Proceedings of:

Principles of Cutting Mechanics:

Applications to Ultra-Precision Machining and Grinding

1993 Spring Topical Meeting

April 12-15, 1993
Westward Look Resort
Tucson, Arizona

The American Society for Precision Engineering (ASPE) is a multidisciplinary professional and technical society concerned with research and development, design, manufacture and measurement of high accuracy components and systems. ASPE activities encompass relevant aspects of mechanical, electronic, optical and production engineering, physics, chemistry, and computer and materials science. Membership is open to anyone interested in any aspect of precision engineering.

Founded in 1986, ASPE provides a new focus for a diverse but important community. Other professional organizations have covered aspects of precision engineering, always as a sideline to their principal goals. ASPE is based on the core of generic concepts necessary to achieve precision in any application; independent of discipline, ASPE intends to be the focus for precision technology — and to represent all facets from research to application.

ASPE — The American Society for Precision Engineering
401 Oberlin Road, Suite 108
P.O. Box 10826
Raleigh, NC 27605-0826
Phone (919) 839-8444 Fax (919) 839-8039

Preface

The 1993 ASPE Spring Topical Meeting focused on understanding and applying ultra-precision machining and grinding process mechanics. The Invited Lecture Session was included to introduce the basic aspects of material removal processes. Following sessions focused on specific examples, applications, and current work.

This topical meeting was organized to provide an informal forum for researchers to exchange ideas with those who find limitations in the processes that affect the quality of their final products. The organizers hope this meeting has helped researchers select future work that is both interesting and potentially beneficial to those designing processes for manufacturing ultra-precision products.

This Volume of Abstracts is intended to convey the informality of ASPE Spring Topical Meetings — authors were not required to submit extended abstracts. The intent of the meeting was to encourage discussions of current and ongoing work; therefore, some results reported here may not be final. We request that individual authors be contacted prior to quoting results reported in the abstracts in this volume.

The Organizers of the
Spring Topical Meeting:

Dick Rhorer
Don Lucca
Tony Gee

1993 Spring Topical Meeting

Contents

Preface — Organizing Committee . . . . . *ii*

Contents . . . . . *iii*

Program . . . . . *iv*

Technical Paper Index *1-2*

Technical Papers *5-94*

Author Index *95*

1993 Spring Topical Meeting

Program

Monday, April 12		Tuesday, April 13	Wednesday, April 14	Thursday, April 15
	8:00	CONTINENTAL BREAKFAST		
	8:30	ON-SITE REGISTRATION	TECHNICAL SESSIONS	
	9:30	OPENING SESSION		
	10:00		BREAK	
	10:30	INVITED LECTURES	TECHNICAL SESSIONS	
	12:00			
		LUNCH	LUNCH	
	1:00	INVITED LECTURES	OPEN FOR DISCUSSIONS	CLOSE OF CONFERENCE
	2:30			
	3:00	INVITED LECTURES	TECHNICAL SESSION	
	5:15			
ON-SITE REGISTRATION AND BAR OPEN	6:30	BAR OPEN	BAR OPEN	
	7:30	DINNER	DINNER	
	8:30	REVIEW & DISCUSSION BAR OPEN	REVIEW & DISCUSSION BAR OPEN	
	9:30			

Technical Paper Index

Opening Session

Tuesday, April 13, 9:30 a.m.

Welcome and Introductions — *R. L. Rhorer*
Conference Outline and Goals — *A. E. Gee*
Overview of Conventional Cutting Mechanics — *D. A. Lucca*

Invited Lectures I

Tuesday, April 13, 10:30 a.m. - 12:00 p.m.

1. ***Material Removal Processes: Engineering Mechanics Consideration***
   C. A. Anderson (Advanced Engineering Technology Group, Los Alamos National Laboratory) . . . . . page 5
2. ***Machining and Grinding — High Rate Deformation in Practice***
   P. S. Follansbee (Materials Science and Technology Division, Los Alamos National Laboratory) . . . . . page 9

Invited Lectures II

Tuesday, April 13, 1:00 - 2:30 p.m.

1. ***Grinding Mechanisms for Metals***
   S. Malkin (Department of Mechanical Engineering, University of Massachusetts at Amherst) . . . . . page 13
2. ***Studies of the Precision Cutting Process****
   R. Donaldson (Precision Engineering Program, Lawrence Livermore National Laboratory)

Invited Lectures III

Tuesday, April 13, 3:00 - 5:15 p.m.

1. ***Indentation Fracture and the Machining of Brittle Materials****
   B. Lawn (National Institute of Standards and Technology)
2. ***Energy Scaling Brittle-Ductile Transitions in Machining***
   K. E. Puttick (Physics Department, University of Surrey at Guilford, U.K.) . . . . . page 14
3. ***Cutting Mechanics for Ductile-Regime Machining***
   R. O. Scattergood (Precision Engineering Center, North Carolina State University) . . . . . page 17

Technical Session I

Wednesday, April 14, 8:30 - 10:00 a.m.

1. ***Molecular Dynamics Simulations of the Precision Machining of Germanium***
   J. A. Patten (NanoTechnology and Precision Engineering Group, University of North Carolina at Charlotte), K. Flurchick (North Carolina Supercomputer Center Research Institute) and J. Beeler and J. Strenkowski (Precision Engineering Center, North Carolina State University) . . . . . page 21
2. ***Atomistic Simulation of Diamond-Tip Machining of Nanoscale Features***
   A. F. Voter and J. D. Kress (Theoretical Division, Los Alamos National Laboratory) . . . . . page 34
3. ***Ploughing on Gold Using a Scanning Tunneling Microscope***
   R. D. Day (Los Alamos National Laboratory) and P. E. Russell (Precision Engineering Center, North Carolina State University) . . . . . page 38

**Paper not available at press time.*

Technical Session II

Wednesday, April 14, 10:30 a.m. - 12:00 p.m.

1. ***Sub-Surface Damage Characterization of Silicon Wafers Using Scanning Infrared Depolarization (SIRD)***
   H. Lundt, M. Kerstan and R. Weiss (Wacker Chemitronic, Germany) . . . . . page 42
2. ***A Non-Destructive Method of Assessing Sub-Surface Damage in Optically Transparent Materials***
   C. F. Kranenberg and K. C. Jungling (Center for High Technology Materials, University of New Mexico) . . . page 46
3. ***Deterministic Microgrinding of Spherical Surfaces on Optical Glasses***
   D. Golini (Center for Optics Manufacturing, University of Rochester) . . . . . page 50

Technical Session III

Wednesday, April 14, 3:00 - 5:15 p.m.

1. ***Investigation of the Potential Machinability of Glassy Carbon in the 'Ductile' Regime***
   Y. Hara and M. Nakao (Mechanical Engineering Research Laboratory, Kobe Steel Ltd., Japan) and A. E. Gee (School of Industrial & Manufacturing Science, Cranfield Institute of Technology, U.K.) . . . . . page 54
2. ***Change of Depth of Cut and Damage on Ground Surfaces in Shear Mode Grinding***
   K. Imai and H. Hashimoto (School of Engineering, Kanagawa Institute of Technology, Japan) . . . . . page 58
3. ***Brittle/Ductile Grinding of Soft Basalt Ceramic***
   I. D. Marinescu and J. A. Webster (Center for Grinding Research and Development, University of Connecticut) . . . . . page 67
4. ***Chemomechanical Effects in Ductile-Regime Machining of Glass***
   T. G. Bifano, R. Annear (Precision Engineering Research Laboratory, Boston University) and D. Golini (Center for Optics Manufacturing, University of Rochester) . . . . . page 71

Technical Session IV

Thursday, April 15, 8:30 - 10:00 a.m.

1. ***Effect of Machining Parameters, Set-up, and Tool Geometry on Surface Finish and Roundness of Polycrystalline Diamond Bored Bronze Bearings***
   G. V. Delbrugge, K. Knott, C. O. Ruud and P. H. Cohen (Department of Industrial and Management Systems Engineering, Pennsylvania State University) . . . . . page 79
2. ***Computer Controlled Precision Optical Polishing on the Diamond Turning Machine***
   P. R. Hannah and D. Stewart (Los Alamos National Laboratory) . . . . . page 86
3. ***Observations on Material Removal Processes Based on Removal Rate and Finish****
   R. E. Parks (University of Arizona) and C. J. Evans (National Institute of Standards and Technology)

Technical Session V

Thursday, April 15, 10:30 - 11:30 a.m.

1. ***Chemical Mechanisms of Diamond Wear***
   E. Paul (Stockton College) and C. J. Evans and R. S. Polvani (National Institute of Standards and Technology) . . . . . page 88
2. ***Orthogonal Cutting Experiments: Input to Ultraprecision Process Design***
   R. L. Rhorer (Los Alamos National Laboratory) and D. A. Lucca (Oklahoma State University) . . . . . page 92

Conference Review and Unanswered Questions

Thursday, April 15, 11:30 a.m.

A. E. Gee, D. A. Lucca and R. L. Rhorer

**Paper not available at press time.*

Technical Papers

Material Removal Processes: Engineering Mechanics Consideration

Charles A. Anderson
Advanced Engineering Technology
Los Alamos National Laboratory

presented at the ASPE 1993 Spring Topical Meeting

on

"Principles of Cutting Mechanics: Ultra Precision Machining and Grinding"

April 13–15, 1993
Tucson, AZ

In the material removal process called machining, a layer of material of constant thickness is removed from the workpiece by a wedge-shaped tool that travels parallel to the workpiece at a preselected depth. Even though the speed of relative movement between workpiece and tool is low (typically 1 to10 m/s), the strain-rates in the workpiece near the tool can be high, on the order of 10^4 to 10^5 s^{-1}. When brittle materials or unlubricated ductile materials are machined at low speed, the removed metal (or chip) will be discontinuous and will be made up of small, fractured segments. On the other hand, when ductile material is machined under lubricated conditions, the removed material forms a continuous coil. In this case, we can represent the material removal process as a steady-state process. In this presentation, we will restrict our topic to orthogonal machining in which the cutting edge is perpendicular to the relative motion — a situation also approximated by other material removal processes such as planing, broaching and turning on a lathe.

The general characteristics of material removal processes are as follows:

(i) As mentioned above, even though workpiece velocities are low, strain-rates are large (~10^4 to 10^5 s^{-1}) because of the localized deformation in the workpiece around the tool tip.

(ii) Temperatures around the tool bit can be significantly above ambient for most cases, which can, in turn, influence the strain field through temperature-dependent material behavior.

(iii) The deformations are large and, thus, carry the material into the nonlinear range of behavior characterized by plasticity, vicsoplasticity, or fracture.

(iv) During the entire material removal process, material must be characterized in the chip as elastic, nonlinear plastic or viscoplastic, and back to elastic. Elastic regions co-exist with flow regions. The chip's final shape will depend strongly on the elasticity of the workpiece material.

(v) The unknown frictional condition at the tool — workpiece interface is important in the machining process, just as it is in other metal forming processes.

Various approximate models for deformation, based on engineering mechanics considerations, have evolved over years of studying material removal processes. The earliest model applicable to ductile materials capable of very large deformation assumed that the deformation around the tip of the tool could be described as a line of shear discontinuity emanating from the tool tip and inclined at an angle ϕ with the workpiece. The

shear stress operating on the discontinuity is the maximum shear stress of the workpiece material. Simple equilibrium considerations and an application of a minimum work principle then gave the relationship,[1]

$$\phi = \frac{1}{4}\pi + \frac{1}{2}\alpha - \frac{1}{2}\lambda$$

where α is the rake angle (the angle that the tool face makes with the vertical) and λ is the angle of friction over the area of the contact between tool and the chip. Experiments by Merchant[2] only roughly confirm the above relationship; the errors are attributed to a variety of approximations, including the use of the minimum principle, underestimating of the resolved shear stress, material work hardening, etc.

Several of the solutions developed in the 1950s[1,3] utilize the method of plasticity called slip-line analysis to describe the flow region around the tool tip during material removal processes. These solutions, which would appear to be an improvement to the solution involving an intense deformation over a single shear discontinuity, also disagree with the experimental data. However, when work hardening of the chip formed in the process is included, the results of the more detailed analysis can be brought into somewhat better agreement.[4] Figure 1 compares approximate plasticity solutions with experimental data (from Merchant[2] and from Thomsen, Lapsley and Grassie[5]) for the machining of steel.

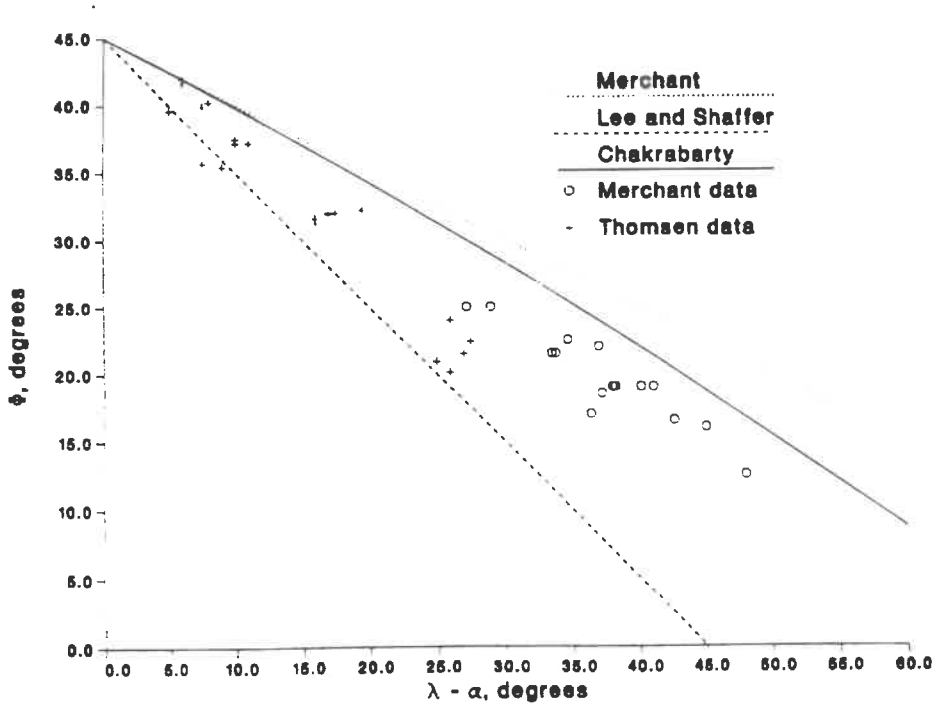

Fig. 1 Shear angle ϕ versus the parameter λ-α, where the λ is the angle of friction and α is the rake angle. Shown are plasticity solutions (Merchant,[2] Lee and Shaffer,[3] and Chakrabarty[4]) and experimental data (Merchant,[2] and Thomsen, Lapsley, and Grassie[5]).

The temperature field around the tool tip has also been calculated using the various approximations about the deformation field around the tool tip. The heat generated internally through plastic flow and along the chip-tool interface through friction can be used as input to the computer codes that solve the heat equation.[6] The advantage of this procedure is that it takes into account the actual geometry of tool and the workpiece. The

MACHINING AND GRINDING -- HIGH RATE DEFORMATION IN PRACTICE

Paul S. Follansbee
Los Alamos National Laboratory
Los Alamos, NM

Introduction

Machining and grinding are well-established material-working operations involving highly non-uniform deformation and failure processes. A typical machining operation is characterized by uncertain boundary conditions (e.g.,surface interactions), three-dimensional stress states, large strains, high strain rates, non-uniform temperatures, highly localized deformations, and failure by both nominally ductile and brittle mechanisms. While machining and grinding are thought to be dominated by empiricism, even a cursory inspection leads one to the conclusion that this results more from necessity arising out of the complicated and highly interdisciplinary nature of the processes than from the lack thereof.

One aspect of machining and grinding operations that is clear is that they both involve highly non-uniform, large strain, and high strain rate deformation mechanisms. Chip formation during orthogonal cutting is described as a localized shearing process involving shear strains of between 2 and 4 and strain rates on the order of 10^5 s^{-1} [1, 2]. Grinding is reported to involve similar strains and strain rates coupled with higher surface temperatures than found in normal machining operations.

With these conditions in mind, the purpose of this paper is to outline the current understanding of strain rate effects in metals.

Rate Effects in Plastic Deformation

Deformation is accommodated in many materials by the generation and motion of defects. In metals, these can be dislocations or deformation twins. The kinetics of deformation processes are defined by the thermally activated interactions of defects with the crystal lattice or with other defects. There are many possibilities for accommodation mechanisms; the rate controlling mechanism depends on the temperature, strain rate and defect population at any instant.

The high strain rates attributed to machining and grinding tend to restrict the options for deformation behavior. For instance, at these strain rates deformation can be assumed to occur under adiabatic rather than isothermal conditions. However, creep mechanisms that require bulk transport (diffusion) are unlikely -- even at the increased temperatures reached during machining -- due to the limited time available for these processes at high strain rates.

The high strain rate deformation literature contains many references to a transition to viscous drag controlled deformation at strain rates exceeding 10^3 s^{-1} or so. Viscous drag deformation is characterized by a linear dependence of flow stress on strain rate -- an

exponent of 1 in a power law relation whereas the exponent at low strain rates is found to be closer to 0.1. A rate dependence of this magnitude, if it were to occur, would dramatically affect flow stress levels as well as the tendency toward strain localization. Recent work, however, has shown that this transition is unlikely except during shock loading [3].

With these restrictions, estimates of adiabatic stress strain curves at the strain rates reported for machining and grinding can be made according to models that describe thermally activated deformation in metals. While simple models for plastic deformation in metals are available, descriptive constitutive laws for machining and grinding need to accurately represent the strain hardening, strain rate dependence, and temperature dependence of the flow stress. Because of the very unique and severe conditions found in machining and grinding independent experimental verification is not always possible, which places a high premium on the foundation used to establish a constitutive relation.

We have developed one model that is capable of describing adiabatic deformation under large strain and high strain rate conditions. It is not the intent in this paper to describe in detail this model, which has been described previously [4,5]. Instead we would like to illustrate the trends predicted by such a model for conditions typical of machining and grinding. Figure 1 shows adiabatic stress strain curves in an austenitic stainless steel at a high strain rates and several initial temperatures. For comparison, a single room temperature (isothermal), quasi-static stress strain curve is included. The adiabatic nature of deformation at high strain rates leads to pronounced "thermal softening" in this material.

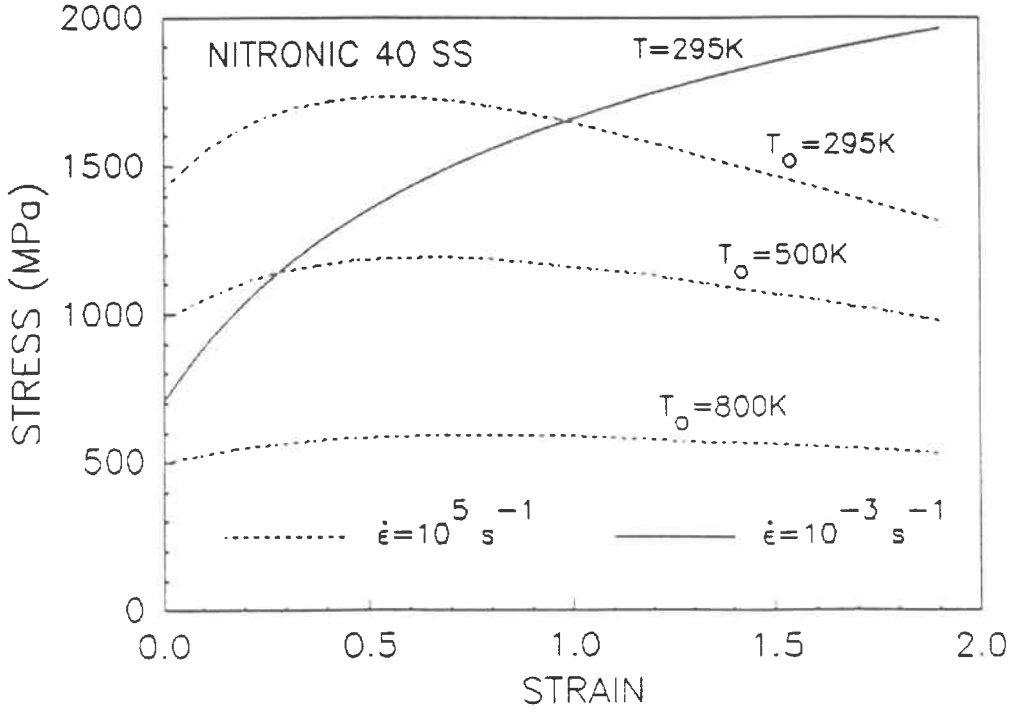

Figure 1: Predicted adiabatic stress strain curves in Nitronic 40 stainless steel at strain rates and temperatures typical of machining and grinding operations.

Strain Localization

In a sense, deformation is always localized due to the crystallographic origin of microstructural deformation mechanisms. Under the appropriate conditions, these microscopic shear localizations can develop into macroscopic shear banding. Metal removal in a machining operating appears to favor a shear localization process. This follows from i) the highly non-uniform stress states and the stress concentrations that exist in the vicinity of the tool/workpiece interface and ii) the adiabatic nature of deformation in machining. The latter is particularly important because the tendency toward shear localization is opposed by the strain hardening ability and strain-rate sensitivity of a material but is assisted by a strongly temperature dependent flow behavior under adiabatic conditions.

Predictions of the initiation of localized straining have proved to be very difficult. Except in a few cases, these necessitate the use of numerical methods. The use of constitutive laws that describe the instantaneous strain, rate, and temperature dependence of the flow stress is essential in analytical or numerical simulations of complicated strain localization behavior.

In general, predictions of the actual failure event in machining operations is very difficult. By failure, we mean the actual mechanism and criteria for formation of the new interfaces making up a chip. However, when localized shearing is severe, this is not as much of a problem as it might appear since the failure plane is well established and the models tend naturally toward a zero stress level as more and more strain (and, thus, heat) builds up in a shear band. This further supports the need to apply descriptive constitutive laws to machining calculations.

Fracture

While machining and grinding mostly involve a localized shearing mechanism, there has always been a need to machine very brittle materials. Because surface cracks are detrimental to the performance of brittle materials considerable effort has gone into the development of grinding and machining operations for these materials. Grinding has been preferred to cutting because i) the higher surface temperatures reached during grinding take the surface above a brittle to ductile transition and ii) the individual "cuts" taken in grinding involve a considerably smaller volume than those taken in machining. In fact, recent work by Puttick has shown that ductile machining response in nominally brittle materials is possible if the depth of cut is maintained below approximately 100 nm [6].

In general, high strain rates lower the ductile-to-brittle transition temperature, i.e., high strain rates assist brittle fracture behavior, through the associated increased stress levels that can drive cracks at higher velocities. The volume effect seen by Puttick and others may have more to do with the microstructural scale and the probability of encountering flaws or microstructural features that can initiate critical cracks. That is, ductile response in nominally brittle materials is possible if the scale over which deformation is imposed is smaller than the microstructural scale of inherent flaws or crack initiation sites.

Conclusions

Machining and grinding are industrial material-working operations that combine several aspects of plasticity, e.g., strain localization and multiaxial deformation, that remain at the forefront of current research. Strain rate and temperature dependent plastic flow are essential aspects of the detailed material removal mechanisms operative during machining and grinding. Successful application of advanced processing modeling and control in these operations will require the use of descriptive constitutive laws.

Acknowledgement

This work was performed under the auspices of the United States Department of Energy.

References

1. Dieter, G. E., Mechanical Metallurgy, Second Edition, McGraw-Hill Book Company, New York, NY, 1976.
2. Black, J. T., "Mechanics of Chip Formation," Metals Handbook, 9th Edition, Volume 16, American Society for Metals, Metals Park, OH, pp. 7-12, 1989.
3. Follansbee, P. S., "Shear Stress Prediction in Shock Loaded Copper," Shock Compression of Condensed Matter 1991, S. C. Schmidt, R. D. Dick, J. W. Forbes, D. G. Tasker (eds.), Elsevier Science Publishers, New York, NY, pp. 415-418, 1992.
4. Follansbee, P. S., and Gray, G. T. III, "An Analysis of the Low Temperature, Low and High Strain-Rate Deformation of Ti-6Al-4V," Metall. Trans., 20A, pp. 863-874, 1989.
5. Follansbee, P. S., and Gray, G. T. III, "Dynamic Deformation of Shock Prestrained Copper," Mater. Sci. Engnr., A138, pp. 23-31, 1991.
6. Puttick, K. E., Rudman, M. R., Smith, K. J., Franks, A., and Lindsey, K., "Single-Point Diamond Machining of Glasses," Proc. Royal Society of London, A426, pp. 19-30, 1989.

We began our experiments with simple indentation and scratching of crystalline silicon, which is the best characterized of all materials. We used a Vickers indenter and verified that in both types of experiment there is a sharp transition to brittle fracture at a penetration depth of about 110 nm, though the resultant pattern of cracking is a function of orientation relative to the crystal lattice (Puttick and Hosseini 1980).

In collaboration with Dr Albert Franks and the late Kevin Lindsey of the N.P.L. we then constructed a highly stiff machine for a study of the single diamond point turning of brittle materials. This consisted essentially of a vertically mounted air bearing carrying the specimen on the end of the spindle, and a tool actuated by a piezoelectric transducer. With this machine we were able to verify the possibility of ductile machining of fused silica, notoriously the most difficult of optical glasses to work. SEM observations of the turned surfaces, however, occasioned some surprise: it appeared that a substantial amount of the material removed in the form of spiral ribbons was in fact detached after the passage of the tool, not ahead of it. We believe that this is due to the operation of a strong compressive residual stress which provides enough strain energy to propagate a shear crack along the boundary of the subsurface plastic zone (Puttick et al 1989).

This machine was subsequently improved, to enable us to machine continuously at high speeds, by Dr Tony Gee of Cranfield Institute of Technology. He installed a Fizeau interferometer to monitor the orientation of the workpiece axis relative to that of the spindle ("specimen run-out"). We have now achieved surfaces approaching good optical quality (R_{max} ~ 3 nm), using various types of diamond tool and cut depths of 100 - 120 nm.

Recently we turned our attention to the depth of subsurface damage, which for many applications in the optical and electronic fields may be as important a determinant of quality as surface profile or form. We compared the damage inflicted by our single point turning machine with that associated with very high precision cup grinding by the Cranfield seven-axis machine tool, again using substrate quality silicon crystals. Observations were made by the non-destructive techniques of Rutherford ion beam backscattering and X-ray topography, and by the destructive method of transmission electron microscopy of cross sections of machined surfaces. The results show that although the mean depth of damage is not very different for the two machining processes, the maximum depths and the nature of damage exhibit dramatic contrasts. The SPDT surface layers exhibit a particularly simple type of plastic flow by dislocation movement predominantly on a single slip system at any given position, which seems to be generated mainly by the cross feed of the tool. The ground specimens, with R_a ~ 11 nm but R_{max} of about 100 nm, showed subsurface layers consisting of dense irregular arrays of dislocations with a variety of Burgers vectors, together with occasional cracks extending to depths of 600 nm or more.

We believe that the highest quality of machined surface of ceramics and glasses, such as is increasingly required by advanced technology, can be achieved only by a single point.

Though such surfaces may apparently be fabricated by grinding, in reality very few of the abrasive grains participate in material removal.

Acknowledgements

In addition to the contributions of colleagues mentioned above, I wish particularly to thank Myke Rudman and Sheila Rudman of the University of Surrey and Paul Shore of Cranfield Institute of Technology.

References

Puttick K E 1980: *J. Phys D: App. Phys.* **13**, 2249

Puttick K E and Hosseini M M 1980: *J. Phys. D: App. Phys.* **13**, 875

Puttick K E, Rudman M R, Smith K J, Franks A and Lindsey K 1989: *Proc. Roy. Soc.* A426,19

Puttick K E, Jeynes C, Rudman M R, Gee A E and Chao C L 1992 *Semicond. Sci. Tech.* **7**, 255

Roesler F C 1956 *Proc. Phys. Soc.* B69, 981

CUTTING MECHANICS FOR DUCTILE-REGIME MACHINING

Ronald O. Scattergood
Precision Engineering Center
North Carolina State University
Raleigh, NC 27695-7918

Introduction

The advent of high-precision computer-controlled diamond turning and diamond grinding machines has made it possible to machine brittle materials in a "ductile regime" wherein fracture damage in the finished surface is eliminated. This has important applications for the manufacturing of precision glass or ceramic components with complex surface forms. While there is a comprehensive literature dealing with material-removal mechanisms for the machining of ductile metals [1], the mechanisms operative for brittle materials are less familiar and relatively poorly understood. In addition, the deformation response of brittle materials can depend sensitively on microstructure, environment and stress-loading conditions, which complicates an assessment of machinability. The present paper provides an overview of the fundamental cutting mechanics for brittle materials. Certain limitations imposed by material properties will also be discussed.

Cutting Mechanics

The loading due to the cutting tool used in either a single-point turning or grinding operation has the feature that the stresses produced are spatially localized. Further insight into the deformation mechanisms is provided by the extensive literature on indentation of brittle materials by sharp diamond (hardness) indenters [2,3]. If the depth d of the indentation is less than a critical value d_c, the response will be plastic flow. If $d > d_c$, fracture in the form of lateral and median-radial cracks will be generated. In its simplest representation, the critical depth is given as

$$d_c = \beta \left[\frac{T}{H}\right]^2 \qquad (1)$$

where T is the toughness (fracture resistance), H is the hardness (plastic-flow resistance) and β is a constant that depends on indenter geometry and other process parameters. Eq. (1) follows from the fact that as d increases, the spatial extent of the plastic deformation zone under the indenter increases. At a critical zone size, fracture (surface energy) becomes favorable relative to plastic flow (volume energy). While the dynamic loading conditions for cutting tools are not equivalent to those for quasi-static indentation, spatial localization is present in both cases and it is reasonable to expect that a transition from plastic flow to fracture will occur at a critical machining depth d_c.

The cutting mechanics for the machining of a brittle material are an interplay between material response governed by d_c and the cross-section profile of the machining chip. Single-point diamond turning using a round-nose tool provides the simplest means to understand this relationship. Fig. 1a is a projection of the [uncut] chip cross section viewed along the cutting direction. Due to the combined action of the cutting and feed motions, the chip cross section is the area bounded by the circular arcs separated by the feed/rev f. The effective depth-of-cut d varies from zero at the tool center to a maximum at the top of the uncut shoulder. At a critical value d_c, there will be a transition from plastic flow to fracture damage, and the crack depth generated at d_c will have a characteristic size scale. The fracture damage progresses upward along the tool nose to the top of the uncut shoulder. If the crack depth at d_c in Fig. 1a does not replicate below the plane of the finished surface (dashed line), ductile-regime machining conditions have been achieved. "Ductile-regime" machining does *not* preclude the occurrence of fracture as a material removal mechanism, the essential requirement being that the damage produced does not replicate into the

finished surface. The tool feed f, as opposed to nominal cutting depth h (Fig. 1a), is a key machining parameter. As f increases, d_c shifts downward along the tool nose, hence, there will be a maximum feed for which ductile-regime machining is possible with a given material and machining parameters.

The optical micrograph in Fig. 1b shows a top-down view of the uncut shoulder region for a (100) germanium crystal machined in the ductile regime. This was obtained by interrupting the machining cut using a fast-tool servo [4]. Fracture damage beginning at a critical depth d_c along the tool nose is manifest in Fig. 1b as the transition from a ductile-cut surface to the fracture-pit damage regime. The experimental observation in Fig. 1b is consistent with the cutting mechanics depicted in Fig. 1a. Further analysis of the geometry in Fig. 1a [4] provides a set of geometrical-model equations that allow values of d_c to be determined experimentally from measurements of the fracture-pit transition point on the uncut shoulder region in Fig. 1b. The size scale for the crack depth in Fig. 1a can be determined from the same analysis. Machining chips also reveal a ductile-to-brittle transition point that can be used to estimate the values of d_c [5].

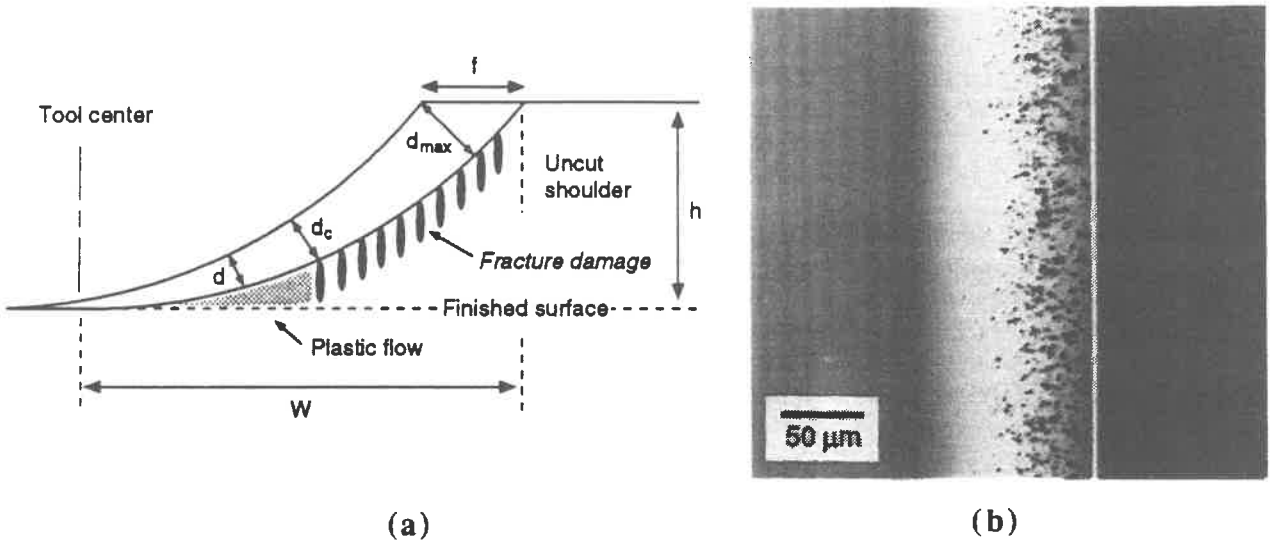

Figure 1. a) Plasticity-fracture transition along tool nose. b) Uncut shoulder (top view).

A more quantitative understanding of the cutting mechanics for brittle materials requires the analysis of the stress-loading conditions. Because of the very small aspect ratio (h:W) of the chip cross section, the cutting process can be approximated as a series of plane-strain orthogonal cuts of varying depth d. Finite-element analyses have been made using this approach [6,7]. A simplified analysis can be made using the stress-field solution for an oblique line force P acting on a half space in Fig. 2a. The line force represents the combined action of the cutting and thrust components of the tool force. The stress field is radial with tensile and compressive stresses occurring behind and in front, respectively, of a line projected normal to the force direction. Plastic deformation occurs in the shaded zones (Von Mises criteria). Mode I fracture will occur along the tensile stress trajectories behind the tool. For given P, there will be a maximum value K_{max} of the stress intensity factor for crack initiation along the Mode I trajectories. Since K_{max} scales with P, which in turn scales with cutting depth d, a critical value of d_c follows from the the crack initiation criteria $K_{max} = T$. The result of this analysis produces Eq. (1) and gives an explicit form for the parameter β. The latter depends upon the rake angle and the rake-face friction coefficient μ.

Fig. 2b shows experimental d_c values (points) for (100) germanium crystals machined along an [011] cutting direction [4]. The dashed line shows predicted d_c values obtained from the stress model in Fig. 2a in conjunction with measurements of T/H and μ. Similar agreement was

obtained using a more sophisticated finite-element model of the cutting process [6]. It therefore appears that the crack initiation process is controlled by the cutting-tool forces. The increase in d_c with increase in [negative] rake angle is essentially a geometric effect. At larger rake angles, the tool force P tilts toward vertical in Fig. 2a, which rotates the tensile stresses out of the subsurface region. This requires a larger value of d_c to obtained the critical force P for crack initiation.

In contrast to critical cutting depths, the agreement obtained between measured and predicted values for the depth of the cracks initiated at d_c in Fig. 1a is poor. The measured values exceed predicted values by an order of magnitude. Either the driving force for crack growth is not directly related to the tool forces or there is subcritical crack growth. While this is not yet understood, both factors may play a role. Subsequent to crack initiation, the cutting tool moves away from the crack and the unloading of the tool force produces a biaxial residual stress state that is compressive very near to the surface and tensile at larger depths [8]. This driving force is not accounted for in current machining-stress models. It can play a significant role if the cracks penetrate into the residual tensile stress region. In addition, cutting fluids can enter the cracks after they are generated and this can contribute to environmentally-assisted subcritical crack growth.

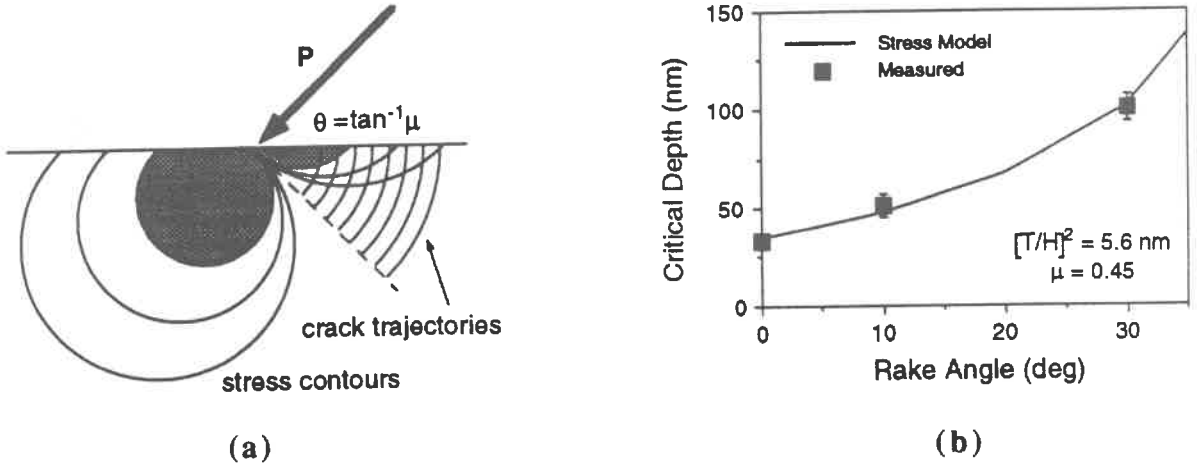

Figure 2. (a) Line-force model for machining stresses. (b) d_c *vs* tool rake angle.

The same cutting mechanics that govern single-point turning will apply to grinding processes. However, the tool geometry and chip cross-section profiles are more difficult to evaluate in this case. Nevertheless, a ductile-to-brittle transition at a critical depth d_c on the "nose" of the active grinding media must occur, and this has been confirmed [9]. This transition will determine the maximum feed for which ductile-regime grinding conditions can be maintained. Recent research has been directed toward a model-based characterization of grinding chip profiles [10]. Even with simplified models, the complexity and sensitivity of the chip profiles to small changes in grinding parameters becomes apparent. Stresses due to the cutting forces should play a similar role to those already analyzed for single-point turning. However, the effective tool-workpiece forces are difficult to assess in a grinding operation. The size and distribution of the grinding media on the grinding wheel, as well as the the bonding agent (resin or metallic), will determine the compliance of the cutting tool. Load spreading due to changes in compliance will affect the active cutting forces [11]. A more comprehensive analysis of the cutting mechanics for grinding operations on brittle materials remains as a challenge for future research.

Material Properties

Fracture toughness T is a key property in controlling deformation response, as is evident in Eq. (1). For many ceramic materials, the toughness plays a subtle and somewhat unexpected role

because of microstructural effects. In contrast to monolithic materials such as optical glasses, the toughness of many commercial ceramics will vary with crack size due to interaction of the cracks with microstructural features such as grain boundaries or second-phase particles. This is especially significant with "high-toughness ceramics" because they can in fact have a very low toughness at the crack-size scales commensurate with precision grinding. Techniques have been developed to measure the toughness variation as a function of crack-size scale [12]. Fig. 3a shows the toughness *vs* crack size curve for a toughened glass ceramic (Canasite), which displays high toughness in the long-crack limit. However, the short-crack toughness drops sharply as shown. The grindability of Canasite is remarkably poor, as manifest by the grinding transition curve in Fig. 3b. In comparison, a very low toughness material like soda-lime glass displays better grindability than the toughened glass ceramic.

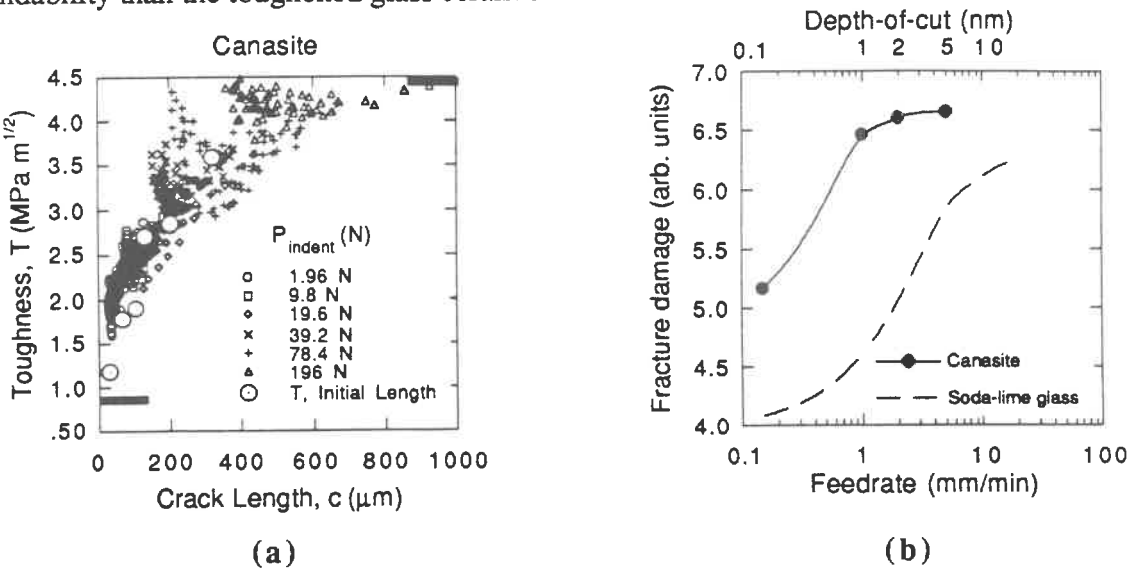

Figure 3. (a) Toughness *vs* crack size. (b) Fracture damage *vs* depth-of-cut transitions.

Summary

The critical cutting depth d_c which governs the initiation of fracture damage is an essential feature of the cutting mechanics for brittle materials. Equally important, however, is the role played by the cross-section profile of the machining chip. Together, these dictate the limits for ductile-regime machining. Material properties also play a pertinent role, and the microstructure can adversely affect grindability for toughened ceramics.

References

1. M. C. Shaw, "Metal Cutting Principles", Oxford Press (1984).
2. B. R. Lawn and T. R. Wilshaw, J. Mater. Sci., 10, 1049-81 (1975).
3. R. F. Cook and G. M. Pharr, J. Am. Ceram. Soc., 73 [4], 787-817 (1990).
4. W. S. Blackley and R. O. Scattergood, Prec. Engr., 13 [2], 95-103 (1991).
5. W. S. Blackley and R. O. Scattergood, submitted to J. of Engr. for Ind. (1993).
6. G. D. Hiatt and J. S. Strenkowski, Proc. ASPE 1992 Annual Meeting, 29-32 (1992).
7. K. Ueda, T. Sugita and H. Hiraga, Annals of CIRP, 40 [1], 61-4 (1991).
8. R. G. Sparks and M. A. Paesler, Prec. Engr., 10 [4], 191-98 (1988).
9. S. C. Fawcett and T. A. Dow, Prec. Engr., 13 [4], 270-76 (1991).
10. G. Storz and T. A. Dow, PEC Interim Report, 37-40 (1992).
11. M. Miller and T. A. Dow, PEC Interim Report, 33-37 (1992).
12. S. M. Smith and R. O. Scattergood, submitted to J. for Mater. Res. (1993).

Molecular Dynamics Simulations of the Precision Machining of Germanium

John A. Patten

University of North Carolina at Charlotte
NanoTechnology and Precision Engineering Group
Charlotte, North Carolina 28223

Ken Flurchick

North Carolina Supercomputer Center
Research Institute
Research Triangle Park, North Carolina

Joe Beeler & John Strenkowski

North Carolina State University
Departments of Material Science and Mechanical Engineering
Precision Engineering Center, Box 7910
Raleigh, North Carolina

ABSTRACT

Results from a molecular dynamics (MD) machining simulation model of single crystal germanium, are presented. The germanium model interaction potential is taken from the work of Ding and Andersen [1,2] after Stillinger and Weber [3]. The machining simulation model is based on our previous work [4,5,6]. The germanium-germanium interaction includes a two body pair potential and a three body angular dependent term. The pair term establishes the equilibrium interatomic spacing of germanium (2.45A), while the three body term provides for the equilibrium diamond FCC (or tetrahedron) structure. The bond angles are approximately 109deg and the lattice constant is approximately 5.66Å for the unit cell.

Equilibrium simulations at room temperature (300 K) have been completed and show the model system remains stable up to 50,000 time steps. Each time step is 1 femtosecond. The model system contains 288 atoms, based upon a 3x3x4 unit cell construction of 8 atoms per cell. The code executes at approximately 50 Mflops, thus, 50,000 cycles require about 25 minutes of cpu time on a Cray Y-MP.

The machining process modelled in the simulation uses a diamond cutting tool, atomic separation 1.54Å, interacting with the germanium atoms via a pair potential. This pair potential is derived from a modified germanium and diamond interatomic pair potential. Machining simulations are run using orthogonal cutting conditions at speeds of 1 m/s to 30 m/s and with depths of cut of 1-10 nanometers. Resulting chip widths are 1-2 nanometers. Machining simulations cover the (001) plane with [010] or [011] direction machining conditions. Other simulations for the (110), (111) and (100) planes with various cutting direction combinations are described.

The Advanced Visualization System (AVS) is used predominately in this research project, both to study the simulations and to present the results of our work. The various slip systems, available for plastic deformation to occur, are readily identified with the visualization tools used in this research. Examples of this work are included in this paper.

1. Background-Molecular Dynamics Simulations

An atomistic description of the machining process can be determined by solving Newton's equations of motion. These equations require as input the forces acting on each particle of the system.

1.1. Atomic Forces and Positions

Interatomic force fields are conservative with no dissipative forces acting, thus the forces acting on individual atoms can be expressed as the gradient of a potential function. This force can be thought of as an intrinsic lattice resistance or frictional force. These potential functions are described by either polynomials or Morse functions, and depend on the particle positions, only. Two and three body terms (which include angular contributions) are used for covalently bonded ceramics. To obtain the total force acting on a single atom, the interactions with all of the neighboring atoms are summed, including any appropriate damping forces, e.g. thermostating boundary forces, etc. Newtons's equations of motion are then integrated numerically to determine the acceleration, velocity and updated positions. From this integration, the evolution of a non-equilibrium system can be determined. Properties of the system can be determined by averaging the trajectories, which is equivalent to phase space averages via the ergodic hypothesis [16].

For the particular models used in this study, boundary forces are included which represent the interaction of the simulated material with its environment. These forces include cutting forces due to the contact and penetration of the cutting tool (simulated diamond) against the material, and the interaction of the material with the environment via heat transfer. These forces, which are included in the model described, are not addressed specifically in this paper. Further information can be found in the references [4,5]

1.2. The Inter-Atomic Energy Potentials

In this section, the potential energy functions for germanium are described and discussed.

1.2.1. Potentials for Ceramics

To more accurately account for the covalent bonding nature of ceramics, the model potential functions of Ding and Anderson (DA) [1.2] as taken from Stillinger-Weber (SW) [3] are used. In addition to the atom-atom interaction, three body potential function terms are used to represent the bond angle forces for covalent materials. The material simulated here is crystalline germanium.

The Ge-Ge pair potential is of the form:

$$u_2 = A\left(Br^{-p} - r^{-q}\right)\exp\left[(r-a)^{-1}\right], r < a$$

and,

$$u_2 = 0, r >= a$$

The Ge-Ge-Ge three-body interaction term, for each triplet of germanium atoms is:

$$u_3 = \lambda \exp\left[\gamma(r-a)^{-1} + \gamma(s-a)^{-1}\right]\left(\cos\theta + \frac{1}{3}\right)^2, r < a$$

and,

$$u_3 = 0, r >= a$$

where $A, B, p, q, a, \lambda, \gamma$ are constants, r and s are the interatomic separation distances, and θ is the included angle of the triplet.

The resultant two and three body forces are of the form;

$$F_2 = -A\exp(r-a)^{-1}\left[\frac{-Bpr^{-p-1} - (Br^{-p} - 1)}{(r-a)^2}\right]$$

and,

$$F_3 = -\epsilon\lambda\sin\theta\exp[\gamma(r-a)^{-1} + \gamma(s-a)^{-1}]$$
$$[(\gamma(r-a)^{-2}\frac{(2rs)}{(r - s\cos\theta)} + \gamma(s-a)^{-2}\frac{(2sr)}{(s - r\cos\theta)})$$
$$(\cos\theta + \frac{1}{3})^2 \quad - 2(\cos\theta + \frac{1}{3})]$$

where ϵ is a constant scaling factor.

The three body term provides the bond angle force for the covalently bonded crystalline germanium. Thus, for each atom i we compute a three body term by pairing up nearest neighbors of i, i.e. atoms j & k. see Fig. 1.1. Where the distance R_{ij} is r and R_{ik} is s. We then look at each k^{th} atom as being a pair with a j^{th} atom, noting that the atom triplet ijk is the same as ikj (where i denotes the central atom or vertex of the angle formed by the three atoms ijk, and R_{jk} is t). Thus, the three body term uses the

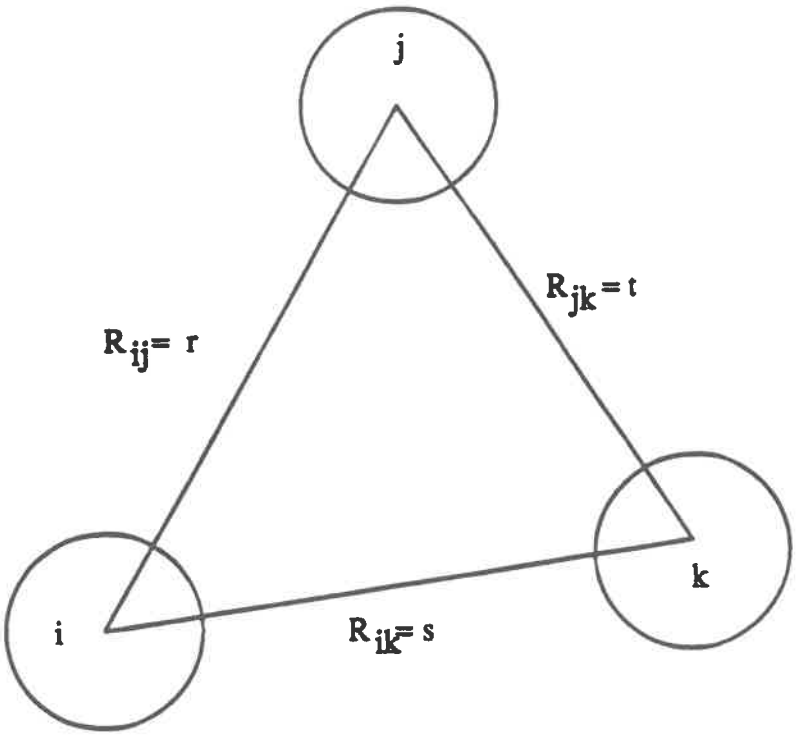

Figure 1.1: Three-body Interaction.

same cutoff as the two body term, namely the vector lengths R_{ij} and R_{ik} are within the cutoff $R_c = a \cdot \sigma$. Fig. 1.2 shows the atoms, angles and bond lengths. The angle θ is defined by the three scalar distances r, s and t (or R_{ij}, R_{ik}, R_{jk} respectively) by:

$$\cos\theta = \frac{r^2 + s^2 - t^2}{2rs}$$

This notation is consistent with the DA model.

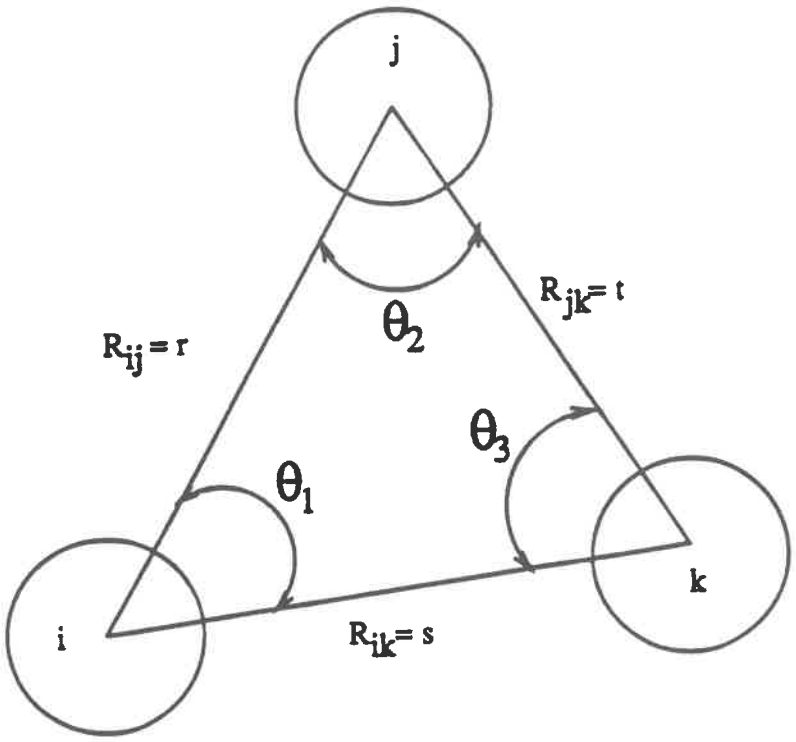

Figure 1.2: Three-body angle terms.

In a method similar to developing a neighbor list, [7,8,9], force terms for each ijk angle in the system are computed. Unlike the pair potential symmetry where $F_{ij} = -F_{ji}$, there is no corollary to this symmetry for the three body terms. Thus, for the three atoms described above, there are three such angle contributions assuming all atom pairs are within the cutoff distance. This is shown in Fig. 1.2 by θ_1 , θ_2 and θ_3.

Therefore for the 3 atoms shown there are three angle force terms and three pair force terms (six total counting both F_{ij} and F_{ji}, etc., but only

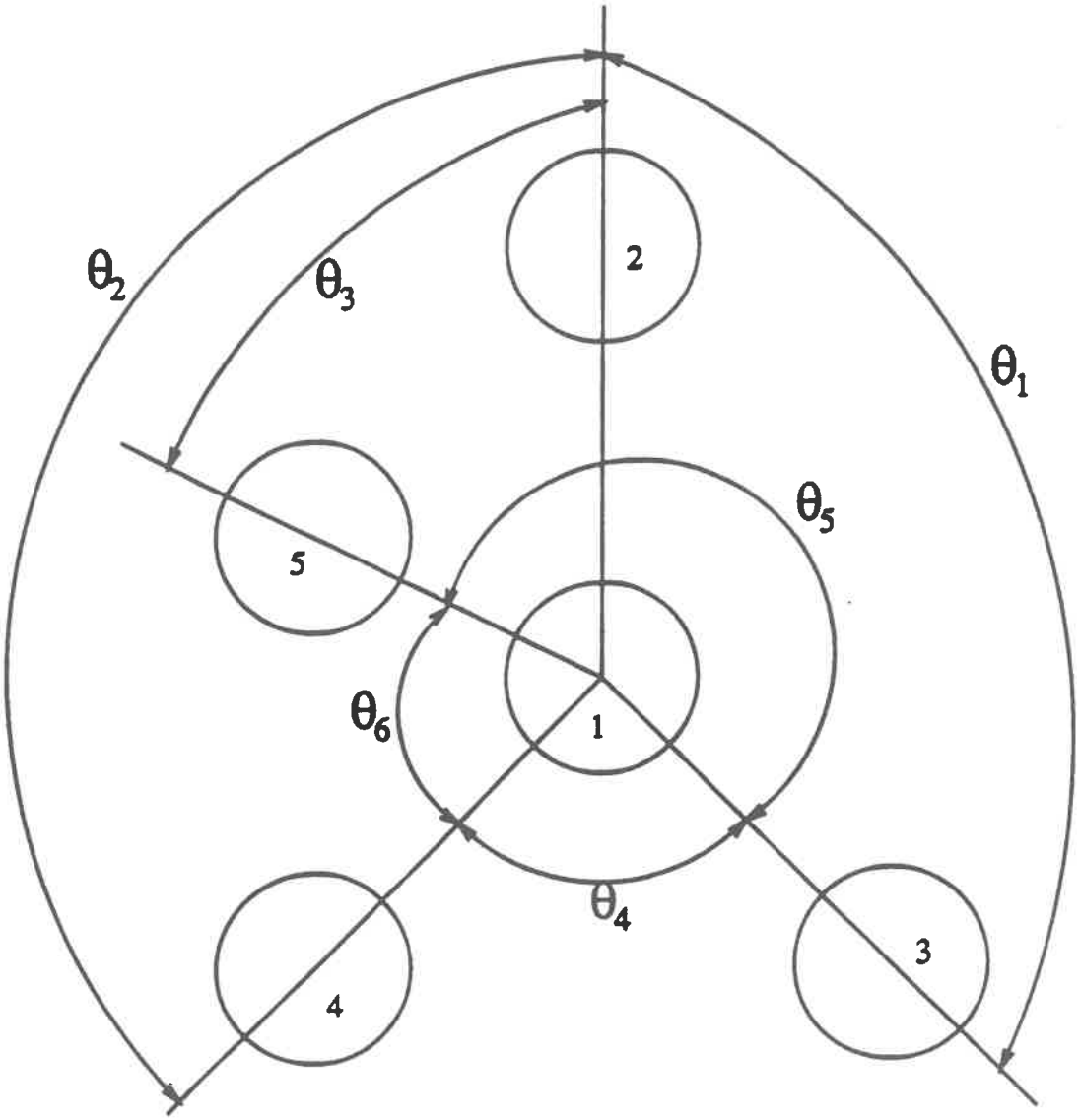

Figure 1.3: Germanium angle terms.

three pair terms require evaluation of the potential function due to symmetry).

For germanium with a diamond cubic structure (FCC), we have six angular terms for the equilibrium five atom tetrahedron molecule. This configuration is shown in Fig. 1.3 where atom 1 is the central atom. i.

There are also four pair bonds represented in this configurations, i.e. the central atom (1) bonded with its four nearest neighbors. The equilibrium positions of all other possible pair bonds, e.g. 2-3, are beyond the cutoff distance R_c, and therefore do not contribute to the potential energy of the system at equilibrium.

The total force acting on an atom is then used to solve Newtons' equations of motion to arrive at particle velocities and updated particle positions due to these interactions [9].

2. Computational Model and Methods

The temperature and the contact pressure (tool/workpiece interface) are allowed to vary. A temperature invariant is imposed at the thermostat boundary to reflect the effect of the stability of the bulk temperature. The finite size of the model can have adverse effects, particularly at the system boundaries. The boundary conditions clearly effect some material properties. All surfaces are explicitly treated in the present model. Most notably the surfaces constitute heat transfer surfaces and interaction with the cutting tool and bulk material are provided.

2.1. Model Approximations

Our present model includes the following approximations:

- Machining in air.
- Neglecting oxidation processes and other chemical processes.
- Treating the convective and radiative heat transfer mechanisms as an exchange of energy between the environment and the atomistic model.

2.1.1. Germanium Workpiece Geometry

The germanium crystal is made up of a number of layers of "movable" atoms and a few layers of non-movable thermostated substrate layers [13]. There is no continuum substrate material in the present model. The crystal is generated by specifying the particular crystal orientation (plane) and the cutting direction. For the present model, the normal to the cutting plane is assumed to be directed upward (orthogonal model) and the machining direction is usually left to right (specified by the cutting direction). The crystal is generated in the model as a structure built upon a unit cell, consisting of 8 atoms. This unit cell is then repeated in the x, y and z directions a specified number of times, in which each repetition is normal

to the cutting plane is considered a layer of material. In this way the width of cut, and maximum length of cut are established by the crystal size so generated. The depth of cut is defined on input, and is implemented as an offset parameter in the simulation. The thermostating boundary layer, generally consists of a single unit layer build as a 2 dimensional array of unit cells.

2.1.2. Diamond Tool

The diamond tool is presently modelled as a perfectly rigid body of dimension 2.5. The rake face and flank face are each made from a single layer of atoms arranged as a close packed structure with interatomic spacing of 1.54Å. The two faces are flat, with an infinite nose radius and an atomically sharp edge radius. The tool rake angle is also specified as an input parameter. The entire tool, comprising all of the diamond atoms, move at a prescribed cutting velocity in the specified cutting direction. As the tool atoms are modeled as perfectly rigid, there are no thermal vibrations associated with the diamond atoms, therefore they behave as an infinite heat sink.

3. Results of Molecular Dynamics Simulations

The results section and discussion are divided into two parts, these are:

1. General discussion of equilibrium conditions.
2. Results of MD simulations of the actual machining process.

3.1. General Discussion of Equilibrium Conditions

Our present modeling strategy incorporates the following practices:

1. A thermostatting boundary layer of atoms is utilized to maintain the workpiece at a preset equilibrium temperature [13].
2. The tool, simulated as diamond, is considered to be perfectly rigid, and an infinite heat sink, i.e. it experiences no thermal vibrations.
3. The environment is considered to be an infinite heat sink, black body, and maintained at a constant 300 K.
4. Thermal initial conditions (TIC) are established by imparting a thermal velocity to each of the workpiece atoms, i.e. all of the energy is initially kinetic energy (KE). The equations of motion are numerically integrated [9] and the system is allowed to

evolve over time. Typically these simulation runs are for 10,000-1,000,000 cycles at time steps of 1-10 femtoseconds. As time progresses the initial KE energy is converted to potential energy (PE), i.e. the atoms are moved from their initial equilibrium positions. Alternate methods of establishing TIC are discussed in [7].

3.1.1. Equilibrium Analysis

With the tool speed set to zero, numerous simulation runs are performed to insure that the model is stable and that the system energy is conserved. For our present model this means that all thermally activated atoms and the environment are at 300 K.

3.2. MD Simulation of the Machining Process

Two models are described.

- Model I: (001) [010]
- Model II: (001) [011]

3.2.1. Simulation Conditions

For the models described, the following conditions apply:

Machining speed:	30 m/s	
Equilibrium Temperature:	300 K	
Material: Crystalline Germanium		
	Interatomic Spacing:	2.45Å
	Structure:	Diamond FCC
	Mass:	72 AMU
Tool Edge Radius:	2.45Å, i.e. atomically sharp	

Orthogonal/Plane Strain Machining

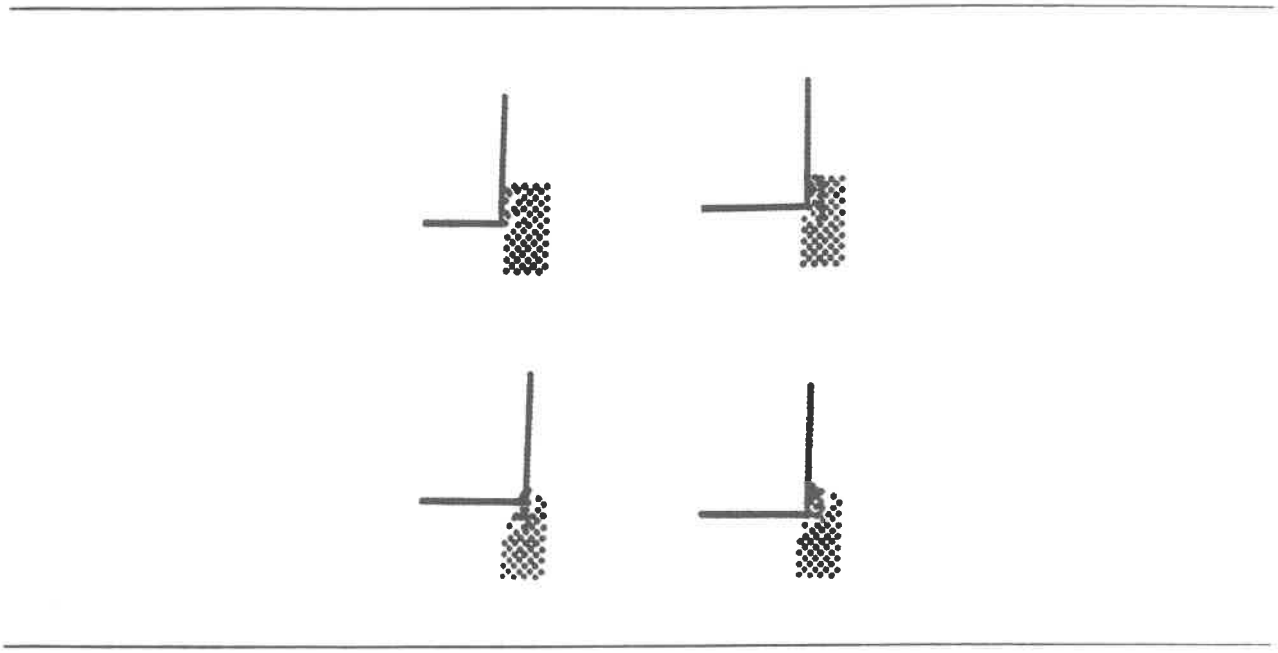

Figure 3.1: Machining Model I

3.2.2. Results for Model I

Fig. 3.1 indicates the position of the modeled atoms part way into the simulation. The spheres to the left, represent the surface of the tool, the bottom layer of the workpiece represents the thermostat atoms and the top layers represent the movable workpiece atoms. This figure clearly shows the deformation process, and the onset of chip formation.

3.2.3. Results for Model II

Fig. 3.2 represents the time evolution of the modelled system. The same three atom regions are indicated as described above, i.e. tool, thermostat layer and workpiece. Since this simulation is for a short time period, the development of the actual chip is not pronounced, i.e. the chip has not yet formed. However, the basic mechanisms of plastic deformation are visible. It is now possible to see the formation of the chip in front of the tool. This action is also assisted due to the thermal activation associated with the atomic vibrations. This latter phenomena causes sharp edges to become rounded as one might imagine occurring during a softening process, prior to material flow due to melting.

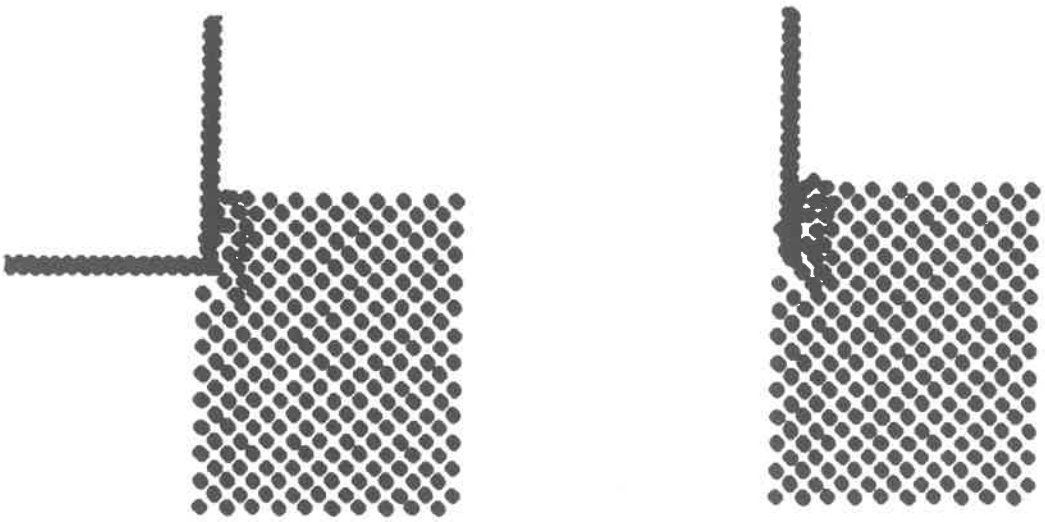

Figure 3.2: Machining Model II

4. Conclusion

The present model can be utilized to study phenomena such as thermally activated processes e.g. crack growth/healing during machining of brittle materials [11].

The computerized experimental work along with other experimental work [14,15], and numerical results [10,12] will eventually lead to a more complete picture and understanding of the machining process of brittle materials.

For the immediate future, work will concentrate on improving the computer code to more accurately reflect the tool-workpiece interaction and to increase the performance and reduce the cpu time per cycle. These changes will permit the simulation of larger systems for longer periods.

Acknowledgements

Support for this work was partially provided by the North Carolina Super Computing Center (NCSC) and the University of North Carolina at Charlotte.

References

1. Ding, K, Andersen, H.C. Molecular-dynamics simulation of amorphous germanium Phys. Rev. B 34, 6987 (1986).
2. Ding, K, Andersen, H.C. Molecular-dynamics computer simulation of amorphous molybdenum-germanium alloys Phys. Rev. B 36, 2675 (1987).
3. Stillinger, F.H., Weber, T.A. Computer simulation of lacal order in condensed phases of silicon Phys. Rev. B 31, 5262 (1985).
4. Patten, J.A., J. Beeler Jr., J. Strenkowski, K.M. Flurchick, Molecular Dynamics Model for Precision Fabrication, submitted to the Journal of Nanotechnology.
5. Patten, J.A., K.M. Flurchick, J. Beeler Jr., J. Strenkowski, Molecular Dynamics Simulationof the Precision Machining Process Including Radiative and Convective Heat transfer Mechanisms, submitted to Journal of Modelling and Simulation in Material Science and Engineering, February 20, 1993.
6. Patten, J.A., Flurchick, K., Optimization of Molecular Dynamics Simulations. submitted to the Computational Materials Science journal, Jan. 6, 1993.
7. J.R. Beeler, Jr., *Radiation Effects Computer Experiments*, North Holland Publishing Co., (1983).
8. Vogelsang, R., Schoen, M. and Hoheisel, C., Comp. Phys. Comm., 30, 235-241, (1983).
9. L. Verlet, Phys. Rev., 159, 98 (1967); M.Levitt, J. Mol. Biol., 168, 595-620 (1983).
10. Larson, W.C., J.S. Strenkowski, Diamond Tool Wear, *Precision Engineerng Center, 1990 Annual Report*, Volume VIII, p. 137, North Carolina State University, Raleigh NC..
11. Mullins, M, M.A. Dokainish, Simulation of the (001) plane crack in alpha iron employing a new boundary scheme, Phil. Mag. A, 46, No. 5, 771-787 (1982).
12. Hiatt, G., Strenkowski, J., A Fracture Mechanics Model for Predicting the Ductile Regime in Single Point Diamond Turning of Brittle Materials, *PEC. 1990 Annual Report*, Volume VIII, p. 181.
13. Nose, S., A unified formulation of the constant temperature molecular dynamics methods, J. Chem. Phys. 81, 511-519 (1984).
14. Tidwell, M., Scattergood, R.O., Analysis and Modeling of Diamond Turning of Brittle Materials, *ASPE 1991 Annual Conference Proceedings*, Santa Fe N.M., October 13-18, pp. 108-111 (1991).
15. Tidwell, R.M., Scattergood, R.O., Diamond Turning of Brittle Materials. *PEC, 1990 Annual Report*, Volume VIII, p 153, NCSU, Raleigh NC.
16. Heermann, D.W., *Computer Simulations Methods in Theoretical Physics*. Springer-Verlag, 1986.

ATOMISTIC SIMULATION OF DIAMOND-TIP MACHINING OF NANOSCALE FEATURES

Arthur F. Voter and Joel D. Kress

Theoretical Division
Los Alamos National Laboratory
Los Alamos, New Mexico 87545

As part of an effort to investigate the limits of stylus-based machining as a nanofabrication technique, we report on molecular dynamics (MD) simulations of machining "experiments" at the nanometer scale. Such MD "experiments" have been used recently to simulate orthogonal cutting of copper[1] and indentation and scraping by a hard diamond-like tool of copper and silver surfaces.[2] Using a many-body form of interatomic potential for the silicon-carbon system, we model a small diamond tip cutting through a nanometer-sized nub of Si on the Si(100) surface. We have examined horizontal cutting speeds from 12.5 m/s to 800 m/s. Although the diamond tip and the silicon feature are both smaller than is experimentally realizable at present, this prototype system allows us to begin an examination of the theoretical limits of physical manipulation with an STM or AFM tip. Properties we wish to examine include the nature of the cutting event (plastic versus brittle), the cleanness of the cut, the fate of the removed material, the force on the cutting tip, the temperature in the machining region, and the effect of different cutting speeds and geometries.

The diamond tip/silicon system is simulated using classical molecular dynamics. The best available interatomic potential for the Si-C system is used: the Tersoff many-body form.[3] The silicon substrate consists of a 10x20x10 Å nub sitting on a Si(100) face. (The nub atoms are lightly shaded for clarity in Figs. 1 and 2). Periodic boundary conditions are imposed in the two directions parallel to the surface. The bottom two layers of substrate are fixed, and the next two layers are thermostatted to a temperature of 300 K using the Nosé-Hoover method.[4] The diamond tip is 20 Å in diameter and is also oriented in the (100) direction. (The tip atoms are black in Figs. 1 and 2.) The innermost core atoms of the tip have horizontal velocity fixed at the desired tip speed, with the next few shells near this core thermostatted to 300 K. The total simulation size is 2184 atoms. The system is warmed for about 10 picoseconds (ps) before the tip cutting motion begins. The slowest horizontal cutting speed considered is 12.5 m/s. (For reference, a table saw blade cuts at about 48 m/s.) The fastest cutting speed considered is 800 m/s.

In Fig. 1, we show four snapshots in time from a machining simulation for a tip cutting speed of 50 m/s in the +x direction. Initially, at t=0, the axis of the tip is aligned with the edge of the Si (100) surface and the bottom of the tip is aligned with the center of the nub. (Also, see the first panel of Fig. 2.) At t=38 ps, the tip is in contact with and centered in the nub. Here the upper half of the nub has deformed to accomodate the tip. At t=76 ps, lifting of the tip begins, so that the tip velocity has an additional component of 100 m/s in the +z direction. At this point, some of the removed silicon sticks to the tip. At t=89 ps, the tip has lifted away in the +z direction, and yet there still remains a "strand" of silicon "fiber" connecting the tip with the nub. In Fig. 2, side views of the machining simulations are shown. The first panel shows the initial snapshot. The second and third panels show the final snapshot for tip speeds of 50 and 400 m/s, respectively. The final results at both speeds look very similar; the tip has pushed material beyond the original dimensions of the nub. In fact, the final results for all cutting speeds examined so far (12.5 to 800 m/s) are very similar.

In conclusion, we find that at all cutting speeds examined (12.5 to 800 m/s), the silicon flows plastically while the tip is unperturbed, and that the nature of the cutting process and the final geometry are very similar. Some removed silicon sticks to the diamond tip, while most is left at the exit of the cut. The maximum force on the tip ($\sim 3 \times 10^{-8}$ Newton) is similar for all cutting speeds examined, with a slight reduction at the higher speeds. A plot of the tip force versus time (not shown) exhibits oscillations that probably result from vibrations in the nub and/or the tip. The silicon nub heats up considerably, reaching a temperature of 700 K during the 50 m/s simulation, and higher temperatures in the faster runs. Thus, the local heating is very speed dependent.

It is a pleasure to acknowledge the collaborations with Robert Day, Bruce Lamartine, and Marilyn Hawley. This work was performed under the auspices of the U. S. Dept. of Energy and was funded by Laboratory Directed Research and Development.

References

1. J. Belak and I. F. Stowers, Proc. of the 1990 Annual ASPE Meeting.
2. J. Belak and I. F. Stowers, submitted to the Proc. of the International Conference of Metallurgy Coatings and Thin Films, preprint UCRL-JC-109024, 1992.
3. J. Tersoff, Physical Review B **39**, 5566 (1989).
4. S. Nosé, J. Chemical Physics, **81**, 511 (1984); W. G. Hoover, Physical Review A **31**, 1695 (1985).

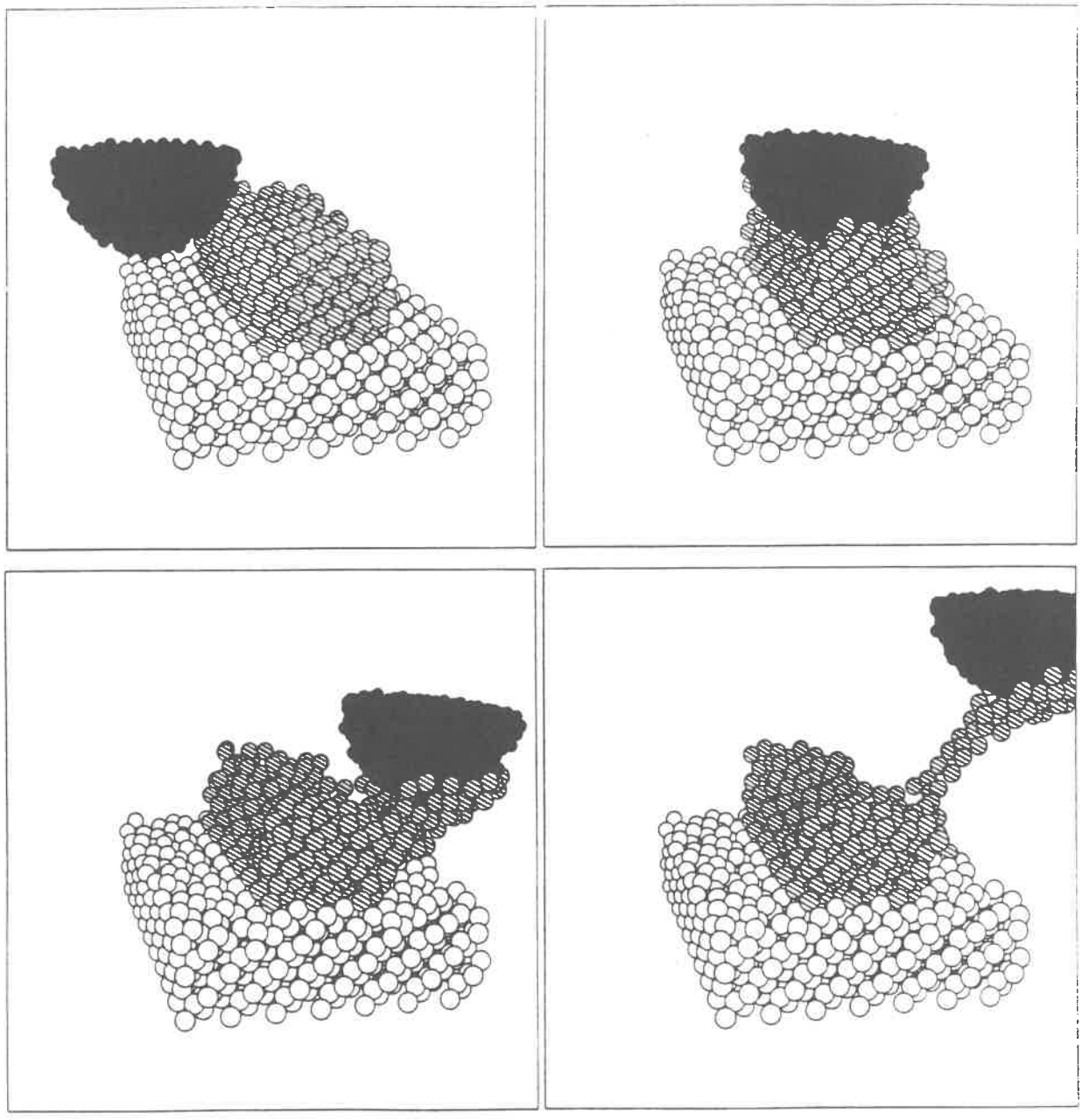

Figure 1. Snapshots from molecular dynamics simulation of diamond tip machining of silicon nub on silicon substrate. **Upper left panel**, t=0 picoseconds (ps). **Upper right panel**, t=38 ps. **Lower left panel**, t=76 ps. **Lower right panel**, t=89 ps.

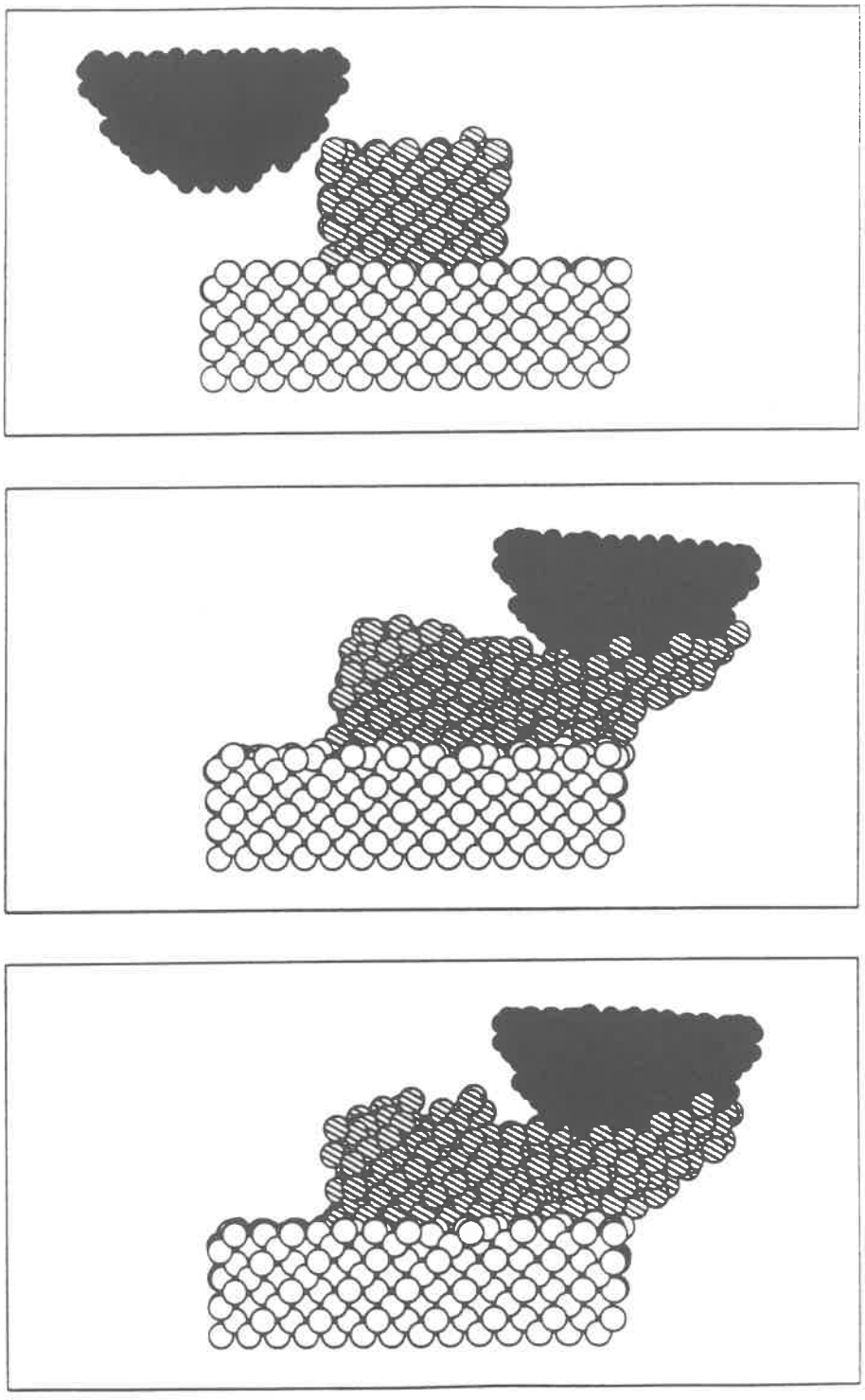

Figure 2. Side view of tip and nub showing similarity of cut. **Upper panel**, before cut. **Middle panel**, after cut, cutting speed of 50 m/s. **Lower panel**, after cut, cutting speed of 400 m/s.

Ploughing on Gold Using a Scanning Tunneling Microscope

Robert D. Day
Los Alamos National Laboratory, Los Alamos, NM, USA

Phillip E. Russell
North Carolina State University, Raleigh, NC, USA

INTRODUCTION

The Scanning Tunneling Microscope (STM) is a scanned probe imaging instrument which uses the principle of quantum mechanical electron tunneling to obtain a topographical image of a surface. To acquire this data the STM positions a sharp conductive tip close enough to the surface of the sample being imaged to induce a quantum mechanical tunneling current. As the tip is scanned across the surface an image is acquired. More details on the image forming process can be obtained from reference [1]. These instruments are capable of controlling the tip placement to a precision of less than 0.1 nm in all three dimensions . It is our desire to exploit the precision and imaging capabilities of the STM for studies in the mechanics of material modification at the nanometer level.

In quantum mechanical tunneling the tip should never contact the surface. However, since the tip is so close to the surface, inter atomic forces and forces caused by tunneling through a contamination layer on the surface can deform the surface elastically. The magnitude of the forces encountered in normal STM imaging in air lie in the range of 10^{-6} to 10^{-7} N [3-6,9]. The purpose of the our experiments is to measure the normal force on the sample induced by the tip as a function of voltage and tunneling current and use the imaging capabilities of the STM to determine if the sample material's surface can be deformed plastically in a controlled manner by the tip. In our investigations we use the tip as a ploughing tool which can be moved in a line to create a furrow, or can be scanned in a plane to displace a pocket of material. This abstract describes how we measure the tunneling force, presents some of the data we have acquired to date, and shows evidence of plastic deformation caused by the tip.

EXPERIMENTAL CONFIGURATION

The simultaneous measurement of force while using a STM has been performed by numerous other investigators. References 2-6 is a representative list of work performed in this area. In general, the reported measurements were made using Scanning Force Microscopes (SFM's) with conductive tips so they could also be used as STM's. Most commercial STM's (ours included) do not allow forces to be measured while scanning the surface. Therefore we devised a way to measure this force by adapting our stand-alone STM head to a Mettler AE 163 [7] semi-micro balance. This instrument measures the change in current to a magnetic coil that is required to keep the balance pan at a constant height as the force on the pan is changed. This arrangement is ideal for the types of measurements required. The AE 163 has a resolution of 10^{-7} N with a 6.5 decade dynamic range. This measurement range is considered to be appropriate for our investigations. Using this set-up to measure tunneling forces has a number of good features: 1) it is inexpensive, 2) it is flexible, 3) the balance is easy to calibrate, 4) the working principle behind the balance is a mature technology, and 5) the balance has a very broad linear measuring range.

Figure 1 is a drawing of our experimental configuration. The stand-alone STM head of our Nanoscope II® [8] is mounted to the balance's frame by means of a fixture. The sample is placed on the balance's pan. Electrical contact between the sample and the STM is made by means of a gold band that is glued to the sample and the fixture using conductive paint. The calibration of the balance was checked using calibrated weights before and after the data had been taken to assure that the experimental configuration was not influencing the balance's measuring ability.

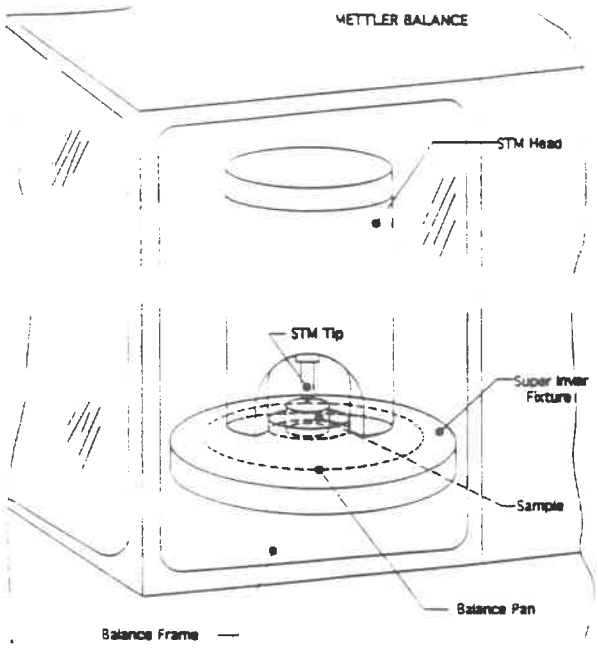

Figure 1 - Drawing of experimental configuration for obtaining tunneling force data using a semi-micro balance

When obtaining the data, the STM's scan size was set to 1 nm so essentially point-force data was obtained. (Forces for any scan size could be measured, however.) The tip materials used were conductive diamond and Pt-20%Ir. The (111) planes of two gold single crystals were used as the samples. One of the samples had an etched surface the other's surface was mechanically polished. Absolute forces were determined by measuring the difference in force when the tip was engaged with the sample, at a particular bias voltage, and when it was withdrawn by 2 μm or more. All of the data were taken in air.

DISCUSSION OF DATA

The diamond tips were doped single crystals obtained from Digital Instruments [7]. A plot of force vs. voltage is shown in figure 2 (Positive forces are compressive.). Each series of data plotted is taken at a different position on the sample. These data show that there is a general trend towards an increase in force with a reduction in voltage. The data also show that there can be a significant variation in force as a function of lateral position on the surface.

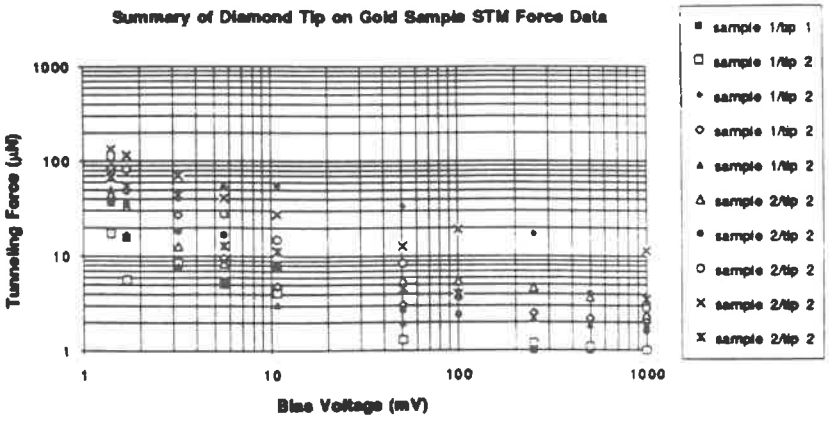

Figure 2 - STM force data for the diamond tips on the (111) plane of the gold samples

Ellipsometry was used to obtain an estimate for the thickness of the contamination layer on our samples. The determination of the absolute thickness depends upon a knowledge of the index of refraction of the contaminant. This is a difficult parameter to obtain but reasonable estimates for this value can be made. Based upon these estimates a layer which could range in thickness from 3 to 5 nm was measured. The role of contamination on the forces induced during STM imaging of graphite in air has been discussed by Mate et. al. [4] and Mamin et. al. [9]. Forces in the range of 10^{-7} to 10^{-6} N were required to push a Pt-13%Rh tip through the postulated contamination layer in order tunnel to the graphite surface for a tunneling current of 1nA and a voltage of 200 mV. The effect of contamination on our surfaces is a likely explanation for the force vs. voltage trends we see in our data.

The value of dln(I)/dS, where I is the tunneling current and S is the tip-to-sample distance, is a measure of the tunneling barrier height. This measurement was made for the diamond tips and for the Pt-Ir tips. The value for the diamond tips was about twice that of the Pt-Ir tips. This implies that a diamond tip must be closer to the surface to achieve the same tunneling current at the same voltage than a Pt-Ir tip. As a result, the force induced by the diamond tip should be greater and more sensitive to contamination layer thickness variations than the Pt-Ir tip. A summary of the force vs. voltage data for Pt-Ir is shown in figure 3. The repeatability of the measurements for the voltages above 20 mV has a standard deviation of 0.1 μN. At 1.4 mV the data has a standard deviation of 1.4 μN. Comparing these data with those presented in figure 2 demonstrates that the forces induced by the diamond are greater and more erratic as a function of sample and position than those for the Pt-Ir. This is what is expected if contamination is playing a role in the generation of the tunneling force. The negative forces seen at the higher voltages for Pt-Ir are probably caused by capillary forces induced by the interaction of the contamination layer with the tip where the layer is relatively thin.

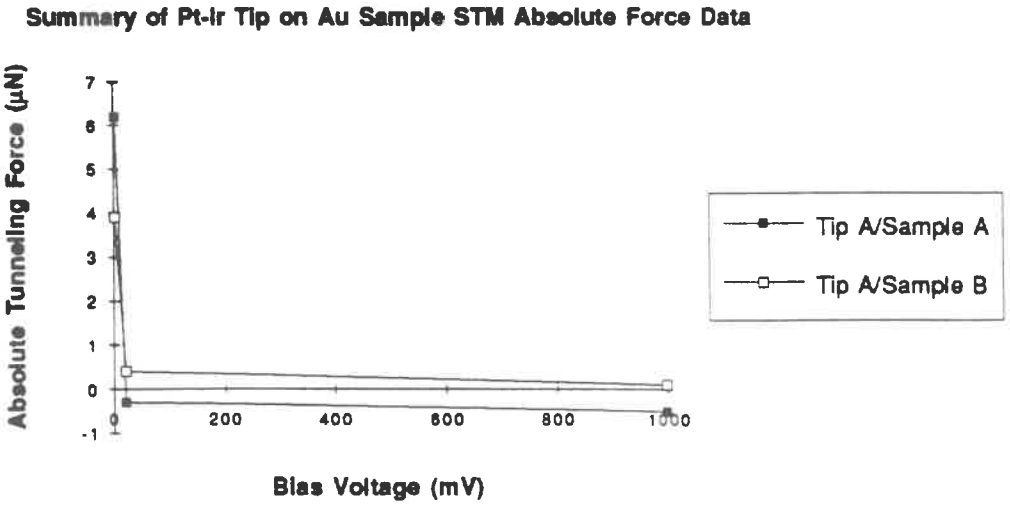

Figure 3 - STM force data for the Pt-Ir tips on the (111) plane of two different gold samples

Plastic deformation was observed at low voltages. Figure 4 (a) shows a 75 nm deep plough on the (111) plane of the single crystal lapped gold surface. The plough was created at a tunneling current of 1 nA and a voltage of 1.4 mV. The force induced was 50 μN. Figure 4 (b) shows a 600 nm square X 4 nm deep pocket which was produced in a sputtered gold surface at a tunneling voltage of 20 mV and a current of 1 nA. (These images were produced at a 1 volt bias voltage by the same tip which that performed the material modification. This high bias voltage does not

induce enough force on the sample to cause plastic deformation.) Azarkhim and Richmond [11] have developed a rigid-perfectly plastic model of ploughing. We are currently comparing our data with their theory. The results of this comparison are encouraging but they are too preliminary to present at this time.

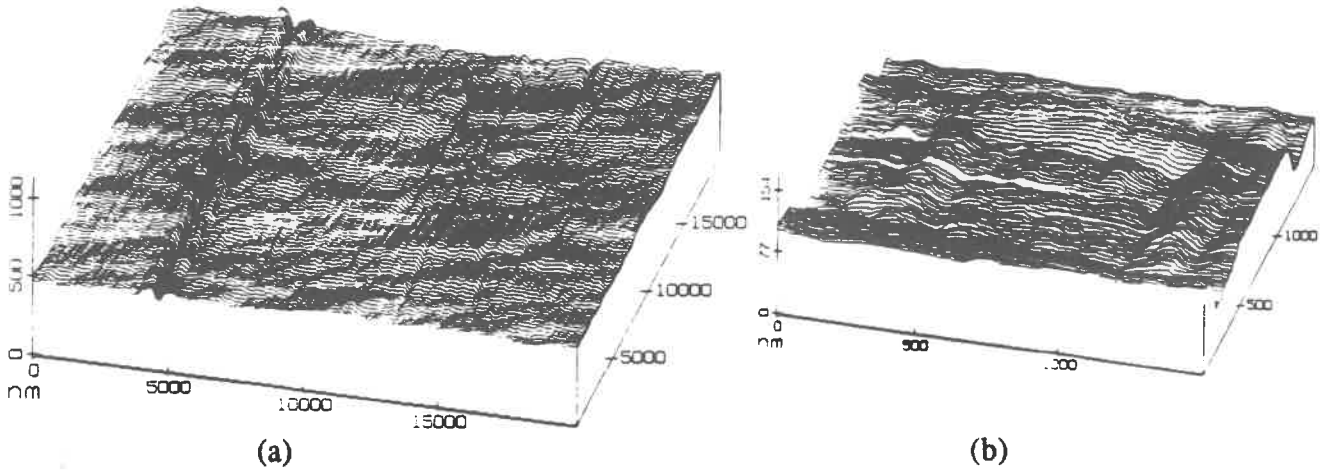

Figure 4 - (a) An STM image of a plough produced on the (111) plane of a single crystal gold surface by a diamond pyramidal shaped tip. (b) A square pocket produced on a sputtered gold surface by the same tip as used in (a).

SUMMARY

In summary, a commercial balance can be used to easily and inexpensively measure point and average scan forces during an STM experiment. It is likely that contamination plays a role in the magnitude of force induced as a result of the tunneling parameters. This was demonstrated by the fact that Pt-Ir, which has a smaller tunneling barrier height than diamond, does not induce as much force on the sample as the diamond. Plastic deformation was observed with the diamond tip at voltages of 20 mV and below with a 1 nA tunneling current.

The authors are grateful to Bruce Lamartine, Bob Marsters, Tony Rollett, and Phil Hannah for their advice and encouragement. A special thanks is extended to Phil Hannah for his production of the drawing used in figure 1 and to George Perrault for his help and advice in setting up the balance.

REFERENCES

[1] H.J. Guntherodt, R. Wiesendanger, Scanning Tunneling Microscopy I, Springer-Verlag Press (1992)
[2] P.J. Bryant, R. G. Miller, and R. Yang, Appl. Phys. Lett. 52 (26), p. 2233- 2235 (1988).
[3] D. A. Grigg, Ph. D. Thesis, North Carolina State University, Dept. of Materials Science and Engineering (1992), p. 74-77
[4] T. R. Albrecht, Ph. D. Thesis, Stanford University (1989), p. 75-89
[5] C. M. Mate, R. Erlandsson, G. M. McClelland, and S. Chiang, Surface Science 208 (1989) pp. 473-486
[6] S.L. Tang, J. Bokor, and R. H. Storz, Appl Phys. Lett. 52 (3), pp. 188-190
[7] Mettler Instrument Corp, Hightstown, NJ USA
[8] Digital instruments, Santa Barbara, CA, USA
[9] D. Sarid, Scanning Force Microscopy, Oxford University Press, 1991, p. viii
[10] H. J. Mamin, E. Ganz, D. W. Abraham, R. E. Thomson, and J. Clarke, Phys. Rev B 34, 12, pp. 9015-9018.
[11] A. Azarkhim and O. Richmond, Wear, 157 (1992) pp. 409-418

SUB-SURFACE DAMAGE CHARACTERIZATION OF SILICON WAFERS USING SCANNING INFRARED DEPOLARIZATION (SIRD)

H. Lundt, M. Kerstan, R. Weiss
Wacker Chemitronic
P.O. Box 1140, 8263 Burghausen, Germany

Introduction

The sophisticated present-day semiconductor device and integrated circuit technology demands an extremely high surface and sub-surface quality of the silicon wafer. Any residual damage due to the mechanical processes of the wafer preparation (slicing, lapping, and grinding) has to be minimized and finally removed to avoid negative effects for the final device production. The depth of this damage significantly influences the duration of subsequent processes of the wafer production like etching and polishing and thus it influences the the wafer geometry. But reducing the sub-surface damage (SSD) is not only necessary to improve the wafer quality, but is also demanded for cost reduction due to the high value of the large diameter ingot material.
Unfortunately the SSD due to the precision machining of the wafers can not be estimated or calculated from the parameters of these mechanical processes. A method to measure the SSD with high accuracy, sensitivity, and local resolution needs to be applied. Already in the early days of the semiconductor technology several methods have been developed to meet these requirements. The three most common methods which are of practical importance and still used in the industry today are constancy of the etch rate /1/, metallographic taper-sectioning /2/, and planar polishing /1/. It should be mentioned that many other methods, like for example x-ray topography and raman spectroscopy, can be applied /3/. Each of these methods has certain disadvantages with respect to sensitivity, local resolution or applicability in an industrial environment.
The purpose of the present work was the development of a new method to detect SSD in precision machined silicon wafers with a high sensitivity for industrial applications faster than previously possible.

Experimental Method

Precision machining causes a damaged and stressed surface layer of the silicon wafer. The stress induces birefringence in the otherwise optically isotropic silicon crystal (photoelastic effect). Thus the stress can be visualized by examining the machined wafers between crossed polarizers. In the case of most glassy isotropic materials visible light can be used while for silicon crystals IR light needs to be applied due to the band gap energy of this semiconductor. Lederhandler /4/ and Takasu and coworkers /5/ used an IR lamp as a light source and identified the degree of stress in the wafer from the gray scale of the pictures they obtained.
In the present work the beam of a helium-neon laser with a wavelength of 1152 nm was transmitted through the machined wafer to measure the depolarisation due to sub-surface damage (s. fig. 1). The optimum wavelength depends on the doping level of the ingot. The wafer is located

between crossed polarizers and a pair of quarter-wave plates (circular polarization). Employing circularly polarized light has the advantage that the depolarization does not depend on the angle between the plane of polarization of the incident beam (linearly polarized light) and the wafer orientation (with respect to a rotation around an axis perpendicular to the wafer center). If the wafer can be kept at a constant orientation the measurement can be performed without quarter-wave plates, which leads to a higher sensitivity.

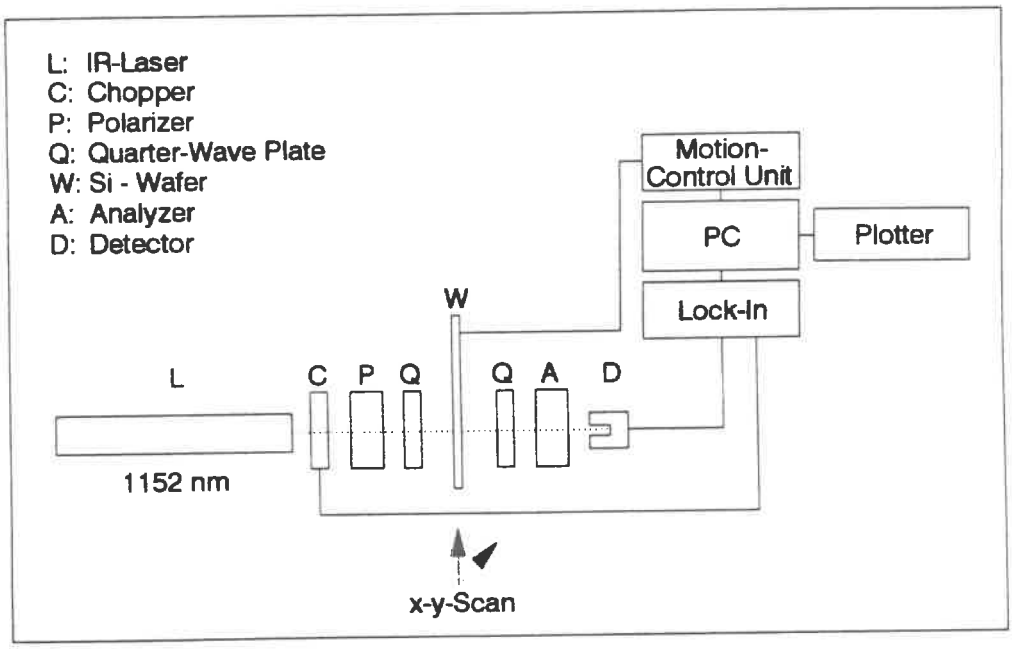

Fig.1: Schematic diagram of the experimental set-up

Instead of a gray scale a quantitative value DP for the degree of depolarisation can be obtained:

$$DP = L_c / L_p$$

L_c: light intensity with crossed polarizers, L_p: light intensity with parallel polarizers

The depolarization ratio DP is a qualitative measure for the subsurface damage. Thus a damage map can be created by scanning the wafer with the laser beam. In the current experiments an unfocused beam is used which allows a 1 mm resolution (about 17000 data points per 6" wafer). By focusing the laser beam a much higher resolution is possible.
Unfortunately the depth of the SSD can not be determined quantitatively from the depolarisation ratio DP alone. A depth profile of the sub-surface damage can be obtained by combining the depolarization technique with subsequent etching. Measuring the depolarization after each etch step yields a decay curve for DP. After a removal of all damaged layers the light intensity for crossed polarizers decays totally. From this decay curve the depth of damage can be determined.

Results

Inner diameter (ID) slicing is the conventional present-day silicon wafering technology. The saw blade used for this process has a diamond cutting edge electrodeposited on the inner diameter. Such an ID blade is a bonded abrasive grinding wheel which cuts a deep, narrow slot in the ingot material. This grinding process leads to high stress fields which cause cracks and dislocations ahead and to the side of the blade. The side damage is left as sub-surface damage in the sliced wafer. Naturally the slicing is a rather coarse mechanical process compared with lapping and flat grinding.
A damage map of an as-cut wafer created with scanning infrared depolarisation (SIRD) reveals rather high values of depolarisation often with strong local fluctuations ("roughness" of damage).
A removal of the upper damage layer by etching reduces the depolarisation and smoothens these fluctuations. The upper layer with the highest degree of destruction of the silicon crystal causes the strongest stress fields and its removal reduces the stress induced birefringence. This stress decreases dramatically (exponential decay) in the first few microns beneath the surface (crack zone in the model of Hadamovsky /6/). After etching even further the depolarization decays weaker which can be attributed to a zone of single, deep reaching cracks and elastic deformation of the crystal lattice /6/.
A plot of the depolarisation ratio DP and the light intensity with crossed polarizers L_C versus the material removal shows the total decay curve.

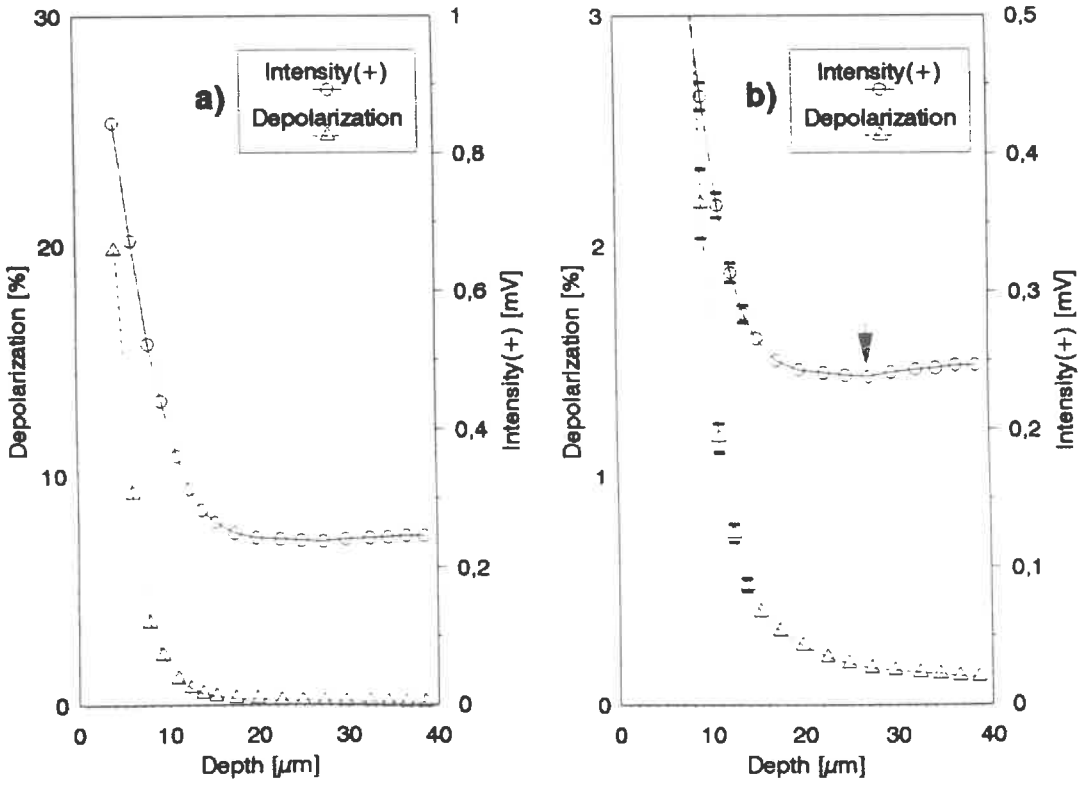

Fig. 2: Depolarisation decay curve for a sliced wafer:
(a) total decay curve, (b) enlarged segment

After the removal of the damage L_c reaches a constant level and after further etching it slightly increases again. This increase is due to a higher transmissivity of the thinner wafer after etching. Thus DP decreases even further (but linearly in the range of a few microns) after the damage removal ($DP = L_c/L_p$). The lowest point in the decay curve of L_c gives the quantitative value of the depth of damage. The error of measurement depends on the local resolution of the scanning and the depth resolution due to the subsequent etching.

For sliced silicon wafers typical values for the SSD are 20-45 µm with an error margin of 1-2 µm. The SSD depends strongly on the grain size of the diamonds deposited on the cutting edge of the ID saw blade. In order to reduce the SSD in sliced wafers the use of a fine diamond grain is favorable. But machine parameters like forward feed rate and rotation speed have also an impact on the SSD.

The damage maps of lapped wafers look much more uniform compared with sliced wafers, and the depth of damage is much lower. Again the depth of the SSD depends strongly on the size of abrasive grain of the lapping powder.

SIRD is a new method to characterize the sub-surface damage of precision machined wafers. It is a fast, non-destructive method to obtain a general overview about the uniformity of the SSD. In combination with subsequent etching the depth of the SSD can be measured with high accuracy (destructive). Thus SIRD can be used to characterize all mechanical processes of the wafer production in order to improve the wafer quality by reducing the the sub-surface damage.

References

/1/ R. Stickler and J.W. Faust, Electrochem. Techn., 4, 399, 1966

/2/ E.N. Pugh and L.E. Samuels, J. Electrochem. Soc., 108, 1043, 1961

/3/ E. Brinksmeier, Precision Engineering, 11, 211, 1989

/4/ S.R. Lederhandler, J. Appl Phys., 30, 1631, 1959

/5/ S. Takasu, Y. Matsushita, H. Kotake and T. Wada, in: Semiconductor Silicon 1977, Edt.: H.R. Huff and E. Sirtl, Proc. 3rd Int. Symp. on Materials Science and Technology, Philadelphia 1977

/6/ H.F. Hadamovsky, "Werkstoffe der Halbleitertechnik", Verlag für Grundstoffindustrie, Leipzig 1985

A Non-destructive Method of Assessing Sub-surface Damage in Optically Transparent Materials

Christian F. Kranenberg, Kenneth C. Jungling
Center for High Technology Materials
University of New Mexico
Albuquerque, New Mexico

Various methods of assessing sub-surface damage in optically transparent materials are either destructive or non-destructive to the optic. Although destructive techniques, such as dimpling[1], microindentation[2], and acid etching[3], provide ways to indicate the amount and depth of sub-surface damage the quality of the measured optic is compromised. Non-destructive techniques are desirable when the surface quality must not be altered.

Some of the non-destructive methods currently used are scatterometry[4], fluorescent confocal microscopy[5], and total internal reflection microscopy (TIRM)[6]. The TIRM method offers a means of quickly assessing the amount of surface and sub-surface damage of transparent optics by utilizing the standing wave characteristics of a s-polarized and p-polarized coherent light source. Figure 1 shows a schematic of the TIRM setup. When illuminating at the critical angle with s-polarized light the first antinode is located at the surface of the optic. Therefore, any defects situated at or near the surface will frustrate the total internal reflection and scatter light into the acceptance cone of the microscope objective. Any scattering sites below the surface at or near antinodal locations will also scatter light out of the surface. When the illuminating beam is switched to p-polarization the first node of the tangential component is at the surface of the optic. The normal component of p-polarized light does not contribute to scattering if the scattering sites are small (depolarization upon scattering does not occur). Since a node is at the surface any defects, such as pits and scratches, that do not extend ~1/10 of the illuminating wavelength below the surface do not scatter light and are therefore not observable[6]. Again, any defects below the surface in the neighborhood of an antinode will scatter light.

The ability of TIRM to locate sub-surface defects is shown in Figures 2 and 3. The depth of focus is 1.2 μm for each micrograph. Figure 2 is a micrograph focussed on the surface of the optic illuminated by s-polarization, and Figure 3 is a p-polarized illuminated micrograph focussed on the same site 3 μm below the surface.

The TIRM technique has been employed as an in-process diagnostic to monitor thin film growth[7]. The technique has also been used as a quality indicator during the polishing process of transparent optics. Two inch diameter fused silica samples are either optically contacted or epoxied to a six inch diameter fused silica plate. The

epoxy has optical characteristics close to that of fused silica. Periodic inspection of the surface and sub-surface quality of the samples is achieved by placing the backside of the plate on top of the index fluid covered prism surface.

Two improved methods of TIRM are under development. Image processing can provide the ability to subtract known surface features from a TIRM image thereby highlighting the sub-surface features. Utilizing a confocal imaging system can reveal the depth of damage.

References:

[1] L. Dettman, "Estimation of Subsurface Damage Depth By Dimpling", Technical Digest on Science of Optical Finishing, Optical Society of America, Washington, D.C., 1990, vol. 9, pp. 52-56.

[2] R.S. Polvani, C.J. Evans, "Microindention as a Technique for Assessing Subsurface Damage in Optics", 1989 Symposium on Optical Materials for High Power Lasers.

[3] P.P. Hed, D.F. Edwards, and J.B. Davis, "Subsurface Damage in Optical Materials: Origin, Measurement and Removal (Summary)", Optical Fabrication and Testing, Technical Digest Series, Optical Society of America, Washington, D.C., 1988, vol. 13, pp. 14-22.

[4] K.C. Hickman, et. al., "Correlation Between Substrate Preparation Technique and Scatter Observed from Optical Coatings", to appear in Applied Optics, Optical Society of America, Washington, D.C., vol. 32, 1993.

[5] W.E. Smith, et. al., "Non-Destructive Estimation of Subsurface Glass Damage Using Fluorescent Confocal Microscopy", Optical Fabrication and Testing Workshop, Technical Digest Series, Optical Society of America, Washington, D.C., 1992, vol. 24, pp. 148-150.

[6] P.A. Temple, "Total Internal Reflection Microscopy: A Surface Inspection Technique", Applied Optics, Optical Society of America, Washington, D.C., 1 August 1981, vol. 20, no. 15, pp. 2656-2664.

[7] F.L. Williams, et. al., "Observation and Control of Thin-film Defects Using In-situ Total Internal Reflection Microscopy", SPIE vol. 1624, Laser-Induced Damage in Optical Materials: 1991, pp. 256-269.

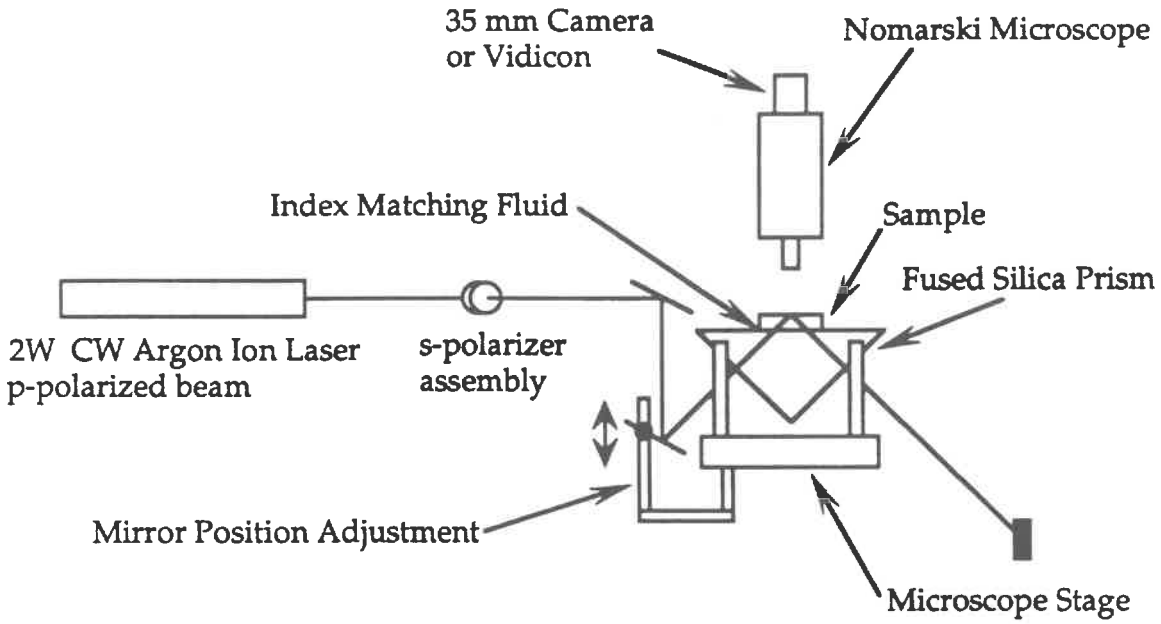

Figure 1. Schematic of Total Internal Reflection Microscopy Apparatus

Figure 2. S-polarized illuminated TIRM of optic surface.

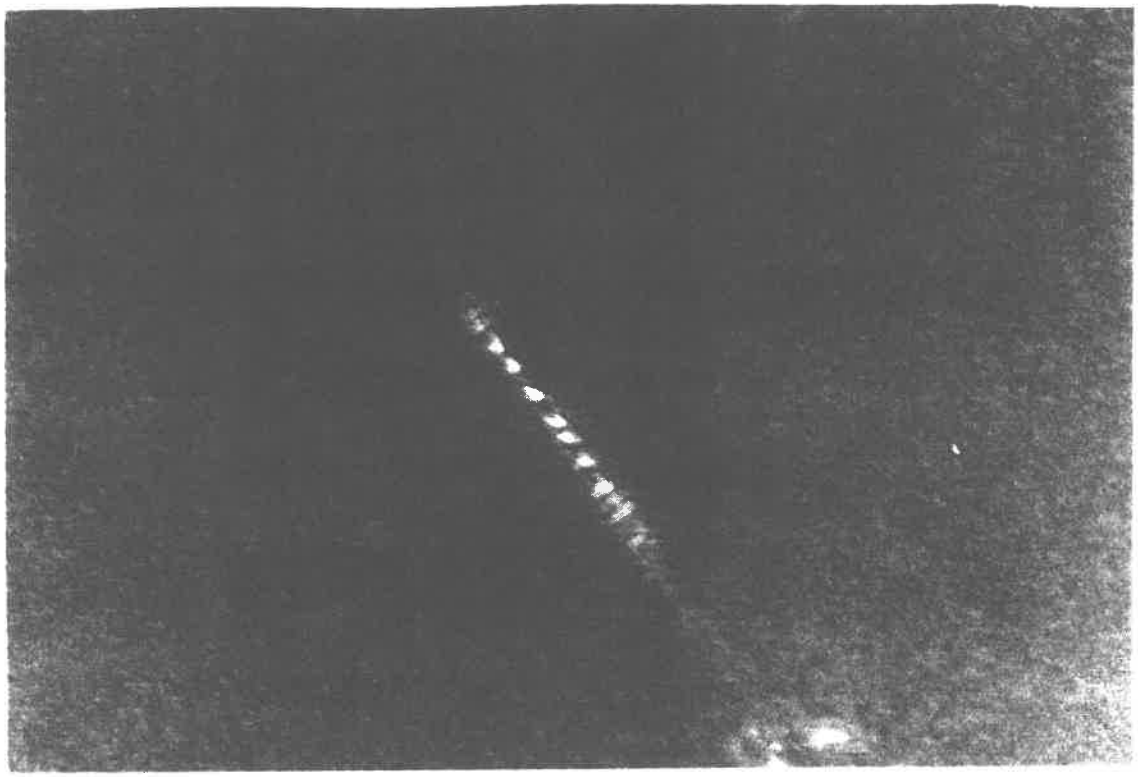

Figure 3. P-polarized illuminated TIRM focussed 3μm below surface.

Deterministic Microgrinding of Spherical Surfaces on Optical Glasses

Donald Golini
Center for Optics Manufacturing
250 East River Road
Rochester, NY 14627-8886

Summary

Over 100 samples of various optical glasses have been deterministically microground with bound diamond metal bonded tools at high spindle velocities and low infeed rates. The Opticam SM, a precision machine tool located at the Center for Optics Manufacturing, served as an exceptionally capable testbed, with tool velocities approaching 15,000 surface feet per minute (30,000 rpm) on a precision airbearing spindle, and infeed rates as slow as 0.1 microns per second. At these feeds and speeds, the geometrical depth of cut is 2Å per tool revolution. A surface roughness of under 75Å and as low as 25Å rms has been achieved on several optical glasses, with figure accuracy as low as $\lambda/5$ peak to valley at 0.6328 microns. These 40 mm radius convex surfaces were produced from plano blanks, with three different grit size grinding tools, in less than ten minutes each. Additional issues to be discussed include machine alignment and radius of curvature accuracy, with particular attention paid to the unique nature of the minor subsurface damage found on surfaces with rms roughness under 100Å.

Background

The grinding geometry on the computer numerical controlled (CNC) Opticam SM uses a bound abrasive cup wheel that is rotated at high speed and tilted at a very precise angle. The lens blank, also rotating, is fed into the tool at a slow constant infeed rate. The cutting edge (circumference) of the ring tool (inner diameter for convex surface and outer diameter for concave surface) must be aligned precisely on the center of rotation of the lens blank to achieve a perfectly spherical surface.

Both the tool and work spindles are Federal Mogul Westwind airbearings. The tool spindle has a dynamic range from 6000 to 30000 rpm, while the maximum work spindle speed is 250 rpm. The linear resolution on both the x and z axes is 0.1 microns, and the slowest allowable infeed rate on the z axis is 0.1 micron per second. The angular accuracy of the B axis is +/- 3.5 arc seconds. These capabilities represent a substantial advance beyond the current machinery available to produce spherical optical surfaces. In particular, they allow extremely high cutting velocities and computer controlled infeed rates not achievable on conventional equipment. Most importantly, the SM is capable of

achieving a geometrical depth of cut per revolution of 2Å when running at a tool spindle speed of 30000 rpm and an infeed rate of 6 microns per minute.

Depth of cut per revolution is a much more meaningful value than tool velocity, since it accounts for both rpm and infeed. It also allows one to discuss constant infeed grinding in terms of critical depth of cut. While tool velocity may play a role, our data suggest that once a "critical velocity" is exceeded, the dominant parameter is depth of cut per revolution, and velocity has only a secondary effect.

Surfaces cut on the Opticam SM were evaluated over a range of spatial frequencies, broadly characterized as: low frequency (spatial features > 6% of full aperture), high frequency (spatial features < 1.5% of full aperture), and mid frequency (spatial features between 1.5% and 6% of full aperture). Each category is attributable to different sources. Surface figure error (deviation from a spherical shape) and radius of curvature error (deviation from an absolute spherical radius) are the two principle low order (global) errors observed in deterministic microgrinding. Surface microstructure, microroughness, and subsurface damage are the high order features that are inspected and evaluated. More difficult to detect and characterize are the low magnitude, mid spatial frequency error components. These are commonly observed in the ring tool geometry, and are referred to as "cutter marks", "rosette", "swirl", "cross", and probably a long list of other names. Each of these surface features will be discussed.

Machine Alignment

When all of the machine components in the ring tool geometry are perfectly aligned, a perfect spherical surface will be produced. Perfect alignment means that the edge of the ring tool passes directly over the center of rotation of the lens (x-axis), and the tool spindle axis (tilted) lies in the same plane as the work spindle axis (y-axis). An error in the x axis results in a radius of curvature error, as well as a cosmetic error (a nub at the center of the lens never gets cut). An error in the y axis (height) produces a toroidal shape instead of a spherical shape, since only half of the ring tool is cutting (figure error). In practice, the likely error in alignment is some combination of x and y displacements, resulting in low order errors.

The Opticam SM has produced lenses with p-v figure error as small as $\lambda/5$ (Zygo MarkIV) and no measurable radius of curvature error (micron spherometer). Nearly half of the surfaces cut on the Opticam have figure error less than 1λ p-v. Displacement errors in x and y as small as 1 or 2 microns will result in measurable figure and radius error. The SM was initially aligned statically with tooling balls and ten thousandth of one inch indicators, but the final true alignment test is to cut parts. The first repeatability test, consisting of 118 lens surfaces, resulted in very predictable machine motions over the course of a work day. Machine movement in x and y produced figure error as low as $\lambda/5$,

and as large as 5λ p-v, which according to initial sensitivity analysis, corresponds to displacements of less than 25 microns. The next task is to engage in controlled studies to measure machine motions with capacitance probes. Sources of system instability to be investigated include thermal differentials across the machine base caused by small changes in coolant temperatures or environmental conditions, thermal spindle growth, and dynamic machine deflections.

Material Dependence

The six glass types cut on the Opticam SM were BK7, K7, SK7, F7, SF7, and KZF6. Although low order error was material independent (purely a function of machine alignment), high order features were solely dependent on material properties. Each sample was inspected using optical profilometry (Zygo Maxim), and an etching/dimpling technique developed at the COM for measuring subsurface damage. SEM and Nomarski microscopy were also used to investigate microstructural features of the glass samples, as well as the grinding tools.

The finishing cuts were done with a 2-4 micron diamond bronze matrix tool at 75 concentration. The finish tool was typically run at 18500 rpm (240 rpm work speed) and 6 microns per minute infeed rate. The geometrical depth of cut per revolution was 3.25Å. The surface microroughness on F7, SF7, and SK7 was consistently under 200Å rms over the entire 40 mm convex spherical surface, with many samples having an rms roughness under 100Å. With a 20x objective in the Mireau mode, the Zygo Maxim evaluates microroughness over a 0.5 mm square area on the surface. These deterministically microground surfaces are specular. The roughness values reported are representative of the entire surface, and not isolated spots. The surface roughness on BK7, K7 and KZF6 was typically about 1500Å rms. The difference in grinding behavior of these six glass types is the subject of further work at the COM.

Subsurface damage is the true measure of grinding performance, as this property (combined with surface figure) defines how much post-grinding work is required. The samples were lightly etched with HF and dimpled to measure subsurface damage. Interestingly, the SSD depth did not vary significantly with glass type or grinding mode. The average damage depth for all six glass types was under 3 microns. The significant difference in SSD was not depth, but spatial distribution or density of damage. The glasses that ground in a predominantly brittle regime had a very high distribution of damage sites, while the very smooth surfaces had a much lower distribution of damage. On a 55Å rms surface, for example, there are very few damage sites with a depth of about 1 micron. This is encouraging because it indicates the potential to eliminate all damage with process improvements. From a process standpoint, however, it may take longer to polish through this infrequent damage than it would to polish out a surface with orders of

Indentation tests were conducted on instruments with ranges from 25 to 1000g and 1 to 20g. Figure 1 shows the relationship between the indenter load and ratio of measured resultant plastic-to-elastic deformation calculated from the indenter shape. The latter is around 1.4%, an extremely small value compared with 30-60% for glasses and 80% for aluminium (see Schinker and Doll[2]) indicating the material to be both highly elastic and brittle.

No fracture was observed at loads less than 100g. Puttick et al[1] showed the critical depth of cut for brittle fracture to be

$$d_c = aER/Y^2,$$

where
E = Young's modulus,
R = specific work per unit area,
Y = yield stress for plastic flow,
a = a numerical parameter,

from which the critical depth d_c for glassy carbon is of the order of 10nm.

3 Single-point Machining

A high-stiffness diamond turning machine[1] was used for single-point machining tests employing a chisel single-crystal diamond tool, truncated with a 1um land. Cutting speeds between 1.8 and 43m/minute and cut-depths from 0 to 0.7um were used.

Figure 2 Talystep Trace of Ductile Groove Profiles

Figure 2 shows profiles of parallel grooves measured with a Talystep (0.1um stylus). These indicate cut-depths of 40-60nm including 'shoulder' pile-up, and cut-width of 1um, (the width of the tool). Brittle fracture, observed on occasion, indicated the critical depth was perhaps less than 60nm. However the indenter tests suggest that, to obtain this order of cut-depth, the tool depth was probably much larger.

4 Retained-abrasive Wheel Grinding

Grinding trials were conducted on an ultra-precision CNC grinding machine[3] built by Cranfield Unit for Precision Engineering. Samples were ground using a cup/annular cast-iron bonded wheel with electrolytic in-process dressing (ELID)[4,5]. The ranges of conditions are shown in Table 1.

Table 1 Grinding Parameters Used

Wheel Speed (m/min)	1180
Depth of Cut (um)	0.5, 1, 3
Cross-feed Rate (um/rev)	2, 6

Samples were examined using the Nomarski, Wyko TOPO-3D and scanning electron microscopes and Rank Taylor Hobson Talystep. Figure 3 shows the relationship between surface roughness (R_a) and cross-feed rate. At the smaller feed-rate of 2um/rev, good finish (4-7nm R_a) was achieved but, at the higher rate of 6um/rev, the roughness was increased (to 12-13nm R_a).

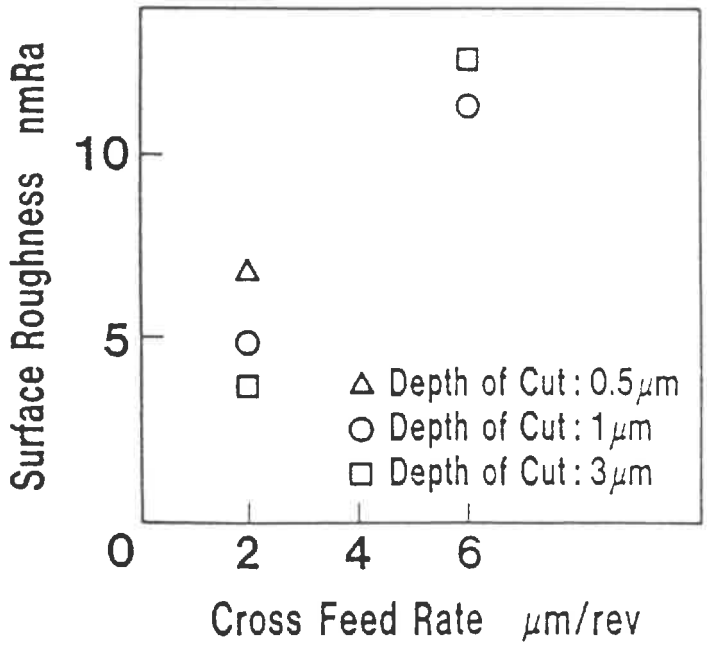

Figure 3 Surface Roughness vs Cross-feed Rate per Revolution (grinding)

5 Conclusions

In glassy carbon, the unusually high elasticity compared with its plastic deformation is apparent from microindentation investigations. However single-point machining and multipoint grinding investigations indicated that it is possible to employ each in the plastic regime.

6 Acknowledgements

Support from Kobe Steel Co, Kobe, Japan, is gratefully acknowledged in respect of a sabbatical year spent by one of us (YH) with the School of Industrial and Manufacturing Science, Cranfield Institute of Technology, UK.

The use of a diamond turning test facility operated at Cranfield with the collaboration of Prof K E Puttick of the University of Surrey, Guildford, UK, is also gratefully acknowledged.

7 References

1 Puttick K E, Rudman M R, Smith K J, Franks A and Lindsey K "Single Point Diamond Machining of Glasses" Proc Roy Soc A **426** 19-30 (1989)
2 Schinker M G and Doll W "Turning of Optical Glasses at Room Temperature" Proc SPIE **802** 70-80 (1987)
3 McKeown P A, Carlisle K, Shore P and Read R F J "Ultra-precision, High Stiffness CNC Grinding Machines for Ductile Mode Grinding of Brittle Materials" Proc SPIE **1320** 301-313 (1990)
4 Ohmori H, Takahashi I and Nakagawa T, "Mirror Surface Grinding by Metal Bonded Super-abrasive Wheel with Electrolytic In-process Dressing" in Seyfreid P, Kunzmann H, McKeown P and Weck M (eds) *Progress in Precision Engineering*, Springer, Berlin, 1991 (Proc IPES7 Conference, Braunschweig, Germany, May 1991) pp153-165
5 Ball M J, Murphy N and Shore P "Electrolytically Assisted 'Ductile' Mode Diamond Grinding of BK7 and SF10 Optical Glasses" Proc SPIE **1573** 30-39 (1991)

Change of Depth of Cut and Damage on Ground Surfaces in Shear Mode Grinding

K. Imai* and H. Hashimoto#

Previous papers[1-3] reported shear mode grinding of BK7 glass using 3000 grit bronze bond diamond wheels. In those experiments the depth of cut was 2 μm, the cross feed rate 150 mm/min, and the material removal rate 0.9 mm^3/min. Forces, work and wheel roughness were monitored while repeat passes were made across the work piece. It was shown that:

* After a number of passes, the normal grinding force reached an approximate steady state;

* During grinding, the wheel surface roughness and cutting performance were invariant; wheel truing and dressing were not carried out;

* Surfaces characteristic of shear mode grinding, ie without pits and fractures, were produced.

* When the feed stock for shear mode grinding was produced by conventional grinding (ie accompanied by brittle fracture), ductile surfaces were produced provided the grinding allowance (ie total stock removed) was 4-5 times the maximum roughness of the preworked surfaces.

Generally, the maximum roughness of the feed stock surfaces (brittle mode surfaces) was about 2 μm, and hence 10 μm must be removed to produce a ductile surface. The results summarized above were those obtained with a depth of cut of 2 μm. Higher productivity will be obtained if shear mode grinding is possible with a larger depth of cut. This paper reports results of experiments in which only the depth of cut was changed. Grinding forces, wheel surface finish, and work piece surface quality are reported.

Experimental method

The surface grinding machine shown schematically in Fig. 1 was used for the experiments. A 4 mm wide bronze bonded 3000 grit diamond wheel was used to

---

* Graduate School, Kanagawa Institute of Technology

Faculty of Engineering, Kanagawa Institute of Technology

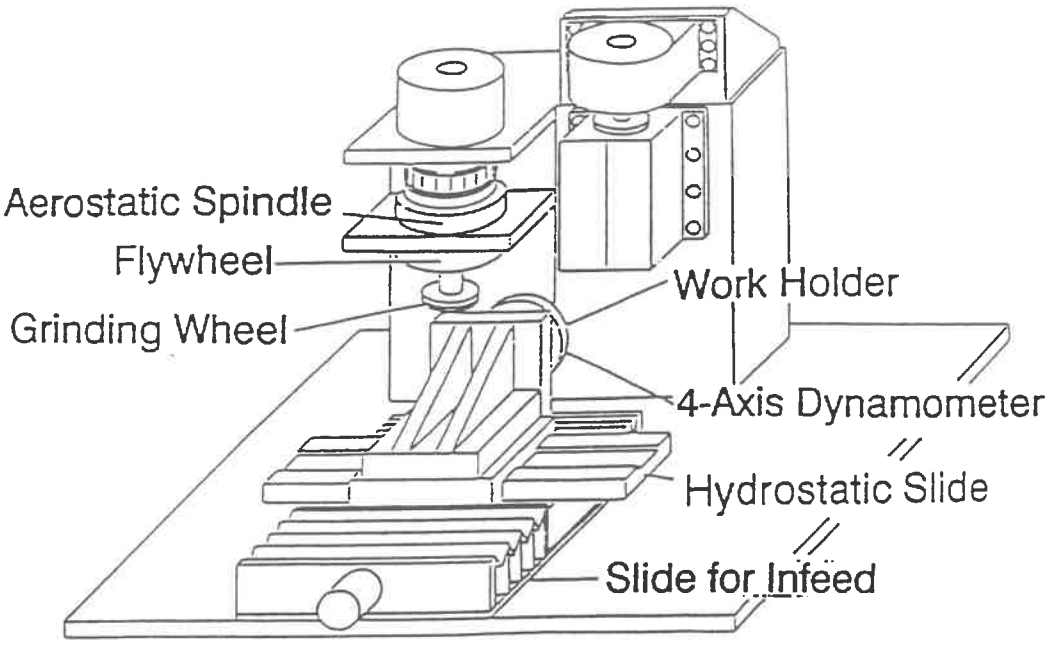

Fig.1 Schematic Drawing of Grinding Machine

Table.1 Experimental conditions

Grinding Wheel	#3000 Metal-bond diamond wheel SD 3000 J75 MB [w4mm ⌀100mm]
Wheel revolution	1500 rpm [7.9 m/sec]
Slide velocity	150 mm/min
Depth of cut	2,6,10,12 um
Specimen	BK7 Glass [w 3x l 50 x t 4]
Grinding Fluid	AL-1 [Yushiro co.]
Static stiffness	8.3 N/um

grind 50 mm long, 3 mm wide samples of the optical glass BK7; an oil based grinding fluid* was used. Wheel speed was 1500 rpm and cross feed rate 150 mm/min. The depth of cut was set up at 2, 6, 10, and 12 μm, (giving stock removal rates of 0.6, 1.8, 3 and 3.6 mm^3/min) and the number of cuts (ie passes across the sample) was 200. The wheel had been previously used in a grinding experiment with more than 500 passes at a depth of cut of 2 μm after truing, and was used in this experiment without further truing and dressing. Grinding forces were measured using a four-axis quartz piezoelectric measuring instrument (Type 9273 made by Kistler Co). Roughness measurements were made using a Surtronic 3P made by Rank Taylor Hobson Co.

Results were evaluated in terms of:

* Variation of normal grinding force
* Variation of the ratio (Ft/Fn) of tangential grinding force (Ft) to normal grinding force (Fn)
* Change in the roughness of the wheel surface. This was measured at eight points on the wheel surface and the mean value of six values except the largest and the smallest values was taken.
* Roughness of the ground surfaces, measured at ten points in the direction perpendicular to the grinding direction.
* Observation of surface damage on the ground surfaces, once normal forces had reached steady state. Samples were etched in an aqueous solution of hydrogen fluoride containing 1.0% HF and 0.5% HCl for 10 min.

Experimental results

Variation of normal grinding force

Change in normal grinding force with depth of cut (up to 10 μm) is shown in Fig. 2. In each case, after an initial period of increasing force, the normal grinding force reaches a relatively steady state. In these conditions the nominal and actual depth of cut are equal. Compliance of this machine is 0.12 μm/N. After spark-out, there is an exponential decrease in normal force in every case. The variation of these normal grinding forces agreed with the results of shear mode grinding at a depth of cut of 2 μm previously reported.

The variation of normal grinding force when the depth of cut was further increased to 12 μm is shown in Fig 3. Clearly, the behavior is different from the variation at depths of cut up to 10 μm. Initially, the behavior is consistent with the results at lower depths of cut; after approximately 5 passes, the normal grinding force begins to level out at a steady state value, but after about 10 passes it starts to increase linearly, reaching 200 N at 16th cut. Grinding was almost impossible under these conditions and grinding burn on the surface occurs.

---

* AL-1 made by Yushiro Kagaku Co.

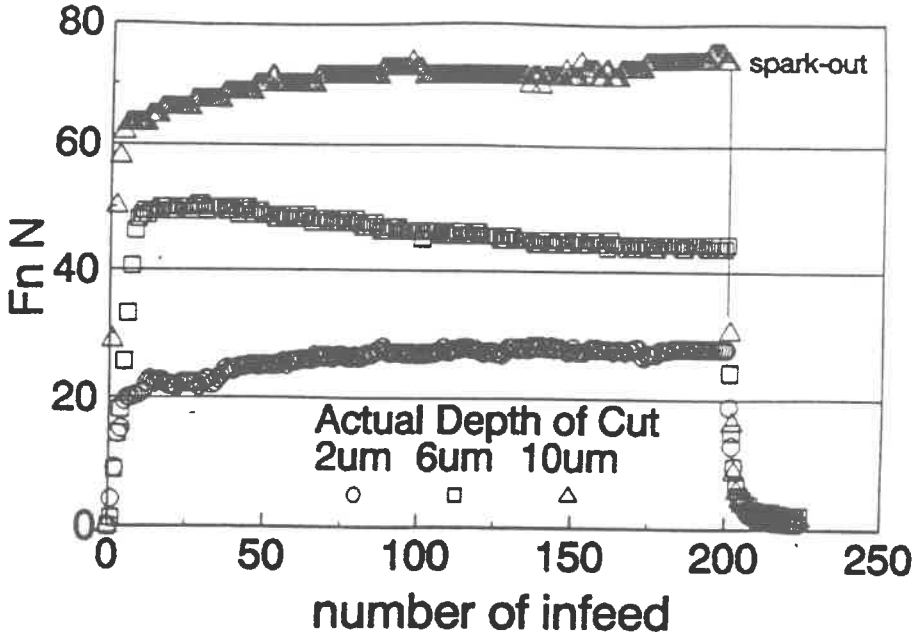

Fig.2 Normal grinding force versus the number of incremental infeeds

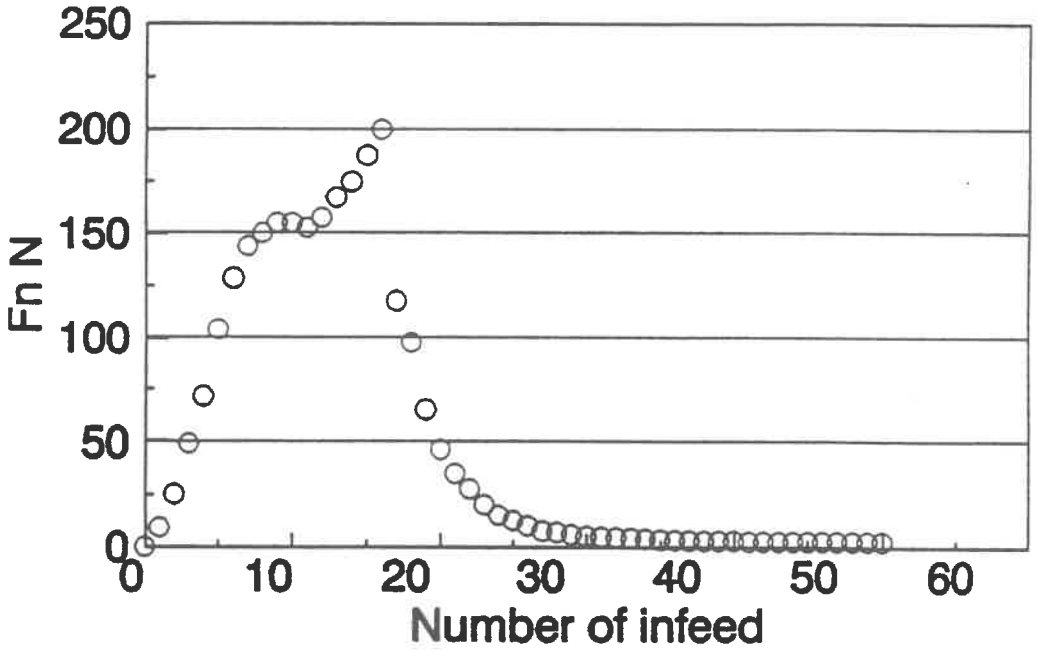

Fig.3 Normal Grinding Force versus number of incremental infeeds [Depth of cut 12um]

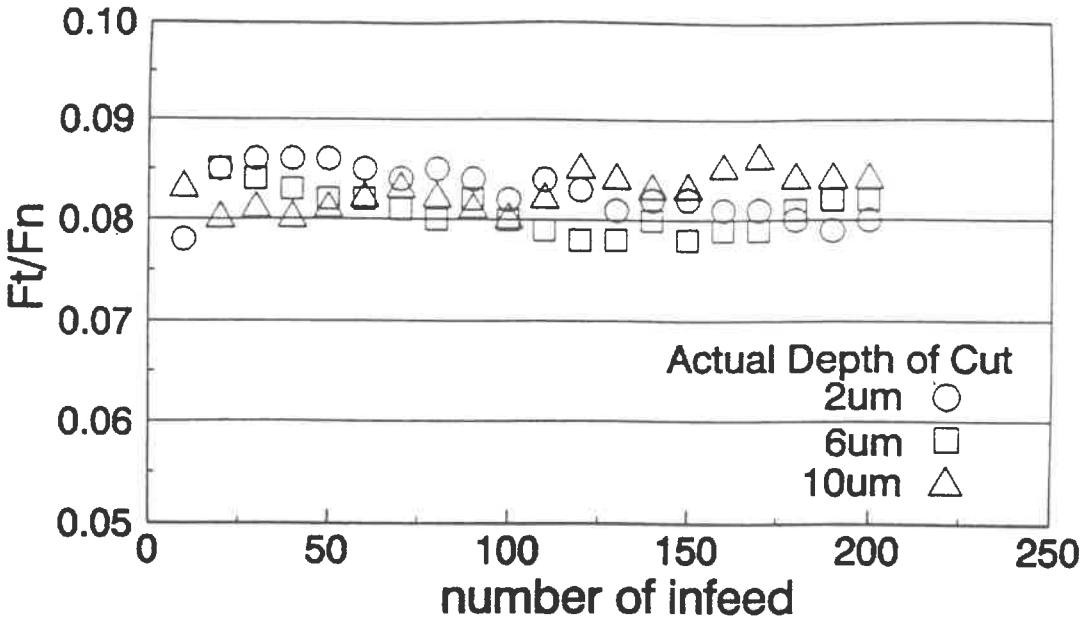

Fig.4 Ft/Fn ratio versus number of incremental infeeds

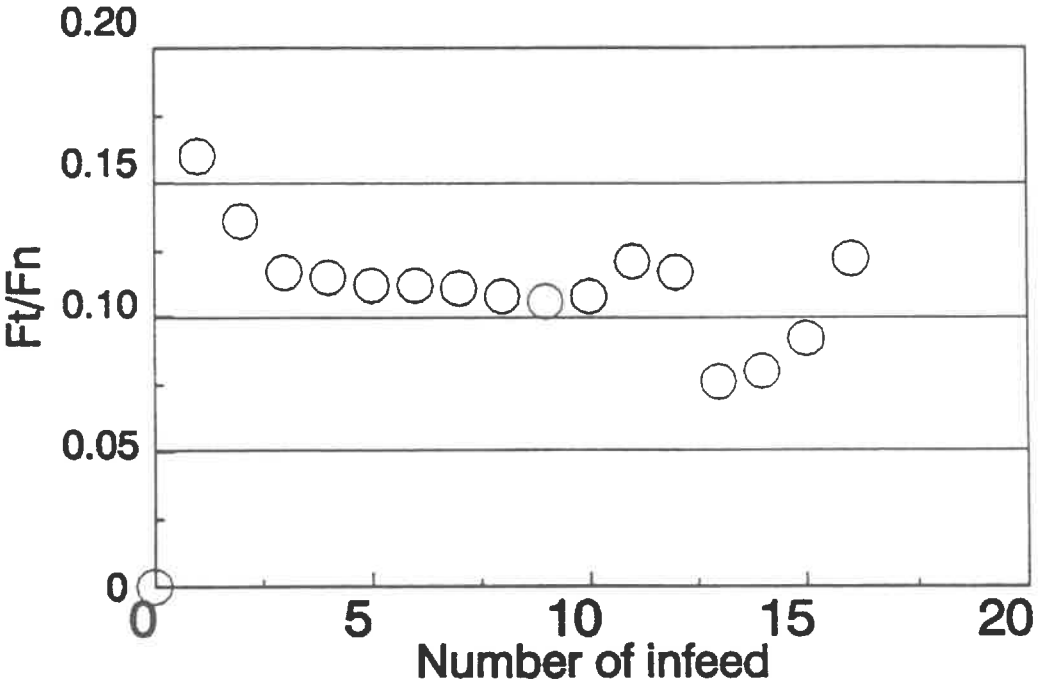

Fig.5 Ft/Fn Ratio [Depth of Cut 12um]

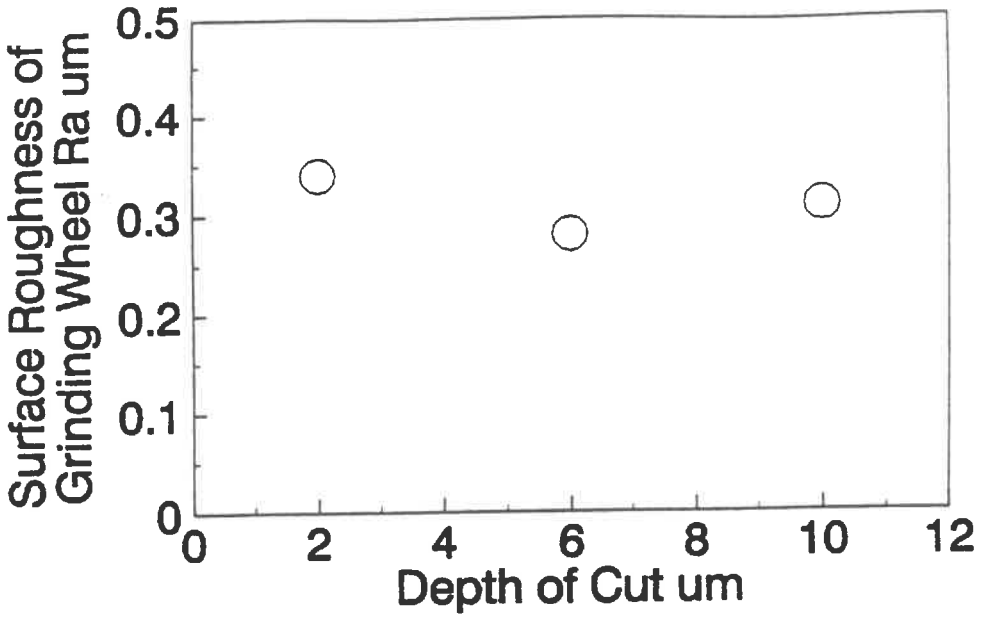

Fig.6 Change in surface roughness of grinding wheel with change in depth of cut

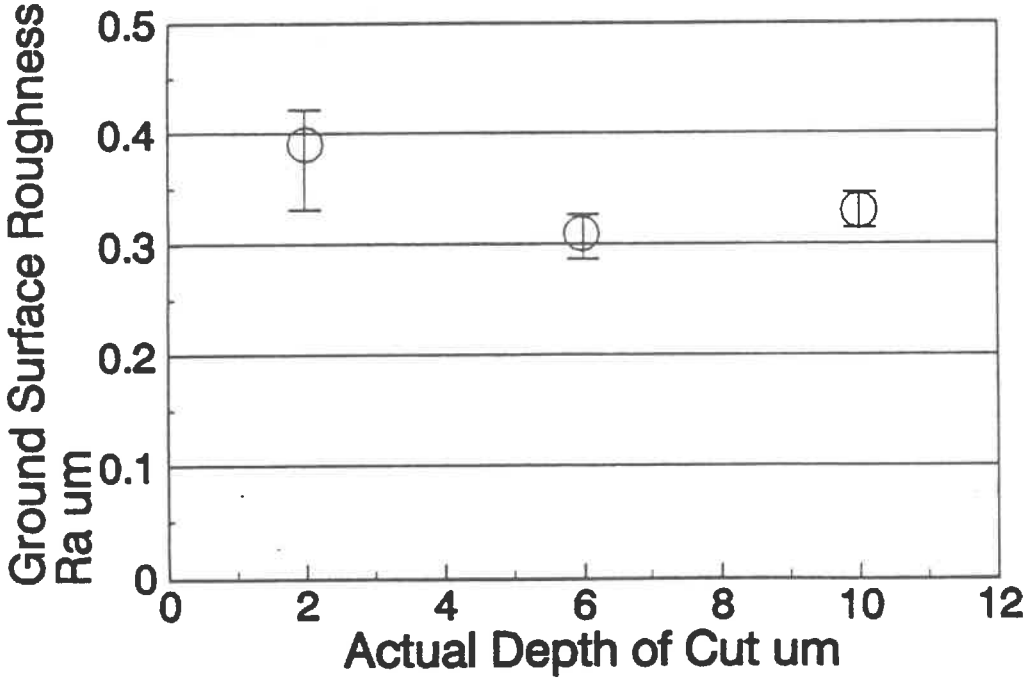

Fig.7 Change in ground surface roughness with change in actual depth of cut

Variation of the ratio of tangential to normal grinding forces

Values of Ft/Fn with depths of cut of 2, 6, and 10 μm are shown in Fig. 4. In every case Ft/Fn is constant at approximately 0.08. By contrast, the values of Ft/Fn when for 12 μm depth of cut are shown in Fig. 5. Initially high values drop to 0.11-0.12 for the next 12 passes, decreased to 0.08 in 13th-15th cuts, and then suddenly increased at 16th cut, and reached 0.12. Presumably this sudden increase correlates with the initiation of burning on the ground surface.

The results given above show that in every grinding experiment at 2, 6, and 10 μm depths of cut, normal grinding forces reached a steady state and, during this period, the values of Ft/Fn were also constant. This suggests that the total area of wear on the flanks of abrasive grains become constant, as does the cutting performance of the wheel.

Wheel surface roughness

Change in the roughness of the wheel surface after the grinding experiments is shown in Fig. 6. The roughness of the wheel surface in the experiment with 2 μm depth was between 0.28-0.34 μm Ra, and when normal grinding force was in the steady state, the roughness did not increase, independent of the number of cuts. At 12 μm depth of cut the roughness increased to the values as large as 0.67 μm Ra.

Roughness of the ground surfaces

The roughness of the surfaces ground at depths of cut of 2, 6, and 10 μm is shown in Fig. 7. The roughness is 0.3-0.4 μm Ra, approximately the same as that of the wheel, and invariant. The surface ground with a 12 μm depth of cut showed cracks and had a higher surface roughness.

Damage on the ground surfaces

The ground surfaces obtained when normal grinding force was in the steady state with depths of cut of 2, 6, and 10 μm are shown in Fig. 8(a). Clearly these are "shear mode" surfaces on which few small pits and other defects can be found. The results of etching the ground surfaces shown in Fig. 8(a) are given in Fig. 8(b). No pits or other defects were revealed by etching.

The surface obtained by grinding with a 12 μm depth of cut (Fig. 9) was clearly different from the surfaces obtained with lower depths of cut. Burn marks and cracks are found in the ground surface.

In summary, in grinding experiments at depths of cut of 2 μm, 6 μm, and 10 μm, when normal grinding force was in the steady state, the roughness of the wheel surface did not change with increasing number of cuts. The ground surfaces are clearly generated in the shear mode, and no pits or sub-surface damage were revealed

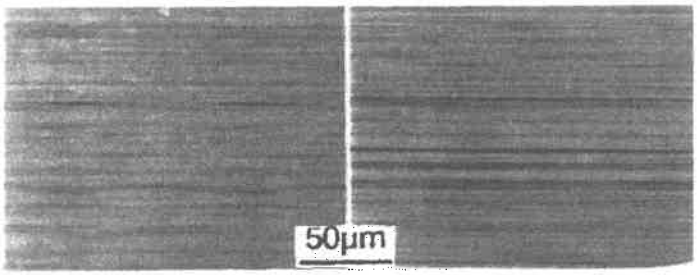

(a)Ground surface [2um] (b)Etched surface

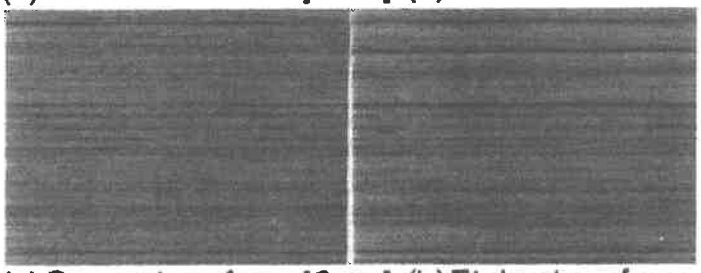

(a)Ground surface [6um] (b)Etched surface

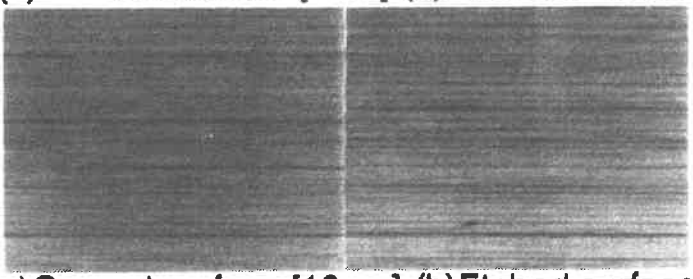

(a)Ground surface [10um] (b)Etched surface

Fig.8 Ground surface of BK7 glass

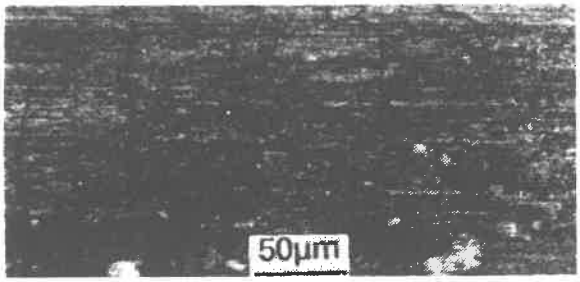

Fig.9 Ground surface of BK7 glass [12um]

by etching. At a depth of cut of 12 μm, the ground surfaces showed burning which leads to cracks.

Conclusions

1. When the depth of cut was set up at 2, 6, and 10 μm, normal grinding force reaches a steady state and, in that state, the actual depth of cut was equal to the set depth of cut. During this period, the values of Ft/Fn was constant at 0.08 independent of the number of cuts. From these facts, it is presumed that the total sum of the areas of wear on the flanks of abrasive grains of the wheel is constant, and also the "cutting quality" is almost constant.
2. The grinding experiment was carried out at depths of cut of 2, 6, and 10 μm without truing and dressing the wheel; 200 cuts were taken. Shear mode surfaces were generated with no defects such as pits etc. Furthermore, no pits were revealed by etching.
3. At the set-up depth of cut of 12 μm, normal grinding force never reached a consistent steady state, and cracks caused by burning appeared on the ground surfaces; therefore grinding was impossible.

The goal of this work was to increase shear mode grinding efficiency by grinding at larger depths of cut. It has been shown that the depth of cut can be increased up to 10 μm (cross feed rate-150 mm/min; wheel speed-1500 rpm) and defect free ground surfaces can still be obtained in BK7.

Acknowledgements

The authors acknowledge to assistance of C. Evans (NIST, USA) in preparing this manuscript.

References

1. H. Hashimoto and J. Takeda: "Shear-mode grinding and ground surface evaluation" The Proceedings of Symposium, JSPE spring meeting, (1991) 36.
2. H. Hashimoto, K. Imari, and K. Blaedel: "Shear-mode grinding to remove residual damage from brittle-mode grinding" The proceedings of OSA, Optical Fabrication & Testing Workshop, Boston, MA, (1992) 126.
3. J. Takeda, K. Imari, and H. Hashimoto: "Shear-mode Grinding of BK7 Glass and Evaluating Ground Surfaces", The Proceedings of ASPE, Santa Fe, (1991) 132.

BRITTLE/DUCTILE GRINDING OF SOFT BASALT CERAMIC

Ioan D. Marinescu, John A. Webster
Center for Grinding Research and Development
University of Connecticut, Storrs, CT 06269-5119

1. Introduction

Natural basalt is an effusive volcanic rock, dark gray to black in color, made up of alkaline plagioclases and ferromagnetic minerals. The hardness of basalt is high and its deformation resistance to compressional stress is also high (1). The technology for sintered "man-made" basalt ceramics was established a few years ago, enabling parts to be produced with a homogenous structure, without cleavages and with good surface quality (1).

2. Experimental

A surface grinder, type Rubin 026 VA II (ELB Schliff) was equipped with instrumentation for measuring the grinding forces, vibration, velocities, diamond wheel wear and consumed energy during the wet grinding of the basalt ceramic.

If grinding is considered as a tribological process, the wear of the workpiece is considered as a desirable mechanism which can be represented by the volume of material removed, by stock removal rate, or by equivalent chip thickness (2). The wear of the grinding wheel is an undesirable mechanism which determines the wheel life, and can be represented by the volume of active abrasive layer worn away. The grinding ratio (G) can be employed to give an indication of wheel life.

From the viewpoint of the chip removal mechanism observed it is obvious that the basalt ceramic is a brittle material. In the case of brittle materials (ceramics, glasses, etc.) the plastic deformation is almost zero. Since the chip removal mechanism is due to elastic microshocks an important process parameter is downfeed. The correlations between downfeed, work speed, specific energy and wheel speed will result in a brittle/ductile regime.

3. Test results

A major problem with basalt ceramic grinding is obtaining the best quality of surface. From Figs. 1 and 2 it can be seen that the value of roughness average (R_a) is a linear function of the equivalent chip thickness (h_{eq}). The slopes of the curves for the two bonds in Figs. 1 and 2 are approximately equal. Using the method presented in the paper (2) it is possible to establish some polytropic relationships for the main technological parameters using h_{eq}. For example, the surface roughness of surface ground basalt ceramic can be obtained by:

$$(1) \quad R_a = 2.761 \cdot h_{eq}^{0.283} \ [\mu m] \qquad (2) \quad R_a = 2.069 \cdot h_{eq}^{0.274} \ [\mu m]$$

(1) for diamond wheels with metal bond
(2) for diamond wheels with resin bond

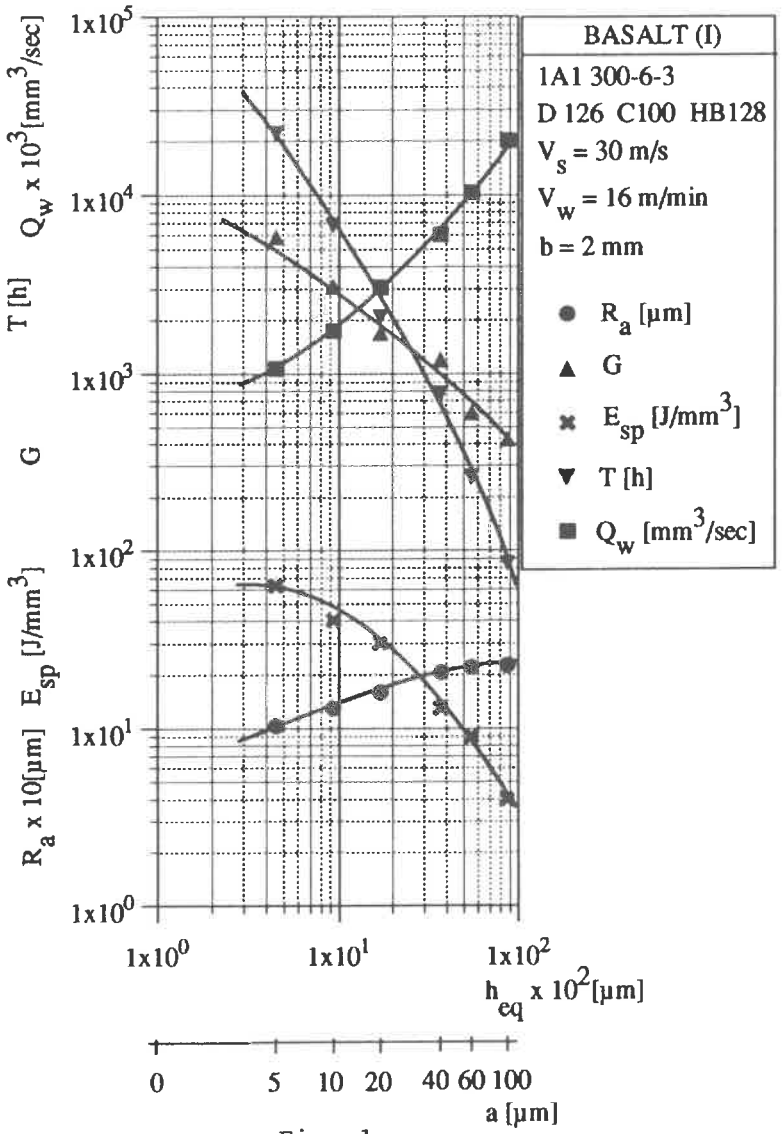
BASALT (I)
1A1 300-6-3
D 126 C100 HB128
V_s = 30 m/s
V_w = 16 m/min
b = 2 mm
R_a [µm]
G
E_{sp} [J/mm^3]
T [h]
Q_w [mm^3/sec]
Q_w x 10^3[mm^3/sec]
T [h]
G
E_{sp} [J/mm^3]
R_a x 10[µm]
1x10^5
1x10^4
1x10^3
1x10^2
1x10^1
1x10^0
1x10^0
1x10^1
1x10^2
h_{eq} x 10^2[µm]
0 5 10 20 40 60 100
a [µm]

Fig. 1

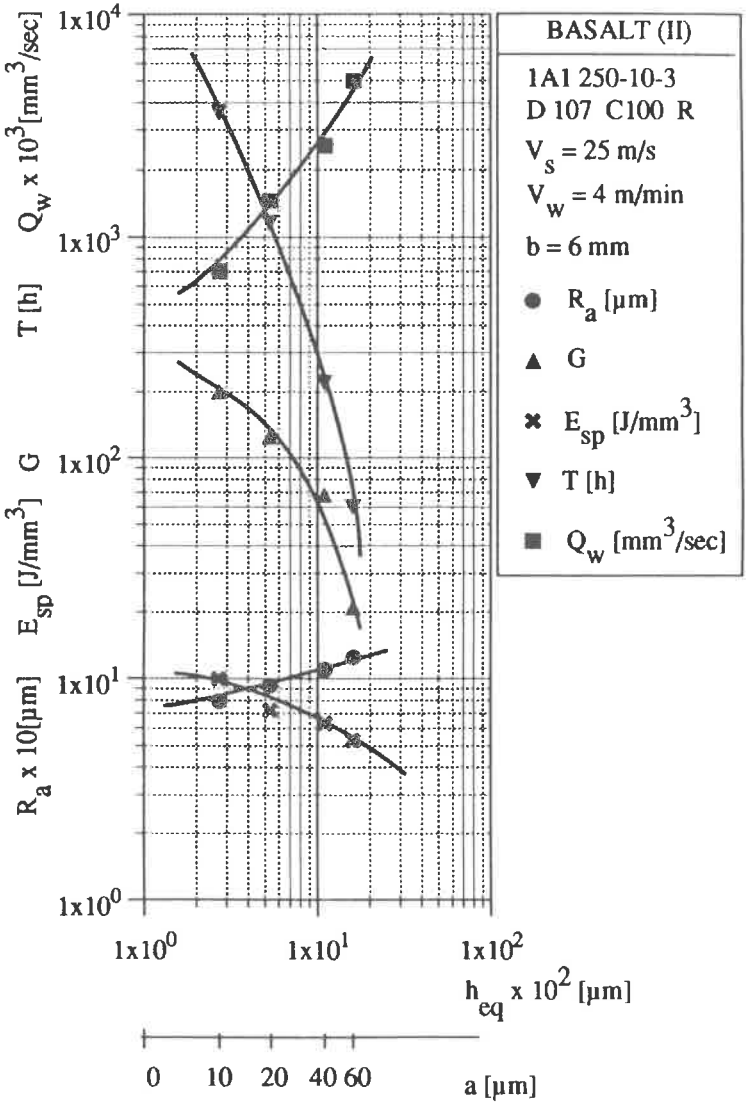
BASALT (II)
1A1 250-10-3
D 107 C100 R
V_s = 25 m/s
V_w = 4 m/min
b = 6 mm
R_a [µm]
G
E_{sp} [J/mm^3]
T [h]
Q_w [mm^3/sec]
Q_w x 10^3[mm^3/sec]
T [h]
G
E_{sp} [J/mm^3]
R_a x 10[µm]
1x10^4
1x10^3
1x10^2
1x10^1
1x10^0
1x10^0
1x10^1
1x10^2
h_{eq} x 10^2 [µm]
0 10 20 40 60
a [µm]

Fig. 2

From Figs. 1 and 2 it can be seen that resin bond wheels give a smaller roughness as compared to metal bond, for the same grinding conditions. Resin bond is, therefore, desirable for the finishing of basalt ceramic parts. Conversely, metal bond grinding wheels are preferable for the roughing stage(3).

From the viewpoint of brittle/ductile regime we can say that in the case of rough grinding the brittle regime occurs when $h_{eq} \geq 0.35\mu m$. This result confirms similar studies (4) that specific energy is larger in the case of ductile regime grinding than in the case of brittle regime grinding.

The same phenomena occurs for fine grinding since the transition point occurs when $h_{eq} \leq 0.05\mu m$. Beyond this value the brittle regime occurs and the specific energy decreases.

The philosophy of using the brittle regime for rough grinding with a metal bond diamond wheel is good for the productivity of the process. For finish grinding a ductile regime is necessary using resin bond diamond wheels, providing the brittle damage can be removed during this stage.

The limiting factor of grinding process productivity (Q_w) is the abrasivity of the basalt ceramic surface (see Fig. 3a and 4a). SEM analysis has shown that material is removed more by fracture and loosening, than by microcutting (Fig.3b). The main wheel wear mechanism of the active composite layer (diamond + bond) is by abrasion (Fig. 3c, d ,e, and 4b, c), combined with fatigue wear of the extra hard grains, resulting from cyclic compressional stresses (Fig. 3f and 4d). The positive effect of the abrasivity of basalt ceramic is the selfdressing of the diamond grains which occurs (Fig.3c, d, e and 4b).

Finally, it is necessary to mention the low energy consumption during grinding of this soft ceramic, with both types of bond. The specific energy E_{sp} decreases slowly with increasing downfeed (a) and upon entering the brittle regime mode of cutting.

CONCLUSIONS

Taking into account the technological and economical aspects for optimum grinding of basalt ceramic with diamond wheels, rough grinding and finishing grinding conditions are recommended.

Utilization of equivalent chip thickness (h_{eq}) to represent the main technological parameters in double logarithmic coordinates permits the optimization of the grinding process by computer.

REFERENCES

1. Marinescu, I.D.,Bouas, D., Some Aspects Concerning the Grinding of Basalt, Proc. 4th International Grinding Conference, October 9-11, 1990, Dearborn.
2. Marinescu, I.D., Dimitrov, B., Gheorghiu, Z., Grigorescu, A., Some Aspects Concerning Wear and Tool Life of Diamond Wheels, Annals of the CIRP, 32 (1983), nr.1.
3. Marinescu,I.D., Webster, A.J., Tribo-Technological Aspects of Ceramic Diamond Grinding. Submitted to ASME for 1993 Winter Annual Meeting.
4. Bifano, T.G., Dow, T.A., Scattergood, R.O., Ductile Regime Grinding: A New Technology for Machining Brittle Materials, Jour. of Eng. for Ind., vol. 113, May 1991.

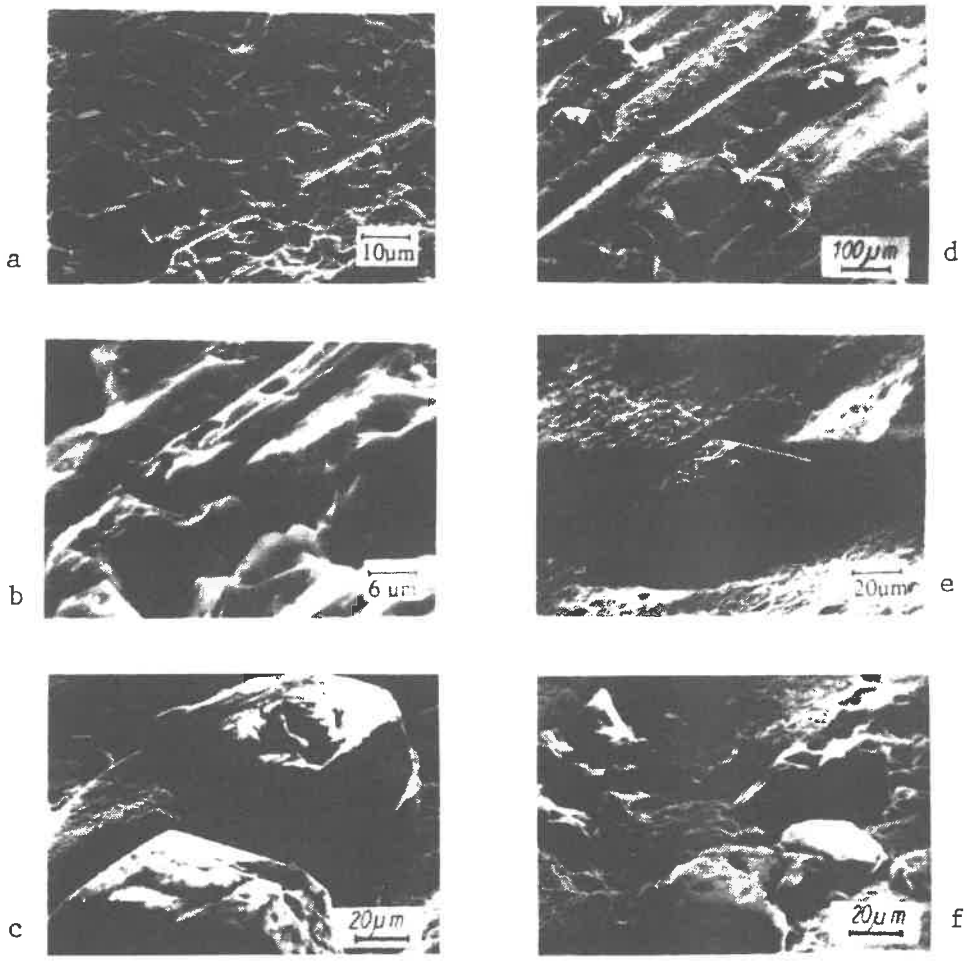

Fig. 3

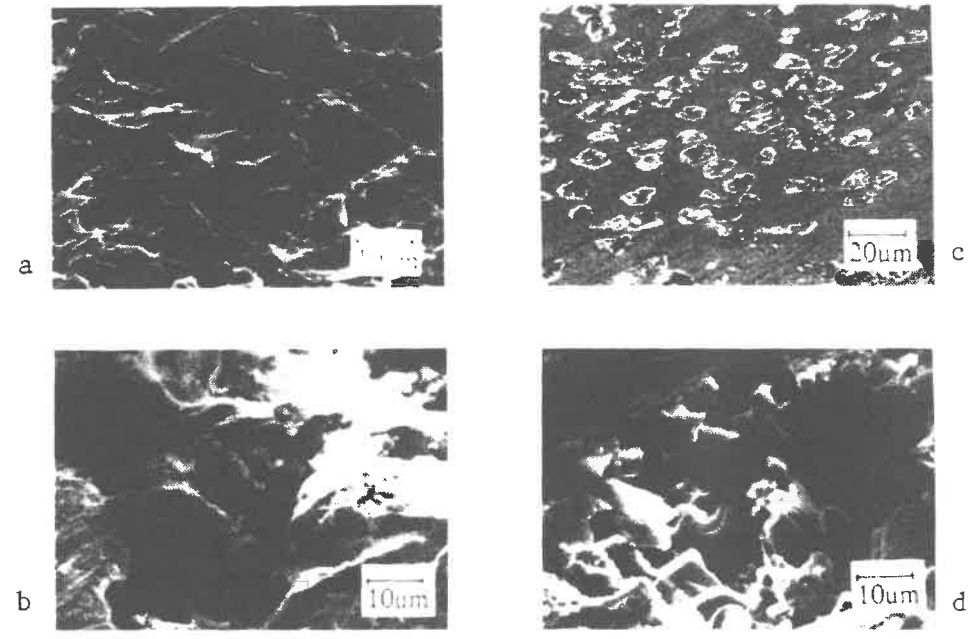

Fig. 4

Chemomechanical Effects in Ductile-Regime Machining of Glass[1]

Thomas G. Bifano
Robert Annear
Precision Engineering Research Laboratory, Boston University, Boston, MA

Donald Golini
Center for Optical Manufacturing, University of Rochester, Rochester, NY

Introduction

It has been demonstrated that brittle materials (glasses, semiconductors, and ceramics) can be ground without inducing fracture damage. Abrasive grain cutting depths less than 50 nanometers are generally required, in a process called ductile-regime grinding [1-5]. Such ultra-precision machining processes, capable of material removal at the scale of nanometers, consist primarily of interactions between *surface* layers of tool and substrate. Although it has been clear since the early development of ductile-regime grinding models that chemomechanical effects can substantially alter grinding processes, to date no basic research has been directed toward an understanding of such effects in bound-abrasive ductile-regime grinding [6]. Chemomechanical effects in small-grain *loose-abrasive* grinding have recently been the subject of a study, in which it was found that damage levels and material removal rate were both influenced by coolant chemistry [7-9]. In this paper, we will describe some empirical results in scratching and micro-grinding of glass in various liquid environments. It will be shown that a possible cause of differences in damage levels when grinding in different environments is ionic adsorption at the surface of the glass, and that electrokinetic measurement of ζ-potential for the glass and liquid environment can be correlated with this effect.

In a study of Rebinder effects [10] in rock drilling, Westwood and others at Martin Marietta examined the influence of various liquids on the hardness and wear resistance of brittle solids [11-17].Their overall conclusion: The surface hardness of a brittle material is maximized when the measured zeta potential (ζ) is zero. The ζ-potential is a parameter of a given liquid-solid interface, describing the voltage existing at the shear plane in the electrolytic liquid double-layer near the surface of the solid. When a solid and a liquid come into contact, the surface of the solid may become charged due to adsorption of ions from the solution. At equilibrium, this *surface charge*, σ, must be balanced by an opposite charge in the solution. ζ-potential is one measure of the charge in the solution: specifically, it is the potential measured at the shear plane in the boundary layer of the solution when the solution is forced to flow past the solid surface.

The dependence of surface properties on ζ-potential has been verified by direct measurement for various crystalline and amorphous solids [11-22]. Again, the primary emphasis of these studies was to improve the efficiency of rock drilling. It was found that ζ-potential could also be correlated to machining efficiency. For impact-drilling of very hard solids with multipoint diamond bits, it was found that environments exhibiting a smaller ζ-potential magnitude resulted in increased drilling efficiency. for finer-scale diamond machining, the opposite correlation was observed: environments exhibiting a smaller ζ-potential magnitude resulted in decreased machining efficiency. Machining efficiency is quantita-

[1] An expanded version of this paper will appear in *Precision Engineering: The Journal of the American Society for Precision Engineering*

tively measured as the *specific machining energy*, the energy input per unit volume of material removed. In constant-force machining, increased efficiency translates into increased material-removal rate. In constant-rate machining, increased efficiency translates into lower machining forces. An exact physical interpretation of the correlation between zero ζ-potential and machining efficiency has yet to be established. It is known, however, that a non-zero ζ-potential affects the adsorption of liquid ions by the solid. Michalske and Bunker [23] recently described some relevant details concerning the chemistry of dissociative adsorption and its influence on fracture in glass, but they did not address electrokinetic effects such as the ζ-potential.

Environmental Effects in Microgrinding

It will be shown in this paper that in *microgrinding* of glass, the lowest machining efficiency correlates with minima in the absolute value of the ζ-potential. Environments composed of one of a homologous series of alcohols or water have been used in glass scratching and glass grinding to demonstrate that reduced machining efficiency in the presence of particular coolant environments is the direct result of a chemomechanically-assisted transition from brittle-regime grinding to ductile-regime grinding. Two important consequences of the brittle-ductile transition accompanying reduced machining efficiency are improved surface finish and reduced sub-surface damage level. The reduction in subsurface damage is a critical chemomechanical effect in glass microgrinding, since removal of subsurface damage is the most time consuming and expensive process in the manufacture of optical components from glass [3]. Based on experimental observations and the ductile-regime grinding model previously reported [1], we conclude that an important chemomechanical effect accompanying the condition of $\zeta \sim 0$ is an increase in *fracture resistance* in the chemically modified surface layer of the glass.

Experimental Observations of Chemomechanical Effects in Scratching and Grinding

To establish a relationship between chemomechanical environment and material-removal processes in micro-grinding, a series of controlled scratching and fixed-abrasive grinding tests were performed on ULE glass (Corning code 7971 titanium silicate low expansion glass). ULE glass was also used in a recent study of chemomechanical effects in loose-abrasive microgrinding [7-9]. Polished ULE samples provided by Litton-ITEK Optical Systems were etched in 40% HF acid for 1 minute to relieve residual polishing stresses and to relieve stress concentrations at the front of any existing subsurface cracks. The samples were soaked in a selected environment for at least one hour before scratching. Different samples, cut from the same original blank and prepared simultaneously, were used for each scratching environment.

All scratching experiments were made using a Wilson Tukon microhardness tester with a Vickers diamond pyramid indenter. The apparatus was modified to permit lateral scratching during the indentation loading cycle, using a motorized micrometer [24]. While scratching, the glass surface was maintained so that it was continually wetted by the selected environmental fluid. Scratches were subsequently analyzed using an SEM, after etching in 40% HF acid for 30 seconds.

Environments tested included a homologous series of nine alcohols and de-ionized water. All scratches were performed at 5 gram normal load and 100 μm sec scratching speed, producing a scratch 4 mm in length. The apparatus was specially calibrated to achieve better than 1 gram resolution on normal scratching load. For each environment, 10-15 scratches

were made. The diamond pyramid used for scratching was checked using high-magnification SEM photographs of the tip before and after the scratch tests. No measurable wear of the diamond tip was observed. Many scratches suffered subsurface damage, appearing in the following sequence of increasing damage: median cracks beneath the base of the scratch, radial cracks nearly perpendicular to the scratching direction, and subsurface lateral cracks extending from the sides or end of the scratch. To evaluate the fracture results, all scratches were categorized as either having subsurface damage (median, radial, or lateral cracks observed) or not having subsurface damage (purely ductile scratch), after examining the entire 4 mm of the scratch length. With the exception of butanol, subsurface damage decreases steadily from the smaller molecular weight alcohols through hexanol. The minimum in subsurface damage level corresponds to hexanol and heptanol. Subsurface damage increases somewhat in octanol, and increases again in nonanol. Damage for ULE samples scratched in a water environment was at the same level as that observed in methanol. Data are plotted along with ζ-potential measurements in Figure 1.

We could find no existing data for the ζ-potential of ULE glass in alcohols. To establish this database, we prepared ULE powder suspensions in each alcohol for use in an electrosonic amplitude (ESA) measurement apparatus (MATEC 8000) that can be used to measure ζ-potential if certain attributes of the powder and liquid environments are known [25]. Specifically, the conversion from ESA to ζ requires the following constants: density and mean particle size of the powder; density, viscosity, and speed of sound in the liquid; and concentration of the colloidal suspension. Sample preparation included pulverizing ULE samples into a powder using a series of ball mills, jet mills, and sieves. The particle size distribution of the powder was measured using a sedigraph, yielding a gaussian distribution with a mean particle diameter of 3.2 μm. All requisite property constants were obtained from the literature for these well characterized, reagent grade alcohols. The concentration of each colloidal suspension was fixed at 0.05% by volume. Ten measurements were made for each suspension. Results of the ζ-potential measurements are plotted along with the scratching results in Figure 1 for ULE glass in the various alcohol environments. For each ζ-potential data point in the graph, the standard deviation of the ten measurements averaged to produce the data is smaller than the size of the plotted symbol.

A correlation exists between the measured occurrence of subsurface damage and the ζ-potential of the scratching environment. The increase in damage for alcohols that are heavier (octanol-decanol) or lighter (methanol-pentanol) than hexanol and heptanol suggests that there is a definite minima in scratching damage level that corresponds to a hexanol or heptanol environment. The ζ-potential measurements show a minimum magnitude in pentanol and hexanol environments. While this does not correspond precisely with the hexanol-heptanol environment that produced minimum damage in scratching, comparison of the graphs in Figure 1 does suggest some correlation between the magnitude of ζ and the likelihood of damage in scratching. It is likely that there are other factors besides ζ-potential and ion adsorption that affect scratching damage in the different alcohols. Some of these factors (i.e., lubrication effects and water content of the different alcohols) have been shown to be less important than ion adsorption in previous studies of glass machining in alcohols [15]. Although the scratches made in a water environment correspond to a large negative value of ζ-potential (60 mv), there are other, more compelling reasons to expect increased damage in water, since its embrittling effects have previously been described and explained by Wiederhorn [26], Tomozawa [27], and Michaelski [23], among others.

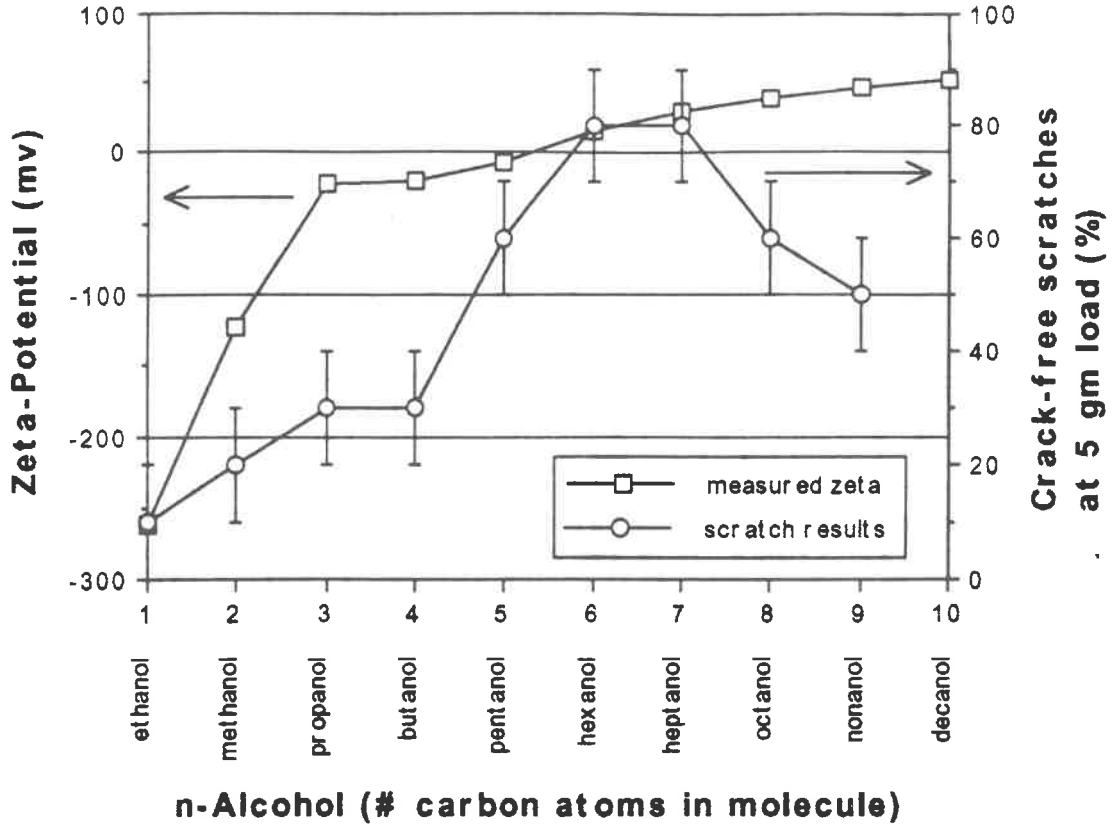

Figure 3: Measurements of scratching damage and ζ–potential for ULE glass in various alcohol environments. Left abscissa is measured ζ–potential. Right abscissa is the percentage of scratches that did not exhibit any fracture in the given environment, for 4 mm long scratches made with a 5 gm normal load and a scratching speed of 100 μm/sec.

Further tests involved ultraprecision machining of ULE on a two-axis diamond grinding apparatus. Samples were pre-polished, mounted with epoxy to the workpiece holder, and soaked in the selected environment for at least one hour before grinding. Different samples, prepared from the same original piece, were used for each environment. The laboratory-scale grinder has a stiffness normal to the grinding contact of 50 MN/m and is controlled in real-time to a precision of 10 nm using piezoelectric actuation and capacitance gage sensing. The entire face of each 5 mm x 5 mm sample surface was ground in each 200 nanometer deep pass, and 100 passes were completed for each test, yielding a total removal depth of 20 μm per sample per test. Wheel wear was measured and found to be negligible (less than 0.25 μm) for each grinding test. The wheel was trued and dressed using a diamond lapping technique [6] before each grinding test. The grinding conditions that were used are described in Table 1. These conditions were chosen to provide a grinding chip thickness (i.e., abrasive grain depth-of-cut) of approximately 180 nanometers: in the brittle regime but within an order of magnitude of the ductile regime calculated for ULE.

SEM photomicrogaphs of the ground, and subsequently etched, ULE surfaces revealed effects in the different environments that were consistent with the results from scratching experiments. It was found that in heptanol and (to a lesser extent) octanol environments, the grinding was largely dominated by plastic flow. In the nonanol environment, grinding

damage levels increased to some extent. In the water environment, the grinding regime was entirely brittle.

The specific grinding energy (which is inversely proportional to machining efficiency) also showed a significant dependence on environment. The measured specific grinding energy for the grinding experiments is shown in Table 2. These results (reduced machining efficiency and reduced subsurface damage in heptanol and octanol, with $\zeta \sim 0$) are consistent with the results observed in scratching tests.

Wheel	100 mm diameter, 6.3 mm wide cup wheel
Configuration	Air bearing spindle and cross slide
Grinding abrasive	4-8 μm natural diamond, 50 conc., resin bond.
Infeed	200 nm/pass, 100 passes per sample
Crossfeed	150 μm/sec
Wheel peripheral speed	7.9 m/sec
Workpiece	5mm x 5mm x 5mm cube
Material Removal Rate	1.5×10^{-13} m^3/s
Cutting Environments	Water, heptanol, octanol, and nonanol

Table 1: Grinding Conditions

Environment	Specific Grinding Energy
Heptanol	9.5×10^{13} J/m^3
Octanol	5.6×10^{13} J/m^3
Nonanol	2.8×10^{13} J/m^3
Water	2.2×10^{13} J/m^3

Table 2: Specific grinding energy for ULE glass microgrinding in various environments.

Discussion

It is important to note that all of these experiments were performed near the ductile-brittle transition in abrasive grain depth-of-cut. In very brittle-regime machining of glass by mul-

tipoint diamond tools, Westwood found that the correlation was reversed: an *increased* machining efficiency accompanied chemomechanical environments in which $\zeta \sim 0$. That a particular environment can enhance efficiency and fracture at high machining rates (brittle-regime grinding) and then inhibit efficiency and fracture at low machining rates was demonstrated by Westwood in a series of experiments on polycrystalline alumina [14]. For diamond grinding of glass, the implications of this phenomenon are significant: the same environment can be used to enhance material removal rate in coarse figuring operations and to inhibit fracture in finishing operations. This phenomenon was first observed in loose-abrasive grinding of glass by Phillips, Crimes, and Wilshaw [28]. In this study, machining rate was measured for constant-pressure, constant-area loose-abrasive grinding in both octanol and water. These experiments were performed with various sizes of abrasive, from 4.5 μm to 105 μm in diameter. It was found that an octanol environment enhanced machining efficiency by up to 100% (compared to a water environment) for large grain sizes (~100 μm), but "[for particle diameters] below 10 μm the effect is reversed and water becomes a more efficient environment [28]." Recent research on loose abrasive microgrinding processes has demonstrated both theoretically and experimentally that a decrease in abrasive size is accompanied by a reduction in fracture damage depth and ultimately leads to a transition from brittle-regime grinding to ductile-regime grinding [7-9]. The critical abrasive size for transition in glass is about 1 μm [29,30]. The results by Phillips, et. al. can be interpreted as follows: if material removal processes are operating in the very brittle regime, octanol results in enhanced fracture and greater machining efficiency. If, on the other hand material removal processes are operating near the brittle-ductile transition, octanol results in inhibited fracture and lower machining efficiency.

Conclusions

Chemomechanical effects in alcohols and water have been explored for microgrinding of glass. It has been shown that significant changes in the surface properties of the glass can be made by changing the machining environment. The material effect of such an environmental change is to alter hardness and fracture resistance in the surface layer, resulting in a net increase in the critical depth-of-cut for a ductile-brittle transition. While the correlation is not perfect, it appears that surface charge and ion adsorption may play an important role in chemomechanical effects. In scratching and grinding tests, the minimum damage observed in ULE glass corresponds to a heptanol environment. Chemomechanical increases in the critical depth-of-cut can be used to facilitate transition from brittle-regime grinding to ductile-regime grinding, without changing other machining conditions and without increased machine precision. This has been demonstrated through models and experiments in this paper. Additionally, chemomechanical environments that enhance ductility in fine microgrinding can be used to enhance fracture at higher machining rates, thereby improving efficiency and increasing productivity.

Acknowledgments

This work was funded through grants from the National Science Foundation Division of Design and Manufacturing Systems, the Survivable Optics MODIL Program at Oak Ridge National Laboratory, and Litton-ITEK Optical Systems. Grinding wheels were donated by Norton Corporation. Special thanks are due to Richard Pober of the MIT Materials Processing Center, Ceramics Processing Research Laboratory, and to Russ Mann of MATEC Corporation for facilities and technical assistance measuring chemomechanical potentials.

References

[1] Bifano, T. G., Dow, T. A., and Scattergood, R. O., 1991, "Ductile-Regime Grinding: A New Technology for Machining Brittle Materials," *ASME J. Eng. for Industry*, Vol. 113, pp. 184-189.

[2] Bifano, T. G., Blake, P., Dow, T. A., and Scattergood, R. O., 1988, "Precision Machining of Ceramic Materials," *American Ceramic Society Bulletin*, Vol. 67, pp. 1038-1044.

[3] Hed, P. P., and Blaedel, K. L., 1986,"Advanced Fabrication of Optical Materials," *Lawrence Livermore National Laboratory, Document UCID-21041-86.*

[4] Stowers, I. F., Komanduri, R., and Baird, E. D., 1988, "Review of Precision Surface Generating Processes and Their Potential Application to the Fabrication of Large Optical Components," *Proc. SPIE 966: Advances in Optical Fabrication and Metrology Including Large Optics*, J. B. Arnold and R. E. Parks, eds., SPIE, Bellingham, WA, pp. 62-73.

[5] Yoshioka, J., Koizumi, K., Shimizu, M., Yoshikawa, H., Miyashita, M.,Kanai, A., "Ultraprecision Grinding Technology for Brittle Materials: Application to Surface and Centerless Grinding Processes," 1985, *Milton C. Shaw Grinding Symposium*, R. Komanduri, D. Maas, eds., ASME PED Vol.16, ASME, NY, NY, pp. 209-227.

[6] Bifano, T. G., 1988, "Ductile-Regime Grinding of Brittle Materials", *PhD Dissertation*, North Carolina State University.

[7] Golini, D., and Jacobs, S. D., 1990, "Transition Between Brittle and Ductile Mode in Loose Abrasive Grinding," *Proc. SPIE,1333: Advanced Optical Manufacturing and Testing*, SPIE, Bellingham, WA, pp. 80-91.

[8] Golini, D., and Jacobs, S. D., 1991, "Physics of Loose Abrasive Microgrinding," *Appl. Optics*, Vol. 30, pp. 2761-2777.

[9] Golini, D., and Jacobs, S. D., 1990, "Chemomechanical Effects in Loose Abrasive Grinding of ULE," *OSA Topical Mtg. on the Sci. of Optical Finishing*, Monterey, CA.

[10] Rebinder, P. A., 1928, *Proceedings 6th Physics Conference*, State Press, Moscow, p.29.

[11] Westwood, A. R. C., and MacMillan, N. H., 1973, "Environment-Sensitive Hardness of Nonmetals," *The Science of Hardness Testing and its Research Applications*, J. H. Westbrook and H. Conrad, Eds., ASM, Metals Park, Ohio, pp. 377-416.

[12] MacMillan, N. H., Huntington, R. D., and Westwood, A. R. C., 1974, "Chemomechanical Control of Sliding Friction Behavior in Nonmetals," *J. Mat. Sci.*, Vol. 9, pp. 697-706.

[13] Westwood, A. R. C., Mularie, W. M., and MacMillan, N. H., 1974, "Chemomechanical Effects in Soda-Lime Glass," *Proc. Symp. on Strength of Glass and Glassware*, University of Sussex, U. K.

[14] Westwood, A. R. C., and Mills, J. J., 1977, "Application of Chemomechanical Effects to Fracture-Dependent Industrial Processes," *Surface Effects in Crystal Plasticity*, R. M. Latanision, J. T. Fourie, Eds., Noordhoff, Leiden, pp. 835-863.

[15] Westwood, A. R. C., Ahearn, J. S., and Mills, J. J., 1981, "Developments in the Theory and Application of Chemomechanical Effects," *Colloids and Surfaces*, Vol. 12, pp. 1-35.

[16] Westwood, A. R. C., MacMillan, N. H., and Kalyoncu, R. S., 1973, "Environment-Sensitive Hardness and Machinability of Alumina," *J. Am. Ceram. Soc.*, Vol. 56, pp. 258-262.

[17] Westwood, A. R. C., Parr, Jr., G. H., and Latanision, R. M., 1972, "Adsorption-Sensitive Machining Behavior of Glass," *Amorphous Materials*, R. W. Douglas and B. Ellis, Eds, pp. 533-543.

[18] Malin, M., and Vedam, K., 1977, "Ellipsometric Studies of Environment-Sensitive Polish Layers of Glass," *J. Appl. Phys.*, Vol. 48, pp. 1155-1157. 1

[19] Czernuszka, J. T., and Page, T. F., 1987, "Characterizing The Surface Behavior of Ceramics: Part 2 - Chemo-mechanical Effects," Chapman and Hall, ltd, pp. 3917-3923.

[20] Cuthrell, R.E., 1978, "The role of Ion Aggregates in Rebinder-Westwood Environmental Effects on Wear as Monitored by Acoustic Emission,"*J. Appl. Phys.*, Vol. 49, pp. 432-436.

[21] Latanision, R. M., and Swain, M. V., 1977,*Surface Effects in Crystal Plasticity*, R. M.Latanision, J. T. Fourie, Eds., Noordhoff, Leiden, p. 3.

[22] Cuthrell, R. E., and Randich, E., 1979, "The Embrittling Effects of Hydrogen on a Variety of Inorganic Materials as Indicated by Acoustic Emission," *J. Mat. Sci.*, Vol. 14, pp.612-618.

[23] Michalske, T. A., and Bunker, B. C., 1987, "The Fracturing of Glass," *Scientific American*, Vol. 122, pp. 122-129.

[24] DePiero, D., and Bifano, T. G., 1991, "Environmental Effects on Subsurface Damage in Glass Machining," *Proc. Am. Soc. Precision Engineering*, Santa Fe, NM.

[25] Obrien, R. W., 1990, "Electroacoustic Equations for a Colloid Suspension," *J. Fluid Mech.*, Vol. 212, pp. 81-93.

[26] Wiederhorn, S. M., and Johnson, H., 1975, "Effect of Zeta Potential on Crack Propagation In Glass in Aqueous Solutions," *J. Am. Ceramic Soc.* Vol. 58, p. 343.

[27] Tomozawa, M., 1985, "Water in Glass," *J. of Noncrystalline Solids*, Vol. 73, pp. 197-204.

[28] Phillips, K., Crimes, G. M., and Wilshaw, T. R., 1977, "On the Mechanism of Material Removal by Free Abrasive Grinding of Glass and Fused Silica," *Wear*, Vol. 41, pp. 327-350.

[29] Kendall, K., 1978, "Complexities of Compression Failure," *Proc.Roy. Soc. Lond. A*, Vol. 361, pp. 245-263.

[30] Brown, N. and Fuchs, B. A., 1988, "Brittle to Shear Grinding Mode Transition for Loose Abrasive Grinding," *Proceedings of the Workshpo on Optical Fabrication and Testing*, Technical Digest Series, Vol. 13, Optical Society of America, pp. 23-26.

EFFECT OF MACHINING PARAMETERS, SET UP, AND TOOL GEOMETRY ON SURFACE FINISH AND ROUNDNESS OF POLYCRYSTALLINE DIAMOND BORED BRONZE BEARINGS

G.V. Delbrugge, K. Knott, C.O. Ruud, and P.H. Cohen

The Pennsylvania State University
Department of Industrial and Management Systems Engineering
207 Hammond Building
University Park, PA 16802

INTRODUCTION

Precision boring with single point, polycrystalline diamond tools has been the focus of laboratory based research. The novelty of this research is that it was carried out using a production type machine, and conducted in an industrial environment. The experiment indicates that techniques used for optimization and analysis of machining in laboratory settings can be adapted to industry. This is so, even though higher production rates and more variables tend to make such analytical approaches less appealing than they are in a laboratory or experimental facility.

EXPERIMENTAL SET UP

Workpiece

The specimen geometry used in the experiment is illustrated in Figure 1. Much of the geometry required for successful manufacture of the bearing is omitted, since it was not required for this experiment. Note, however, that even though the smaller bore is not described in Figure 1, it was also diamond turned using the same set up used for this experiment.

Machine

The CNC machine used for the diamond boring was manufactured by Kellenberger. This machine is actually a cylindrical grinder, designed to grind both inner and outer diameters. The internal grinding attachment was removed and replaced with diamond tooling, as shown in Figure 2.

Tooling on the machine could be positioned in .00001 inch increments, with positional repeatability of .000008 inches.

Workholding Equipment

An air bearing spindle was used to hold and rotate the specimen during the diamond boring operation. A cross-sectional view of the set up is shown in Figure 3.

A unique feature of the experiment was the grinding of the air bearing spindle to fit the bronze specimen after the air bearing was attached to the machine. Grinding was completed before

installing the diamond tooling. By grinding the spindle after clamping it to the machine table, error between the diamond tooling and spindle axis was minimized.

The openings at both ends of the spindle allowed machining of the entire inner diameter without changing the bearing location. This minimized geometric error between the three different bores machined during actual production.

EXPERIMENTAL DESIGN

Obviously, the goal during manufacturing of the bearings was to develop the best process possible by changing the process parameters. The purpose of this experimental design was to quantify the effect of changing some of those parameters, while recognizing the range of variables proven during production of the bearings.

Table 1 shows the experimental matrix. The convention in most diamond turning operations specifies feed in inches per minute, instead of inches per revolution (f_r). For both production and experimental machining of the bearings, 0.5 inches per minute was used for feed. Therefore, the percent deviation from the theoretical finish was evaluated along with the absolute finish results. Theoretical finish is calculated by:

$$f_r^2/(8*TNR) \text{ microinches},$$

where TNR is the tool nose radius, measured in inches.

Tool center height, radial depth of cut, d, and tool geometry (sharpness, R_i) were also variables in the experiment. Measured response variables were axial finish and roundness (out of round) of the bored diameters. The number of tool passes, n, is a calculated parameter given below:

$$n= ((2*TNR*d + d^2)^{1/2})/f_r.$$

The parameter n is more descriptive than using the depth of cut or feed alone, especially when orthogonal machining is not used.

EXPERIMENTAL RESULTS

Measured Finish

By using an experimental matrix, results could be presented and analyzed in a variety of ways. The measured axial finish is presented in Figure 4 by plotting the finish, in microinches, as a function of n, the number of passes required to generate the surface. The plots illustrate the effect of center height on the measured finish. The dependence of the finish on the RPM, which determined the feed per revolution, is also apparent from the figure. The RPM for a given level of n can be determined from Table 1.

The center height and RPM were also determined to be statistically significant variables in an analysis of variance (ANOVA) of the finish. ANOVA was also performed using the percent

difference of measured finish from theoretical. In this ANOVA, the RPM was determined to be the only statistically significant variable. Depth of cut and tool sharpness did not have a statistically significant effect on the measured finish in this experiment.

Roundness

Only the center height had a significant effect on the roundness in the experiment. This effect is shown in Figure 5, which illustrates roundness as a function of n.

Center height was also the only statistically significant variable. ANOVA results indicated that none of the other parameters caused significant variation in the measured roundness.

DISCUSSION OF RESULTS

Surface Finish

The center height of the tool was clearly the most influential variable in the experiment. However, it can be observed from Figures 4 and 5 that the best finish was obtained at the lower center height of .001 inches, while minimal out of round resulted when using the higher center height of .010 inches.

If the finish obtained with the larger center height value had been better than that obtained with the lower one, it would have been easy to provide an explanation for the difference. This is because raising the tool center height in boring operations reduces the friction between the tool flank and the newly formed surface. An increase in friction here can increase tool vibration and distort the theoretical scalloped finish.

However, this experiment yielded a superior finish at the lower center height. One possible explanation is the effect that the center height has on the effective rake angle of the tool. Increasing the tool center height in a boring operation makes the effective rake angle more negative.

As the rake angle of the tool increases negatively, the force required to plastically deform the workpiece also increases, since more compressive, and less tensile stress is being applied to the deformation zone, and compressive yield strength is greater than tensile yield strength for a given material. Therefore, a larger percentage of material in the deformation zone is not sheared away as a portion of the chip. This deformed material remains as part of the formed surface when using the tool with the larger center height, adding to the height of the surface profile and measured roughness.

The higher RPM had the expected effect on the measured surface finish. Theoretical finish at 1000 RPM was 25 microinches; measured finish was better than that in every case. For 1000 RPM, the ploughing of the tool may have actually decreased the value of measured finish, since theoretical finish assumes no distortion of the scalloped surface.

At 4000 RPM, the finish limitations of a polycrystalline tool start to become more significant. Theoretical finish at this speed is 2 microinches; the average grain size of the diamond tool is .00016 inches, and the size ranges from .00006 to .00032 inches.

Single crystalline diamond may be required to improve the measured finish below five microinches, which was the lowest measured finish value in the experimental data. Four microinches was the lowest value obtained with this set up in production.

Roundness

Roundness is not a common variable in diamond turning research. However, it was an important tolerance to maintain in production, where it was quite sensitive to changes in tool center height. The results of this experiment also indicated that tool center height was influential. The higher center height was used to provide a consistently lower value of out of round in the experiment.

Future work that includes force measurement would provide means for a more thorough explanation of the roundness results. However, the results obtained here indicate that the rigidity of set ups like those used for this experiment is sensitive even to small changes in tool geometry. Simultaneous analysis of roundness and finish also shows that optimizing the set up for multiple response variables often requires that improvement of one variable must be done by sacrificing the quality of another.

CONCLUSIONS

1. When used with the correct set up, diamond tooling can be used in a production environment to manufacture parts to microinch tolerances.

2. Analytical techniques can be used to predict optimum machining parameters in production environments.

3. In precision operations used to produce parts with multiple tolerance requirements, measured variables cannot always be analyzed and improved independently.

4. Measured variables are sensitive to the effect of varying the tool center height, which is not a typical variable in laboratory studies.

BIBLIOGRAPHY

- Chaloux, Leonard E. "Part Fixturing for Diamond Machining." Proceedings of SPIE, vol. 508, August 23- 24, 1984, pp. 109- 111.

- Evans, C., Polvani, R., Postek, M., and Rhorer, R. "Some Observations on Tool Sharpness and Subsurface Damage in Single Point Diamond Turning." Proceedings of SPIE, vol. 802, March 31- April 2, 1987, pp. 52- 66.

- Rhorer, R., and Lucca, D. "An Experimental Procedure for Studying Diamond Turning Chip Mechanics." Proceedings of ASPE 1990 Annual Conference, September 23- 28, 1990, pp. 51- 54.

TABLE 1: EXPERIMENTAL DESIGN WITH NUMBER OF PASSES OF TOOL. THE CALCULATED NUMBER OF PASSES, n, IS SHOWN WITH THE STATISTICAL SCHEME CONSISTING OF TWO LEVELS RPM, TWO LEVELS CENTER HEIGHT, THREE LEVELS DEPTH OF CUT, AND TWO LEVELS OF DIAMOND TOOL. MEASURED RESULTS INCLUDE AXIAL FINISH, RADIAL DEFLECTION, AND ROUNDNESS.

RPM	CENTER HEIGHT (IN.)	DEPTH (IN.)	NUMBER OF PASSES OF TOOL, n	
			TOOL A, Ri = .001	TOOL B, Ri = .0001
1000	.001	.0005	2.25	2.25
		.0015	3.94	3.94
		.0030	5.68	5.68
	.010	.0005	9.00	9.00
		.0015	15.78	15.78
		.0030	22.72	22.72
4000	.001	.0005	2.25	2.25
		.0015	3.94	3.94
		.0030	5.68	5.68
	.010	.0005	9.00	9.00
		.0015	15.78	15.78
		.0030	22.72	22.72

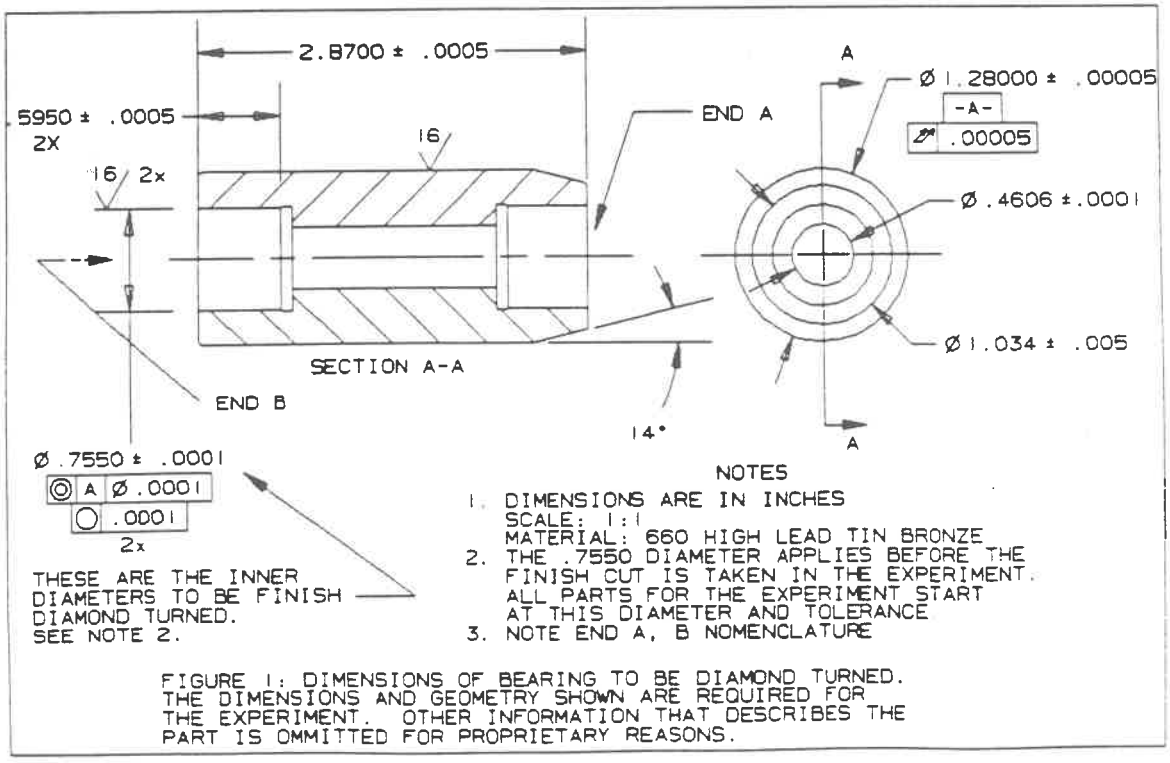

FIGURE 1: DIMENSIONS OF BEARING TO BE DIAMOND TURNED. THE DIMENSIONS AND GEOMETRY SHOWN ARE REQUIRED FOR THE EXPERIMENT. OTHER INFORMATION THAT DESCRIBES THE PART IS OMMITTED FOR PROPRIETARY REASONS.

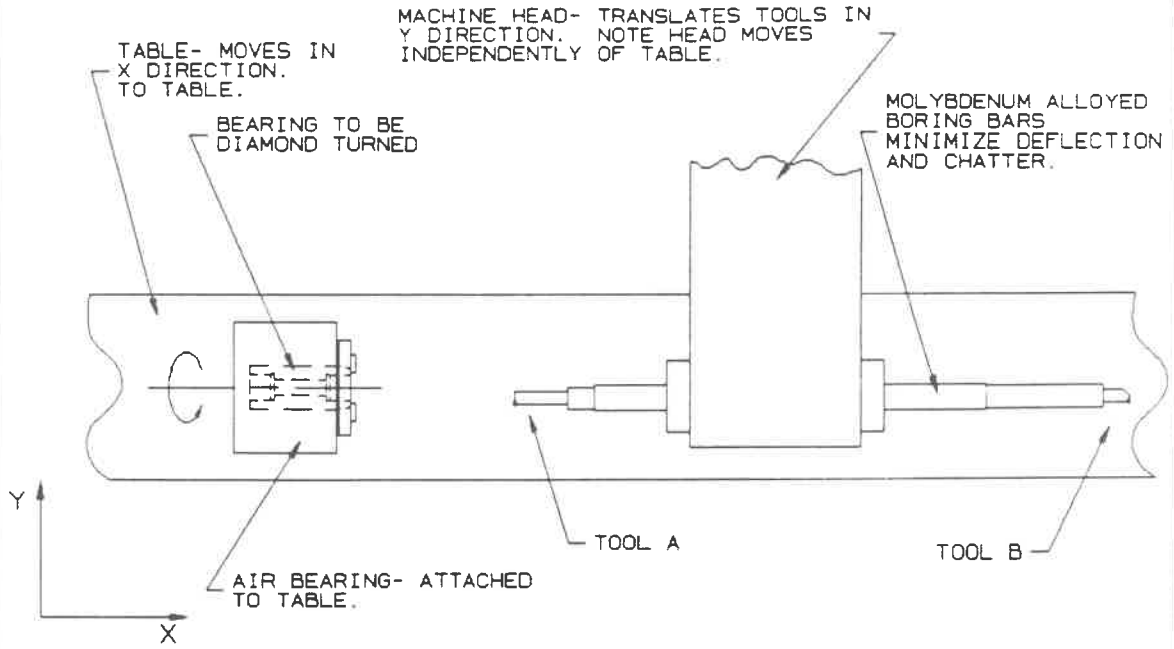
MACHINE HEAD- TRANSLATES TOOLS IN Y DIRECTION. NOTE HEAD MOVES INDEPENDENTLY OF TABLE.
TABLE- MOVES IN X DIRECTION. TO TABLE.
BEARING TO BE DIAMOND TURNED
MOLYBDENUM ALLOYED BORING BARS MINIMIZE DEFLECTION AND CHATTER.
Y
X
TOOL A
TOOL B
AIR BEARING- ATTACHED TO TABLE.

FIGURE 2.: CNC I.D./O.D. GRINDER WITH ATTACHED DIAMOND TOOLING. THIS SETUP ALLOWS PART TO BE BORED FROM EITHER END, WITHOUT INTERRUPTING THE PROCESS. TOOL OFFSETS CAN BE PROGRAMMED INDEPENDENTLY.

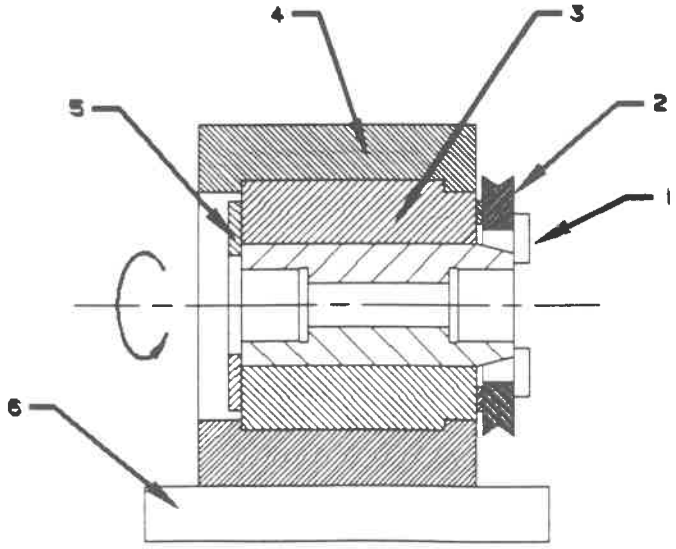

LEGEND

1. CLAMP- TWO EACH, ATTACHED TO PULLEY.
2. V- PULLEY- FASTENED TO FACE OF AIR BEARING SPINDLE. SPINDLE IS BELT DRIVEN BY A SERVO MOTOR, WHICH IS LOCATED ON TOP OF THE AIR BEARING (NOT SHOWN HERE)
3. AIR BEARING SPINDLE- GROUND WHILE CLAMPED IN PLACE SO BRONZE BEARING WILL SLIP FIT WITH LESS THAN .0002 CLEARANCE. SPINDLE RUNS OUT LEASS THAN .00002.
4. AIR BEARING- DOES NOT ROTATE RELATIVE TO SPINDLE.
5. BACKING PLATE- LOCATES END B OF BRONZE BEARING.
6. CLAMPING PLATE- COUPLES AIR BEARING TO MACHINE. THE PART CAN TRANSLATE AXIALLY WHILE ROTATING.

FIGURE 3.: AIR BEARING SPINDLE, WITH BRONZE BEARING. THE BEARING TO BE DIAMOND TURNED IS SHOWN PROPERLY LOCATED AND CLAMPED ON END A, WITH TWO STRAP CLAMPS LOCATED 180° APART.

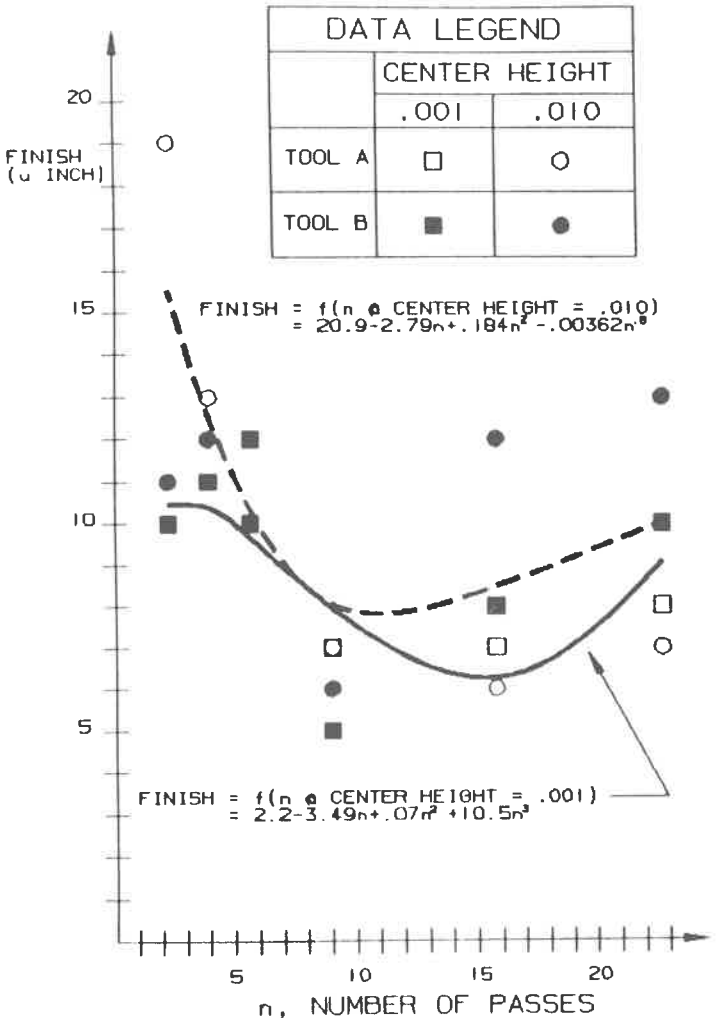

FIGURE 4: FINISH AS A FUNCTION OF n. DATA POINTS ARE PLOTTED AS SHOWN. FITTED CURVES FOR EACH CENTER HEIGHT ARE DRAWN. EQUATIONS FOR THESE CURVES ARE THE MINIMUM SUM OF SQUARE ERROR CURVES FOR THAT DATA SET.

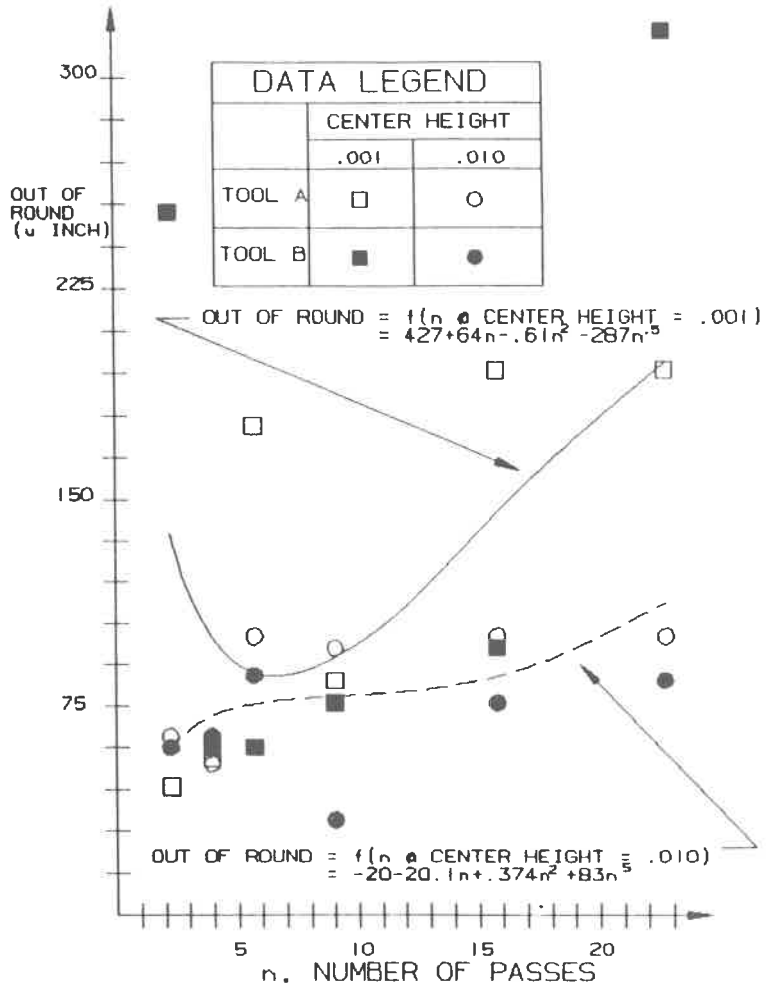

FIGURE 5: OUT OF ROUND AS A FUNCTION OF n. DATA POINTS ARE PLOTTED AS SHOWN. FITTED CURVES FOR EACH CENTER HEIGHT ARE DRAWN. EQUATIONS FOR THESE CURVES ARE THE MINIMUM SUM OF SQUARE ERROR CURVES FOR THAT DATA SET.

Computer Controlled Precision Optical Polishing on the Diamond Turning Machine

Philip Hannah and Delbert Stewart
Los Alamos National Laboratory
Los Alamos, New Mexico

With the growing use and interest in Ductile Regime Grinding (DRG) (specular surfaces from specially prepared grinding wheels), and the increasing use of a post polish after Single Point Diamond Turning (SPDT), it becomes apparent that an "on the machine" polishing device is needed.

It was been currently[1] reported that a measured surface quality of approximately 100 nanometers P-V has been achieved on glass substrates (Spectrasil SiO2) using the DRG technique. Although these surfaces are specular and appear to be polished to the naked eye, microscopic examination will show that the surface exhibits many fine grinding marks left by the wheel. For many applications these surfaces are sufficient. However, for uses in the visible and higher end of the spectrum, especially the ultra-violet, the light scattering from these ground surfaces is sufficient to make them not usable. Most work currently being done in the DRG area is with brittle materials, especially the glasses. Soft metals like aluminum, copper, brass, gold, etc., because the materials removal mechanism is different (brittle vs. ductile), cannot benefit from this process. Fortunately the SPDT process can produce accurate (1/2 wave or better), smooth (25 nm or better) surfaces on a wide variety of materials. The very nature of this process, however, is exactly analogous to machining on a lathe. Unfortunately, like a lathe, there are residual marks left in the part's surface by the passing of the tool. In order to use SPDT surfaces at these shorter wavelengths, a technique of plating and then polishing is used. The plating fills the grooves left by the machining process and the polishing smooths the plated surface, thus producing the desired low scatter performance. This smoothing is accomplished by removing the part from the machine and sending it to an optical shop where conventional lapping and polishing techniques are used to finish it.

As neither DRG nor SPDT are currently capable of producing low scatter surfaces, additional post polishing is required. The need for a simple post polishing technique on the machine, without removing the part, becomes essential.

This paper will report on the latest results of a joint venture project between the Moore Special Tool Co. and the Los Alamos National Laboratory. The object of this undertaking is to develop an on-machine post polishing device and the necessary software to support it. In order to develop the software we will begin the initial experiments using fused silica, as the removal rates are slower and thus the change in figure is more easily controlled.

---

[1] Precision Engineering Journal, Jan. 1991, Vol. 13 No. 1

At this writing a number of 3" diameter, 0.5" thick, plane parallel glass test blanks have been obtained with one side polished. This polished surface has had its figure and cosmetic quality carefully documented prior to the initial polishing runs. After each run interferometric figure and surface quality will be recorded. Once we have the numerical control program developed we will move to the smoothing of ductile ground and diamond turned surfaces.

Chemical Mechanisms of Diamond Wear

Edward Paul
Stockton College
Pomona, NJ

Chris J. Evans and Robert S. Polvani
National Institute of Standards and Technology
Gaithersburg, MD

Tool wear limits the range of materials that may be single point diamond turned economically. To ease this limit, we must first understand the mechanisms of diamond tool wear before we may mitigate its effects either by changing conditions to reduce wear or by predicting wear rates accurately enough to modify part programs to compensate for wear.

A number of different, possibly interacting, mechanisms can contribute to diamond tool wear: abrasion and chipping; adhesion and built-up edge formation; fatigue; and chemical wear, including diffusion, graphitization, and so on. There is a body of evidence to support the contention that chemical mechanisms limit diamond turnability for many materials of engineering interest[1], yet these mechanisms are probably the least well understood.

For the machinist, the critical step in chemical wear of a diamond tool involves the reversible stretching of the C-C bonds in the diamond lattice to form a transition state complex. Understanding the variety of process in complex formation gives insight into differences in diamond tool wear.

In the absence of other materials, diamond will convert to graphite (and vica versa) at a very slow rate. The synthetic diamond industry is founded on the observation that the rate of conversion can be increased substantially when certain metals are present. These metals serve as catalysts to form an intermediate complex with carbon atoms that lowers the energy barrier between diamond and graphite. The solid line in Fig. 1 represents the reaction path of the uncatalyzed process; the dotted line represents the path in the presence of a suitable metal. Studies on diamond wettability[2] and on coal gasification[3] have helped identify which metals act as catalysts and which ones do not. The general pattern is that metals with unpaired d shell electrons can form complexes with carbon atoms.

Table 1 divides metals into two groups; those with unpaired d electrons and those without. Comparison of experimental information on diamond wear with these two groups shows a striking overlap; the metals which form complexes also wear diamond

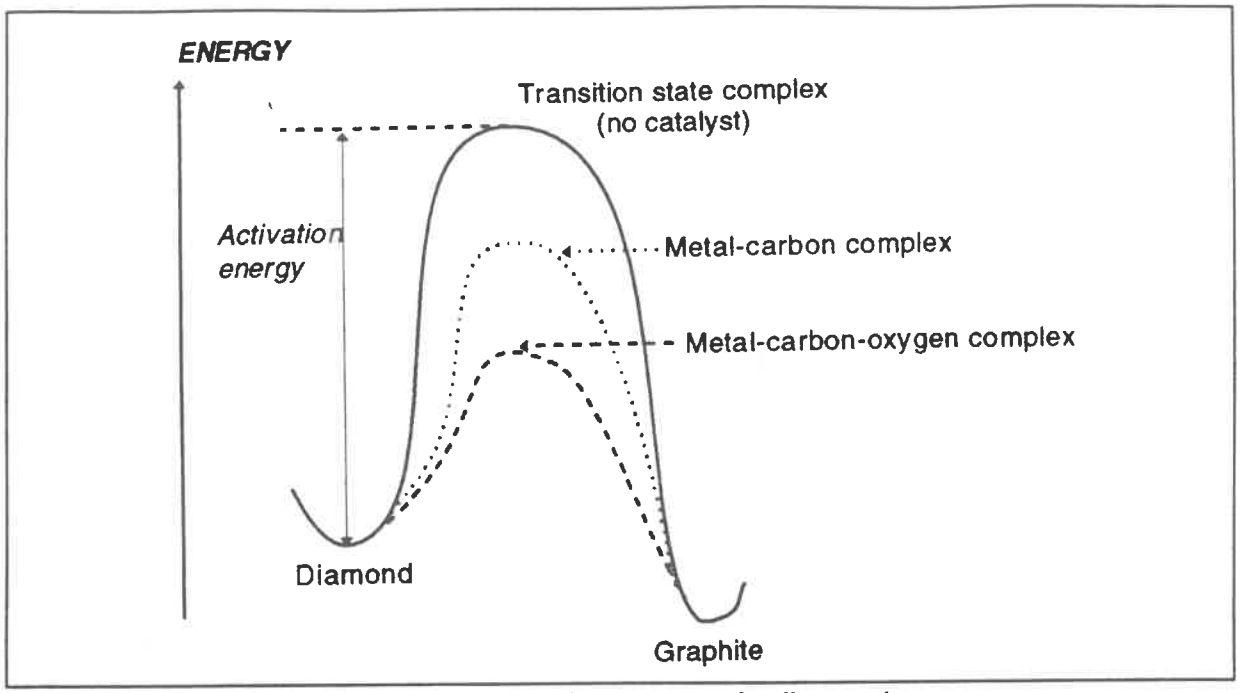

Figure 1 *Reaction pathways for carbons atoms in diamond*

tools rapidly; those which do not form complexes do not give unreasonable tool wear. The three exceptions to these observations - beryllium (Be), plutonium (Pu) and silicon (Si) - are discussed below.

Table 1 Unpaired d electrons and diamond wear

Tool wear	Unpaired d electrons	
	0	Not 0
Low	aluminum copper germanium gold indium lead magnesium palladium silver tin zinc	
High	beryllium silicon plutonium	cobalt chromium iridium iron manganese molybdenum nickel niobium platinum rhenium rhodium ruthenium tantalum titanium tungsten uranium vanadium

Detailed information on the structures of the carbon-metal complexes is not known. Experimental studies have shown that in the presence of oxygen, a carbon-metal-oxygen transition state complex can also be formed. These complexes react even faster than the carbon-metal ones and act as better catalysts. The activation energy associated with their formation is lower than for the other transition state complexes. They are shown schematically by the dashed lines in Fig. 1.

Once a complex is formed, there are several possible results. Since formation is reversible, the stretched carbon bond may contract and the atom may return to the diamond lattice. Alternately, it may break free and form a graphite structure with other carbon atoms, diffuse into the metal if diffusion sites are available, or react with other atoms in the environment. These other reactions might include formation of oxides or nitrides with gases present, formation of various hydrocarbons with materials in the cutting fluid, or formation of carbides with the metal being cut. For some of these reactions, different transition states might form. From the viewpoint of diamond wear, however, these processes must be preceeded by the formation of some sort of transition state complex and the presence of d electrons appears to be a significant factor in this.

Other factors may also correlate with diamond wear. Higher temperatures favor increased wear, for example, as does workpiece hardness which leads to higher cutting temperatures. This is understandable in terms of transition complex formation. Crystal structures and melting points also correlate generally with diamond tool wear. These two factors, however, also correlate generally with the number of unpaired d electrons and in both of these cases, certain elements break the correlation patterns. The insight afforded by the formation of transition state complexes offers the posssibility of understanding the process more fully.

The three elements which are reported to give substantial tool wear without having unpaired d electrons are Be, Pu, and Si. In all three cases, there is some question about whether the material actually machined was pure or whether it contained significant amounts of oxide. In the case of Be, the diamond turning experiments have been performed on materials with highly refined microstrustures and (highly abrasive) BeO on the grain boundaries. Arnold[4] has reported diamond turning beryllium at much reduced feeds and speeds, with the goal of reducing energy input to the cutting edge. Apparently there is a reduction in tool wear at lower speeds. Significantly, there is also a reduction in tool wear when cutting a sputtered grade of beryllium (presumably with no oxides) rather than a bulk 0-50 beryllium.

In the case of Pu, tool wear data may be described as sparse at best, consisting of second hand reports of tests performed with no information given on specific alloys used. As in the case of Be, the grade of Pu generally machined contains significant impurity levels and the rapid wear reported may not necessarily be chemical in origin. Another hypothesis for the case of Pu is the presence of unpaired f shell electrons. The ability of f electrons to form complexes with carbon is not known. Experiments using the lanthanide group elements should help test this hypothesis.

In the case of Si, tool wear may be due to its rapid oxidation to form silicon oxide, a material used commercially to polish diamonds. This hypothesis will be tested by passiviating a silicon surface and then machining it in a helium environment. An alternate possible mechanism for tool wear in these cases is the formation of silicon carbide (or of beryllium carbide when cutting beryllium).

The model of transition complex formation as significant in diamond wear leads to possible strategies for mitigation. One is to change the gas surrounding from air to nitrogen, argon or methane[5] to eliminate the formation of carbon-metal-oxide complexes. Another is to try cutting fluids which can compete with carbon to complex metals at the cutting interface. A third strategy is to introduce alloying elements into the workpiece material that will block the formation of the carbon-metal complex.

This description of the formation of transition complexes between carbon atoms in the diamond tool and metal atoms in the workpiece helps explain the differences in diamond tool wear and suggests further experimental approaches to further improve our understanding of the processes. In addition, it indicates experimental paths to improve cutting performance.

References:

1. Evans C. "Cryogenic diamond turning of stainless steel" *CIRP Annals*, Vol 40 (1991), pp571-5

2. Tanaka T., Ikawa N., and Tsuwa H. "Affinity of Diamond for Metals" *CIRP Annals*, 30, 241-5 (1981)

3. Tamai Y., Watanabe H., and Tomita A. "Catalytic Gasification of Carbon with Steam, Carbon Dioxide, and Hydrogen" *Carbon*, 15, 103-6 (1977)

4. Arnold J., ASPE Spring Topical Meeting, April 1991; Personal communication, February 1993

5. Casstevens J. "Diamond turning of Steel in Carbon Saturated Atmospheres" *Precision Engineering*, 5, 9-15 (1983)

Orthogonal Cutting Experiments: Input to Ultraprecision Process Design

Richard L. Rhorer
Los Alamos National Laboratory
Los Alamos, NM

Don A. Lucca
Oklahoma State University
Stillwater, OK

In recent years in the United States there has been an increase in interest in analyzing material removal processes. This is probably part of a larger trend to replace the "rules of thumb" upon which we relied in the past with more analytical engineering approaches. All analytical methods have to be verified before they can be used for practical process design. This verification is often done by comparing calculated results to careful experiments that have been designed to limit complexities.

In the field of cutting mechanics the orthogonal geometry has historically been used to verify analytical models, and the literature contains extensive studies, both analytical and experimental, of orthogonal machining. In recent years the traditional orthogonal geometry approach has been used for studying material removal in ultraprecision or diamond turning processes. This abstract describes an experimental approach for orthogonal diamond turning studies, which can be used along with analytical models to study the process. Orthogonal machining is the plane strain case where only forces in two orthogonal directions are significant.

In the case of single point ultraprecision machining the orthogonal model is drawn as shown in Fig.1. The shear zone and friction on the rake face, cross-hatched in Fig.1, are the regions where the majority of the cutting energy is dissipated in conventional machining. Many of the analytical and experimental approaches to studying the shearing process are summarized by Oxley[1], and many aspects of these models can be used to study ultraprecision machining. However, in ultraprecision machining a significant amount of the cutting energy may also be dissipated by the plowing effects caused by a finite tool edge radius, and the resultant sliding along the tool-workpiece interface resulting from tool wear and/or workpiece elastic recovery[2]. Attempts at modeling various aspects of the energy dissipation in ultraprecision machining have recently been put forth[3].

In ultraprecision machining the depth of cut often approaches the tool sharpness, or cutting edge radius, as illustrated in Fig.1. The ratio of the thrust force to cutting force is found to be constant when the depth of cut is large compared to the edge radius (as is the case in conventional machining); however, this ratio is seen to increase as the depth of cut approaches the edge radius. This change, which can be shown as a rotation of the resultant force vector, is plotted in Fig.2 for a case where a diamond tool has been used to cut aluminum with different depths of cut. As the depth of cut is decreased, the resultant force vector rotates toward the direction perpendicular to the surface.

It would seem possible that this rotation of the force vector as a function of depth of cut could be used to predict the actual sharpness (or edge condition) of the tool. Also, when cutting with a constant depth of cut, a change in the resultant force vector (or a change in the ratio of the thrust to cutting force) would indicate changes in this condition (i.e., tool wear).

The set-up used for a recent experimental series is shown in Fig.3. The disk with three different coupons is mounted on the spindle and turned at a constant RPM. The depth of cut is fixed by adjusting the cross-axis feed rate which carries the tool into the edge of the moving coupons. The thickness of the coupons is one millimeter and the diamond tool is wide compared to the coupon, producing a thin, wide chip. The force in the direction of the feed rate (thrust force), and the force in the circumferential direction (cutting force), are recorded.

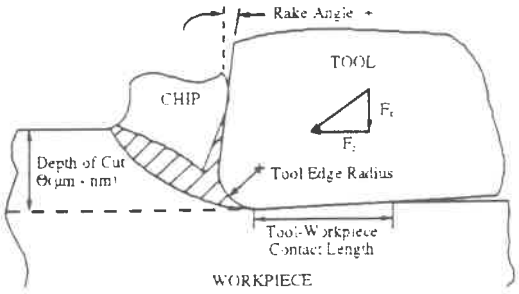

Fig.1. Orthogonal Cutting Geometry at Small Depths of Cut

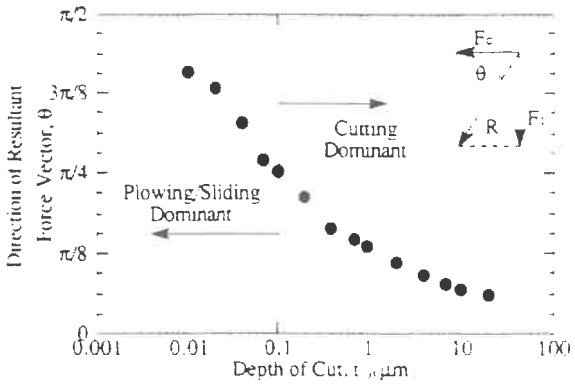

Fig.2. Effect of Depth of Cut on the Direction of Resultant Force Vector in Orthogonal Flycutting of AL 6061-T6

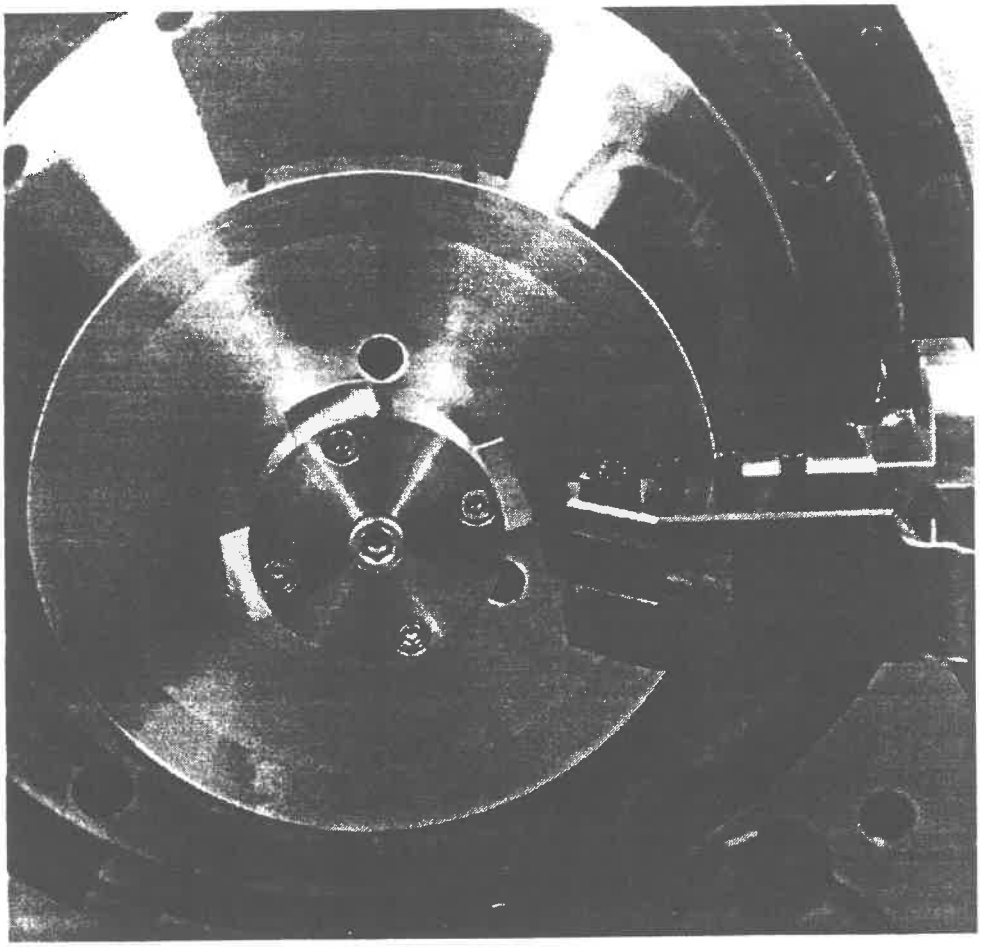

Fig.3. Photograph of Experimental Set-up for Three Different Material Samples

In this experimental set-up we can hold from one to four samples at a time, and we have usually worked with all samples of a series from identical material. For this current series, we mounted one aluminum, one copper, and one stainless steel coupon in the test rig, thereby intermittently cutting the three different materials.

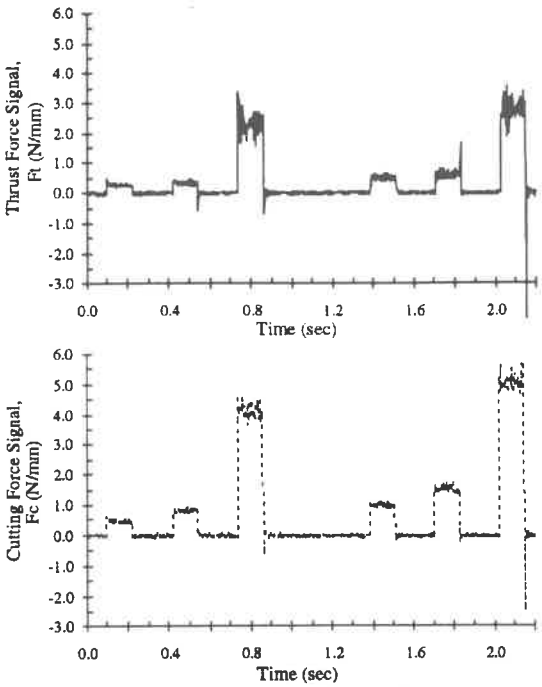

Fig.4. Thrust and Cutting Force Data when Cutting Three Different Materials

Typical data from this series is shown in Fig.4. The first square wave-like signal on the bottom trace is the cutting force when cutting the aluminum coupon, the second is for the copper, and the third (largest force) is for the steel. The upper trace contains corresponding three thrust force signals. It can be seen that the forces are larger for the steel, as would be expected. In addition the ratio of thrust to cutting force, and specific cutting energy can be determined for each of the materials.

The use of such an experimental approach allows for data, devoid of the complexities of a 3-D geometry, to be collected on the cutting and thrust forces, the force ratio, and the resulting specific energies. We have used this overall approach to investigate the effects of plowing and sliding which appear to dominate the force system when the depth of cut becomes of the order of the tool edge radius. The results of cutting the above 3 materials at a depth of cut of 2 micrometers (>> tool edge radius) are found to be consistent with those obtained for the conventional cutting of these materials, as would be expected. We are currently investigating the relationship of the resulting forces and energies in the region of depths of cut where plowing and sliding become important.

---

[1] Oxley, P.L.B., *Mechanics of Machining: An Analytical Approach to Assessing Machinability*. First ed. 1989, Chichester, UK: Ellis Horwood Limited.

[2] Lucca, D.A., Rhorer, R.L., and Komanduri, R., "Energy Dissipation in the Ultraprecision Machining of Copper". Annals of the CIRP, 1991, 40(1): pp.69-72.

[3] Lucca, D.A., Seo, Y.W., and Rhorer, R.L., "Energy Dissipation in Ultraprecision Machining", *Proceedings of the 1993 NSF Design and Manufacturing Systems Engineering Conference*, Univ. of North Carolina at Charlotte, 1993, pp.225-229.

Authors Index

Anderson, Charles A. 5
Annear, Robert 71
Beeler, Joe 21
Bifano, Thomas G. 71
Cohen, P. H. 79
Day, Robert D. 38
Delbrugge, G. V. 79
Donaldson, Robert R.*
Evans, Christopher J. 88
Flurchick, Ken 21
Follansbee, Paul S. 9
Gee, Anthony E. 54
Golini, Donald 50, 71
Hannah, Philip R. 86
Hara, Yoshihiro 54
Hashimoto, Hiroshi 58
Imai, Kenichiro. 58
Jungling, Kenneth C. 46
Kerstan, M. 42
Knott, K. 79
Kranenberg, Christian F. 46
Kress, Joel D. 34
Lawn, Brian R.*
Lucca, Don A. 92
Lundt, Holger. 42
Malkin, Stephen. 13
Marinescu, Ioan D. 67
Nakao, M. 54
Parks, Robert E.*
Patten, John A. 21
Paul, Edward 88
Polvani, Robert S. 88
Puttick, Keith E. 14
Rhorer, Richard L. 92
Russell, Phillip E. 38
Ruud, Clay O. 79
Scattergood, Ronald O. 17
Stewart, Delbert D. 86
Strenkowski, John S. 21
Voter, Arthur F. 34
Webster, John A. 67
Weiss, R. 42

*Paper not available at press time.